STUDY OF FACTORS AFFECTING ON SKIN-CORE STRUCTURES, MECHANICAL AND MORPHOLOGICAL PROPERTIES OF WOOD PLASTIC COMPOSITE DURING CO-INJECTION MOLDING

KRIANGKRAI JONGPRASERTVITTAYA

A THESIS SUBMITTED IN PARTIAL FULFILLMENT
OF THE REQUIREMENT FOR THE DEGREE OF
MASTER OF ENGINEERING IN AUTOMOTIVE ENGINEERING
(INTERNATIONAL PROGRAM)
INTERNATIONAL COLLEGE
KING MONGKUT'S INSTITUTE OF TECHNOLOGY LADKRABANG
2012

KMITL-2012-IC-M-004-019

Thesis Title	Study of factors affecting on skin-core structures, mechanical and morphological properties of wood plastic composite during co-injection molding.
Student	Mr. Kriangkrai Jongprasertvittaya
Student ID.	52600901
Degree	Master of Engineering
Program	Automotive Engineering (International Program)
Year	2012
Thesis Advisor	Dr. Wuttipong Rungseesantivanon Asst. Prof. Nattawoot Depaiwa Prof. Isao Satoh and Assoc. Prof. Takushi Saito

ABSTRACT

The study investigated the behavior of skin-core structures from co-injection molding using several grades of polypropylene (PP) and wood plastic composite (WPC). This work was divided into fourth parts. First part, the co-injection molding machine was designed by CAD/CAE simulation software and invented. Second part, this investigation was focused on the major and minor effects of skin-core formation by various molding parameters such as viscosity ratios, temperatures, injection speeds and volume proportions using in house co-injection molding machine. This can lead to understand skin-core formation and find the optimum condition. Third part, the results from the second part were compared with plastic injection molding simulation software. From these experiments, there were found reduction of skin-core volume proportions, skin injection speeds, skin temperatures and core viscosities lead to high core thickness fractions but a large number of decreasing skin-core volume proportions conduce to core breakthrough. Decreasing core injection speeds, core temperatures and skin viscosities lead to low core thickness fractions. Finished part, this study investigated the mechanical properties and morphology of sandwich specimen with wood plastic composite (WPC). A Maleic anhydride (MA) grafted PP (PP-g-MA) was used as a compatibilizer to improve the poor interfacial interaction between the hydrophilic natural fiber and the hydrophobic matrix PP. On the mechanical properties, increasing wood flour contents in sandwich specimen lead to decrease impact strength but flexural strength increased compared with pure polypropylene. The

morphology and microstructure of fractured surfaces were analyzed and discussed using the scanning electron microscopy (SEM) and Optical microscope that the results show good adhesion between skin and core layers.

ACKNOWLEDGEMENT

This thesis could not be completed without the assistance of many persons to whom I would like to express my sincere appreciation.

First, I would like to sincerely thank my advisor, Dr. Wuttipong Rungseesantivanon, who has given me many helpful suggestions, useful advice and fruitful discussions during the undertaken research.

I would also like to sincerely thank Asst.Prof. Nattawoot Depaiwa for kind advising and helping, Prof. Isao Satoh and Assoc. Prof. Takushi Saito for the suggestion.

I am grateful to National Science and Technology Development Agency (NSTDA), which provided the full scholarship for studying in the master program.

Special thanks go to MTEC PTL laboratory's members for helping me during the experiment.

Finally, I am very grateful to my family for all love, caring, understanding and motivation throughout my life.

Kriangkrai Jongprasertvittaya

CONTENTS

CONTENTS (CONT.)

CONTENTS (CONT.)

CONTENTS (CONT.)

CONTENTS (CONT.)

LIST OF TABLES

LIST OF FIGURES

LIST OF FIGURES(CONT.)

LIST OF FIGURES(CONT.)

LIST OF FIGURES(CONT.)

LIST OF FIGURES(CONT.)

LIST OF FIGURES(CONT.)

LIST OF FIGURES(CONT.)

CHAPTER 1

INTRODUCTION

1.1 Significance and Background

The co-injection molding process (or sandwich injection molding) was first developed by Garner and Oxley of ICI. [1] Two compatible thermoplastic materials flow into the mold cavity through the same gate. First and second polymer melts are injected to make skin and core, respectively. Two thermoplastics are laminated together and take advantage of different properties during the molding phase. This technology consists of sequential and simultaneous injection molding process to combine skin and core materials having different physical and chemical properties. Sequential injection molding process is a independent injection between first(A) and second(B) polymer melt to make skin and core structure in the mold, respectively(A→B). Simultaneous injection molding process is not the same because core structure is combined with first(A) and second(B) polymer melts(A→A+B).

In this study the molding parameters (viscosity, injection speed, volume proportion and temperature) were investigated to find major and minor parameters affecting on sandwich structure using sequential injection molding process. Major and minor effects were examined to create the molding part depending on requirements. Moreover, this study can be applied in automotive parts by using wood plastic composite or recycle plastic. In addition, mechanical properties of sandwich structure could be improved depending on the material to make core structure.

Wood plastic composite (WPC) can be a cost effective alternative to many plastic composites or metals in terms of bending stiffness or weight [2]. Wood fibers are non-abrasive so that relatively large concentrations can be incorporated into plastics without causing serious machine wear during blending and processing. The main applications of WPCs are in building products, such as fencing, rails, decking, decorative trims and so on. These composites are also gaining acceptance in automotive, industrial and marine applications [3]. This thesis may be applied in automotive components by using wood plastic composite to make core or skin structure depending on requirement because wood plastic composites will enhance mechanical

properties, reduce material weight and fuel consumption, lower production cost and improve passenger safety.

The second objective investigated the effect of wood flour contents on the physical properties of polypropylene/wood flour composites by using co-injection molding process. The main problem with wood plastic composite (WPC) has been the poor interfacial interaction between the hydrophilic natural fiber and the hydrophobic matrix PP. Therefore, maleic anhydride grafted PP (PP-g-MA), which is compatible with PP and can react with the hydroxyl groups of the fiber, was used as a compatibilizer in this study.

1.2 Objectives

1.2.1 To study the effects of parameters on co-injection molding process.

1.2.2 To classify the major and minor effects on co-injection molding process and compare with plastic injection molding simulation software.

1.2.3 To investigate the properties of wood plastic composite (WPC) on sandwich specimens.

1.3 Scopes

1.3.1 The first study was on co-injection molding machine. In this work, CAD/CAE simulation software was used to design this machine then created it.

1.3.2 The second study was on the injection molding process by varying molding parameters. The injection process was employed by the sequential injection molding process. Consequently, these specimens were injected in various conditions and then studied their physical properties.

1.3.3 Furthermore, studied the physical properties, mechanical properties, thermal properties and rheological properties including morphological properties of wood plastic composite (WPC) on sandwich specimens.

1.4 Expected Benefits

1.4.1 Understanding the processing method on PP/PP co-injection molding.

1.4.2 Understanding the parameters affecting on sandwich structure.

1.4.3 Understanding the mechanical properties and morphology on sandwich structure (PP/WPC).

1.4.4 Useful research works which can be extended to the actual application in the automotive industries or more advanced applications.

CHAPTER 2

LITERATURE REVIEWS

2.1 Introduction to Polypropylene (PP)

Polypropylene (PP) is a thermoplastic polymer, made by the chemical industry and used in a wide variety of applications, including packaging, textiles (e.g. ropes, thermal underwear and carpets), stationery, plastic parts and reusable containers of various types, laboratory equipment, loudspeakers, automotive components, and polymer banknotes [4]. An addition PP made from the propylene monomer, it is rugged and unusually resistant to many chemical solvents, bases and acids [5].

Structurally, it is a vinyl polymer, and is similar to polyethylene, only that on every other carbon atom in the backbone chain has a methyl group attached to it. Polypropylene can be made from the propylene monomer by Ziegler-Natta polymerization [6] and by metallocene catalysis polymerization[7]. The structure of polypropylene is shown in **Figure 2.1**.

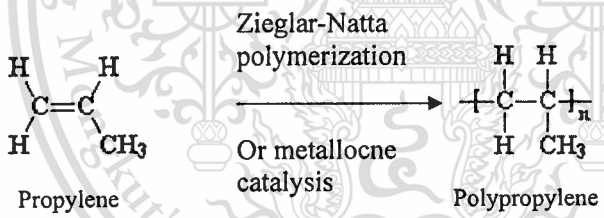

Figure 2.1 The structure of polypropylene

Most commercial polypropylene is isotactic and has an intermediate level of crystallinity between that of low-density polyethylene (LDPE) and high-density polyethylene (HDPE). Polypropylene is normally tough and flexible, especially when copolymerized with ethylene monomer. This allows polypropylene to be used as an engineering plastic, competing with materials such as ABS. Polypropylene is reasonably economical, and can be made translucent when uncoloured but is not as readily made transparent as polystyrene, acrylic, or certain other plastics. It is often opaque or colored using pigments. Polypropylene has good resistance to fatigue. Moreover, the thermal properties of polypropylene are also continually explained. The melting of polypropylene occurs as a range, so a melting point is determined by finding the highest temperature of a differential scanning calorimetry chart. Perfectly isotactic PP has a

melting point of 171 °C (340 °F). Commercial isotactic PP has a melting point that ranges from 160 to 166 °C (320 to 331 °F), depending on atactic material and crystallinity. Syndiotactic PP with a crystallinity of 30% has a melting point of 130 °C (266 °F) [8].

The melt flow rate (MFR) or melt flow index (MFI) is a measure of molecular weight of polypropylene. The measure helps to determine how easily the molten raw material will flow during processing. Polypropylene with higher MFR will fill the plastic mold more easily during the injection or blow-molding production process. As the melt flow increases, however, some physical properties, like impact strength, will decrease.

There are three general types of polypropylene: homopolymer, random copolymer, and block copolymer. The comonomer used is typically ethylene. Ethylene-propylene rubber or EPDM added to polypropylene homopolymer increases its low temperature impact strength. Randomly polymerized ethylene monomer added to polypropylene homopolymer decreases the polymer crystallinity and makes the polymer more transparent.

Polypropylene is liable to chain degradation from exposure to heat and UV radiation such as that present in sunlight. Oxidation usually occurs at the tertiary carbon atom present in every repeat unit. A free radical is formed here, and then reacts further with oxygen, followed by chain scission to yield aldehydes and carboxylic acids. In external applications, it shows up as a network of fine cracks and crazes that become deeper and more severe with time of exposure.

For external applications, UV-absorbing additives must be used. Carbon black also provides some protection from UV attack. The polymer can also be oxidized at high temperatures, a common problem during molding operations. Anti-oxidants are normally added to prevent polymer degradation.

2.2 Introduction to composite material [9]

The definition of a composite is that a composite material contains a chemically and/or physically distinct phase distributed within another continuous phase and exhibits properties that are different from both of these.

Historically, composite materials have been used for centuries in one form or another, for example, straw reinforced mud bricks, paper and concrete. Wood and bone are an example of naturally occurring composites. Artificial composites are based on fibrous materials bound together with resins, one of the earliest synthetic types being glass reinforced polyester.

Composites are especially attractive for their high specific strength (stress/density or σ/ρ) and modulus (stress/stiffness or σ/E) and low density (mass/volume or m/v). This has led to great interest in their research and development in the past few decades, particularly for aero applications where additional payload capacity and engine efficiency are paramount. In more recent times the automotive industry has shown interest in structural (primary load carrying members) composite materials for similar reasons, although the effects of exhaust emissions on the environment has provided the impetus for the lightweight vehicle of the future. Composites also offer numerous advantages over many traditional materials like metals, including low density and enhanced corrosion and temperature capability.

2.2.1 Performance of the reinforcement

Composites may be broadly classified according to the nature of the matrix phase for example, metal matrix composite (MMC), polymer matrix composite (PMC) or ceramic matrix composite (CMC). The scope of this discussion will be limited to those composites that have brittle polymer matrices. Reinforcements may be in the form of single crystal whiskers, platelets, long fibers, short fibers, small particles or precipitates (or a combination of any of these) which are typically supported in a less brittle matrix. Materials in the fibrous form exhibit much greater strengths than in any other form, and furthermore the smaller the diameter of the fiber the greater the strength, see **Figure 2.2**.

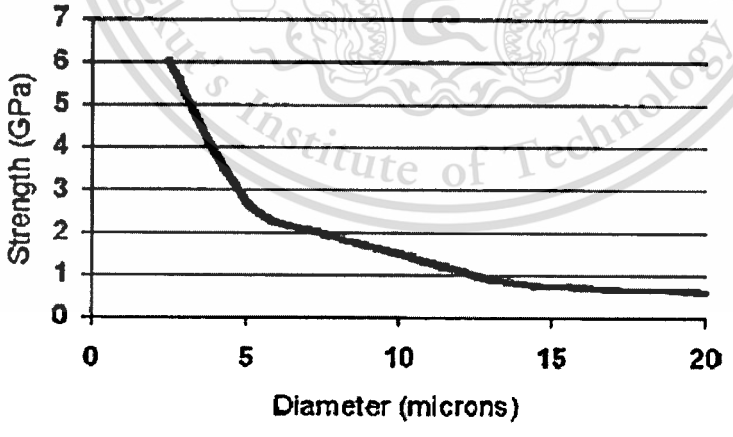

Figure 2.2 Reducing fiber diameter increases tensile strength [10]

This may be explained first by preferred orientation produced during drawing or spinning of fibers and secondly by considering failure as a statistical process induced by flaws. Quite simply, the smaller of the fiber is the less likelihood of its containing a critical flaw. In view

of this fact, it is crucial to composite integrity that the surface of the fiber be protected from damage during fabrication. Hence, a sizing agent of some description is applied, which not only must be compatible with the fiber but also with the matrix material for optimum bonding. In polymer composites this protective coating is the foundation of the fiber/matrix interface which has a very important function. The purpose of the matrix is to allow the fibers to be formed into a useful shape, to transport load to the fibers throughout the composite (via an interface) and to protect them from damage and corrosion. Fibrous reinforcements are available in a variety of diameters but generally fall into the range of 5 to 100 μm. Reinforcements are available in the form of long or short fibers in a variety of architectures including continuous and discontinuous mats and woven roves as well as chopped and continuous strands or laminates. The diameter and length very much dictate the format of reinforcement (and properties). Large diameter fibers, such as silicon carbide or sapphire monofilaments are formed into shape by filament winding for example, where the bend radius on the fiber is shallow. Small diameter fibers such as glass can easily be formed directly into complex mold as mats or roves or if discontinuous may be injected into the cavity. Fibers will generally classify into four categories; glass, ceramic, metal or polymer, as do matrices. The processing route of the composite is usually dictated by the matrix material. Production of polymer composites invariably involves low temperature/low pressure compression and injection of resin into a cavity whereas metal and ceramic matrix composites require high pressure and/or temperature sintering or melting operations.

2.2.2 Categories of Composites

Composite materials are not new or even a human invention, most natural biological materials are composites. Examples include bone, horn, insect shells, plants, teeth and wood. The microscopic structure of these biomaterials are generally very complex and relatively little is still known about them. The mechanical properties of these materials are compared with artificial composites. In some cases the strength to weight ratio of natural composites is better than for some artificial composites. The categories of composites can be classified into five types.

2.2.2.1 Natural Composites

Most of the structural elements found in nature are composites. Examples are wood, horn, and the shells of crustacea. Animal composites have reinforcements made from polysaccharides or calcium salts, matrix materials are often proteins, e.g., collagen, elastin and keratin in bones and teeth or complex phenolic compounds in hard insect shells. Bone has brittle high modulus apatite crystals as reinforcement, bound together with ductile, organic collagen fibres. The bones of birds attain the stiffness required to support the muscle loads required for flight without weighing too much, by means of a honeycomb cored structure. In the plant world cellulose and lignin predominate. Bamboo has a cellulose matrix, with silica reinforcement giving high rigidity and high impact strength; properties exploited in the early days of aircraft manufacture and to date by the makers of kites, and as scaffolding. The microscopic structure of these materials is always complex, and when compared to artificial equivalents the mechanical performance is excellent.

2.2.2.2 Biocomposites

Biocomposites include natural structural materials such as wood, but can also include artificial composites made with synthetic resins and reinforcing fibres such as jute, banana fibre, coconut fibre, and bamboo fibre. Rice husks can be used as the basis for the manufacture of silicon carbide whiskers, and research is being conducted in the use of spider silk as a fibrous reinforcement. The strength of spider silk is in a similar range to that of aramid, e.g., DuPont Kevlar, fibres. Biocompatible bone substitutes (Hapex; Smith & Nephew) are made by producing a polyethylene-hydroxy-apatite composite. This material has similar mechanical properties to bone, and is sufficiently near to bone in a biological sense for the surrounding bone to grow into the artificial material. Applications include long life artificial hip joint mountings and artificial inner ear bones which can restore hearing to the profoundly deaf. Biocomposites are attractive because of the low environmental impact of their product life cycle, they can be locally produced, and they do not add to the net level of carbon dioxide in the atmosphere.

2.2.2.3 Carbon-Carbon Composites

Carbon-carbon composites are made from carbon fibres embedded in a carbon or graphite matrix. Graphite does not melt, it sublimes, passing directly from the solid phase into the gaseous. This physical change occurs at about 3500 °C. Carbon-carbon composites have a density of one-quarter that of steel, a high specific heat capacity and thermal stability in a non-oxidising atmosphere up to 2500 °C (mechanical properties tending to fall off after this point). In an oxidising atmosphere, the material burns to produce extraordinarily expensive carbon dioxide. The matrix is insinuated into the reinforcing material either as a liquid or by deposition of a chemical vapour. The material is densified in a controlled atmosphere at high temperature to produce the composite material. Due to the wide range of reinforcement configurations and processing techniques, the range of properties available in carbon-carbon composites is very large.

2.2.2.4 Ceramic Matrix Composites (CMC)

Ceramic matrix composites are reinforced for fundamentally different reasons to those for polymer and metal matrices. Whereas polymers and metallics are reinforced for increased strength and modulus, ceramics are reinforced to increase their toughness and damage tolerance. Consider the strength of bone china: the Wedgewood company used to demonstrate the compressive strength of its bone china tea cups by balancing a London Transport Routemaster bus (weighing approximately 11,000 kg) on six tea cups (**Figure 2.3**).

Figure 2.3 The compressive strength of ceramics (Source: Josiah Wedgewood and Sons, Ltd.)

However, the reader will be familiar with the effect of rapid sequential compressive and tensile loadings on ceramics (as for example by dropping a teacup onto a hard surface). So, ceramic materials suffer in structural applications not from intrinsic weakness, but from their low flaw tolerance and brittle nature, otherwise ceramics are ideally suited for work in high temperature and chemically aggressive environments. The properties can be improved by the addition of reinforcements; typical reinforcements used are either continuous fibres or discontinuous reinforcements of fibres, whiskers or particulates.

2.2.2.5 Metal Matrix Composites (MMC)

MMC are produced by the addition of reinforcing particles to molten metal (often aluminium), by the infiltration of molten metal into a particulate or fibrous preform (usually silicon carbide), or heating a mixture of reinforcement and powdered metals. MMC outperform metals in terms of wear resistance, better elevated-temperature properties and creep resistance. They also have low coefficients of thermal expansivity. They suffer from high costs, complex fabrication methods, and limited service experience. The desired properties for this application are good thermal conductivity, and wear resistance coupled with lightweight.

2.2.3 Properties of natural fiber reinforced composite material

2.2.3.1 Stiffness of short fiber composites

In composites containing discontinuous reinforcements, stresses are transferred from the matrix to the fibers by shear forces at the fiber/matrix interface. The fibers may still carry a high proportion of the load on the composite, but there is a section at both ends of each fiber where the fiber tensile stress is still building up to it is maximum value and in which region it is reinforcing efficiency is diminished. In general this leads to short fiber composites being less stiff than continuous fiber composites. For most practical composites, the stiffness of the short fiber composites is equal to that of a continuous fiber composite if the fibers are of the order of only 1 mm long (**Figure 2.4**).

It should be noted that in most practical short fiber composites, such as injection molded reinforced thermoplastics or dough molding compounds the fibers will usually not be random but be slightly aligned by the fabrication process. This should be taken into account during detailed design of components.

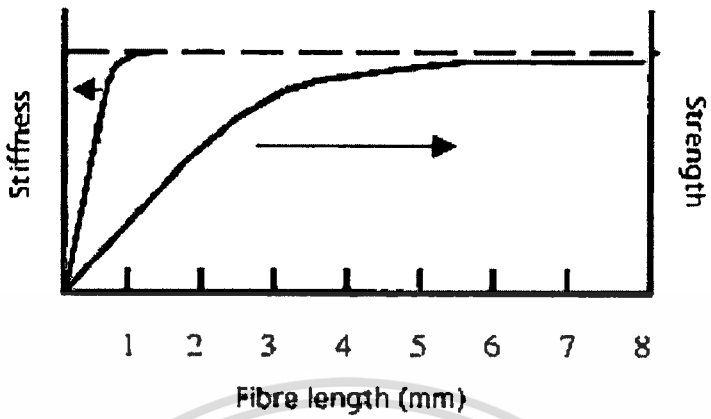

Figure 2.4 Fiber length effects

2.2.3.2 Strength of discontinuous fiber composites

As highlighted in section stiffness of short fiber composites, discontinuous fiber composites are loaded, through or across the fiber matrix interface via shear forces, leading to an ineffective length of individual fibers at each end. Not only does this lead to a decrease in stiffness of the composites (when compared to continuous fiber composites) but also suffer a reduction in strength. As a guide, approximately 95% of the continuous fiber composite strength can be achieved in a short fiber composite with fibers only 8 mm-10 mm long (**Figure 2.4**).

One of the limiting factors on strength of short fiber composites is the fiber/matrix interface strength. The higher the interfacial shear strength the more rapid the buildup of stress at the end of fibers therefore a stiff/strong composite requires stiff/strong interfaces. Though as indicated previously stiffness and strength do not increase with fibers above 8 mm long, the impact properties of a material are improved through using longer fibers. It is generally accepted that a fiber length of approximately 20 mm is required in order to gain the impact properties of a continuous fiber composite (this should be regarded as a rule of thumb – the exact length depend on many things such as geometry of the specimen, fiber/matrix interface strength,etc.

2.2.3.3 Energy absorption and toughness

In section strength of discontinuous fiber composites on short fiber composites, it was noted that the strength of the composites can be improved with a stronger/stiffer interface. It is not always desirable for the fiber and matrix to be strongly bonded and some reasons for this will be discussed. Fiber debonding and pull out is one of the important energy absorbing mechanisms during composite fracture. **Figure 2.5** illustrates a uni-directional (UD) composite which has undergone multiple fiber fracture and debonding in and around a matrix crack. Note that the matrix has failed in a brittle manner without yielding. It can also be seen that the fibers have pulled out of their 'sockets'. This mechanism increases the fracture toughness by dissipating energy. If the fiber/matrix interface is too strong, then it is possible that the composite would crack in a single fracture rather than the crack being diverted by the fibers. This single failure mechanism would reduce the toughness of the composite significantly. Other mechanisms operate in composites based on ductile matrices (such as thermoplastic polymers and metals) to dissipate energy. In most instances polymer matrix composites fail by delamination/debonding, an inherently tough mechanism.

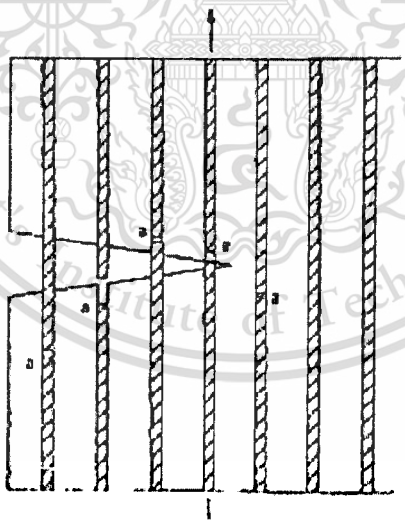

Figure 2.5 Multiple fracture and fiber pull out in a uni-directional composite

2.2.3.4 Voids

Several types of voids may be present in composite materials. These can occur in all forms of composite, although there are variations in their incidence depending on fabrication route and matrix type. Large cavities can form during the manufacture of the

component as a result of gross defects. Small voids often form adjacent to the fibers, either because of incomplete infiltration during processing or cavitation during deformation. Voids also form in matrix-rich pockets or fiber-free regions between laminae.

2.3 Influence of MA-g-PP on abrasive wear behavior of chopped sisal fiber reinforced polypropylene composites [11]

The sisal fiber reinforce polypropylene composites with and without maleic anhydride grafted polypropylene (MA-g-PP) was developed by U.K. Dwivediand and N. Chand [11]. Different amounts of MA-g-PP, 1, 2 and 5-wt% were added to modify the composites. Abrasive wear and mechanical properties of sisal fiber reinforced polypropylene composites were determined. When increasing percentage of maleic anhydride grafted polypropylene, the tensile strength is increased. The improvement in the tensile strength is attributed to the increased adhesion between sisal fiber and PP that facilitates more stress transfer through bonding to the sisal fiber. The adhesion is due to the presence of MA-g-PP, which reacted with the hydroxyl group present in the sisal fiber surface. In another words, the addition of MA-g-PP increased the resistance to pullout the fiber from PP matrix. Percentage elongation of unmodified sisal fiber reinforced PP composite is highest as compared to other sisal fiber reinforced PP composites. Addition of MA-g-PP has reduced the elongation of the composite. Elongation of composites decreased with the increase of MA-g-PP contents. This decrease in elongation is due to the combined effect of (i) improvement in adhesion between fiber and matrix, and (ii) modification of matrix. **Figure 2.6**(a) shows the tensile fractured surface of unmodified sisal fiber reinforced PP composite. It can be seen that sisal fibers debonded easily and pulled out from matrix, which indicates poor bonding at inter face between sisal fibers and PP. Holes are created in the PP matrix as the fiber pullout and visible **in Figure 2.6**(a). Tensile fracture occurred in PP by the pulling of chains and the formation of voids in the bulk polymer material. Some fibers have fractured and broken after pullout. The easy pullout of fibers shows poor adhesion between sisal fibers and PP matrix. **Figure 2.6(b)** clearly shows the poor bonding at the fiber-matrix interface. **Figure 2.6(c)** exhibits the photograph of sisal fiber reinforced PP composite having 1-wt% MA-g-PP, which reflects the improved fiber-matrix interaction at interface. For more clarity at the interface, a micrograph (**Figure 2.6(d)**) of higher magnification of sisal fiber reinforced PP composite having 1-wt% MA-g-PP is incorporated to exhibit the improved fiber-matrix interaction.

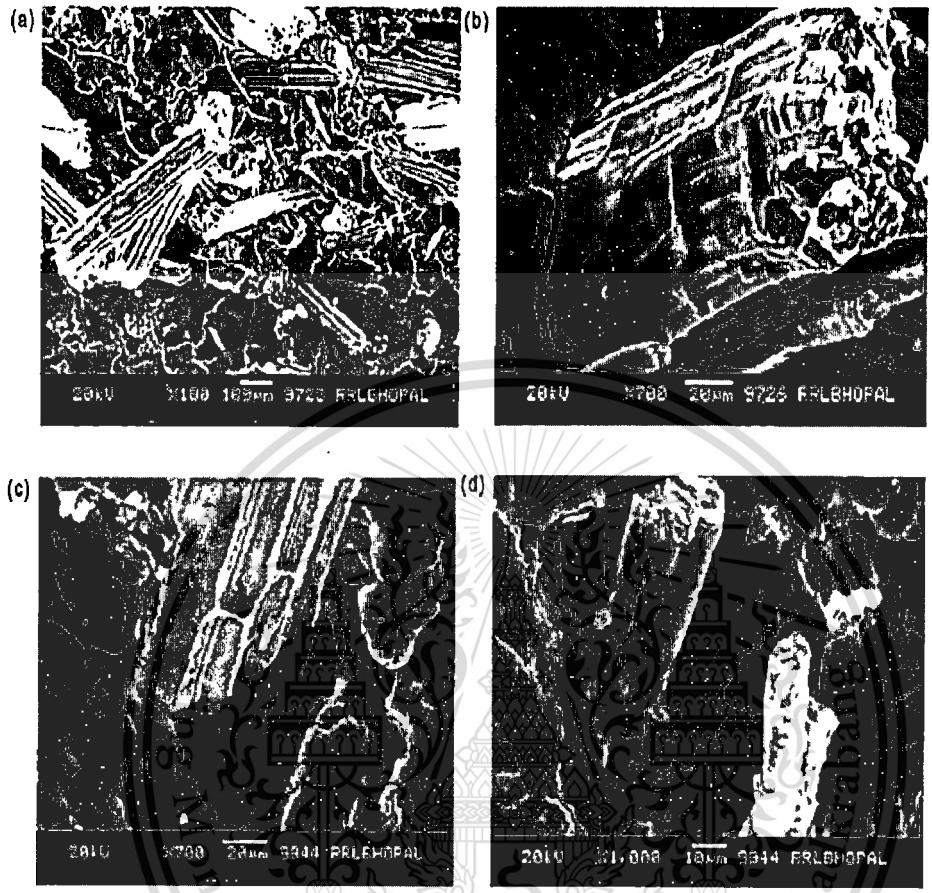

Figure 2.6 (a) shows SEM of tensile fractured surface of unmodified sisal fiber reinforced PP composite. (b) Shows magnified SEM of tensile fractured surface of unmodified sisal fiber reinforced PP composites. (c) SEM of tensile fractured surface of 1-wt% MA-g-PP modified sisal fiber reinforced PP composites. (d) Another SEM shows improved fiber–matrix interaction at interface with more clarity of 1-wt% MA-g-PP modified composite.

2.4 Injection Molding[12]

The injection molding process can be separated in three stages

2.4.1 Plastication

Plastication is the action of mixing and melting the feedstock. The polymer flow rate is governed by the material process conditions of the plastication stage and is a combination of material rheology, barrel temperature, shear, back pressure and screw speed. The basic aim is to produce a homogeneous and formable melt for the next stage where the material enters the mold.

2.4.2 Filling

The parameters of mold filling are of great importance to the quality of the finished article especially when considering factors such as warpage (orientation effects) and surface finish (skin formation). Filling dynamics are the major factor in affecting the levels of residual stress [13]. It is important that injection speeds are reproducible as slight changes can cause variations in the product. Injection speeds that are too high can cause jetting and degradation and thus affect mechanical properties [14]. A low speed may cause an increase in injection pressure requirements due to a thicker frozen layer because the molten material cools at the lower speed. The higher pressures are required to force polymer melt. This can produce incomplete filling of the mold often referred to as short shots.

2.4.3 Packing and cooling

The packing stage's purpose is to add extra material to compensate for the shrinkage caused by the increasing density of the solidifying polymer. If the additional polymer were not injected the component would shrink and warp due to non uniform cooling. Ideally the packing and cooling stages should be such that the final dimension is maintained as close as possible to design tolerances. Variables during this stage are packing pressure, packing time and the mold temperature. Bad mold design can lead to inconsistent cooling along the dimensions of the mold surface which can cause increased residual stresses which lower the mechanical properties of the part as well as causing warpage [15].

2.5 Co-injection molding process

In the co-injection molding process (sandwich injection molding process), two polymer melts are sequentially inject into the mold cavity through the same gate to form skin-core structure. First and second polymer melts are injected to make skin and core, respectively. Two thermoplastics are laminated together and take advantage of different properties during the molding phase.

2.5.1 Techniques for Co-injection Moulding Process[16]

In this section, the different techniques for sandwich injection molding process are classified using the number of melt channels in the nozzle. These are presented as follows.

2.5.1.1 One-channel nozzle

2.5.1.1.1 Single channel technique

The single channel method was patented by ICI in 1970[17] and is schematically shown in **Figure 2.7**. An injection molding machine with two cylinders was used. The polymer melts were injected sequentially into a cold mold through an adjustable valve. The melt injected first forms the skin and surrounds the core, which was injected afterwards. The formation of a skin-core structure could be explained from the mold filling process. The polymer injected first would cool and solidify at the surface as it came into contact with the cold mold wall, while a flowing region of molten polymer still existed at the centre of the flow channel. When the second polymer melt was injected it forced the first forward as the flow front and this would solidify at the surface as it progressed. This continued until the mold was filled and a sandwich part had been formed. The thickness of the skin could be varied by changing injection molding parameters, such as injection velocity, melt temperature, mold temperature, and melt viscosities. A disadvantage with the method is when switching from injection of skin melt to injection of core melt, the mold cavity pressure drops, and the melt front comes to a temporary standstill.

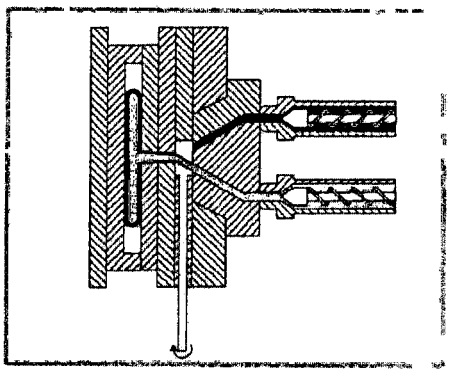

Figure 2.7 Single channel technique(ICI)

2.5.1.1.2 Mono-sandwich technique

The mono-sandwich technique, developed by Ferromatik Milakron [18], used two polymer melts were layered in one injection cylinder, as shown schematically in **Figure 2.8**. This was achieved by melting the skin material in a separate side extruder and leading it through a special hot runner to the front of the screw in the main cylinder. The melt pressure pushed the screw backwards. When a sufficient amount of melted material had accumulated in front of the screw, the screw starts rotating and feeds the core material. The injection was then done in the same way as for normal injection molding by pushing the screw forward. The maximum amount of core material that could be obtained depended on the mold geometry. A standard molding machine could be rebuilt to a sandwich machine simply by connecting a side extruder to the main injection unit. In addition, very thin-walled parts could be produced by this method.

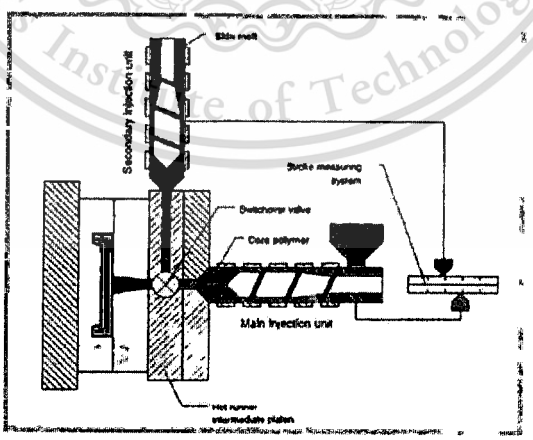

Figure2.8 Mono-sandwich technique (Ferromatic Milakron)[18]

A further advantage was said to be the simplified exchange of materials in the cylinders due to the relatively simple construction. The process control was simple since injection was made in the same way as for normal injection molding. One major disadvantage was the lack of detailed control of the injection process. This made molding of parts having complicated shapes more difficult.

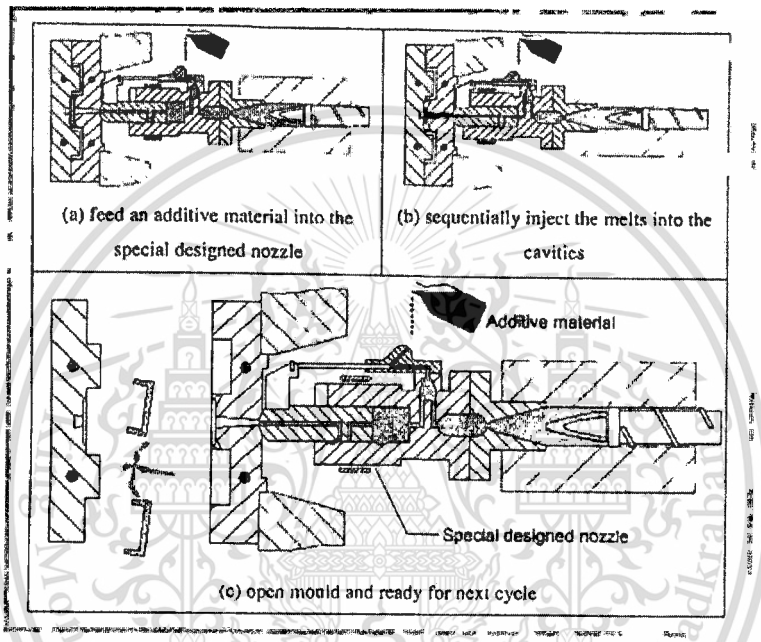

Figure2.9 The Addmix mono-sandwich injection technique[19]

However, there was a modified version of mono-sandwich injection technique, originated by Addmix [19]. In **Figure2.9,** it was a similar technique to the Ferromatik one but without an ancillary extruder. Sufficient amount of materials were regulated from the separate hopper, which was controlled by a stroke measurement system; the polymers were layered and fed into one injection cylinder. The sandwich components were then molded as mentioned previously.

2.5.1.2 Two-channel nozzle

2.5.1.2.1 Dual channel technique

The dual channel method, developed by Battenfeld in the mid 1970s, included a phase of simultaneous injection. Two injection units were united through a specially designed nozzle as seen in **Figure 2.10**. The nozzle was equipped with two separate, concentric channels that could be independently operated, opened, and closed with hydraulics. The duration of the simultaneous injection phase depended on the material and especially on the mold geometry. Typically the duration was 5-25% of the injection time for the skin component. Separate operation of two injection units made it easier to control skin thickness in various parts of a molding. An optimum distribution of core material was obtained if the skin viscosity was kept slightly lower than that of the core. If the same material was used in skin and core, it was recommended to use a 20-30°C higher temperature for the skin.

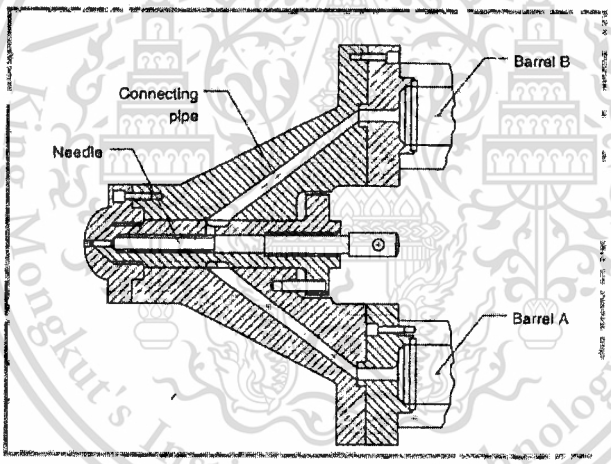

Figure 2.10 Two-channel nozzle technique (Battenfeld)

An advantage with the two-channel technique was the increased flexibility, such as the possibility to separately control the velocity profile of both skin and core during mold filling. Therefore the skin thickness could be adjusted in various parts of a molding. Further amounts of skin material could be injected during holding time to seal the gate area with extra skin material and prepare for the next cycle.

2.5.1.3 Three-channel nozzle

A main disadvantage of those techniques described above was that, firstly, the skin thickness close to the gate area might become very thin, because frictional heat from the flowing melts could make the skin re-melt and be flushed away in this region. Secondly, as expected, in the case of incompatible skin and core materials, the adhesion between both interfacial layers were poor. Thus, compatibilisers were needed.

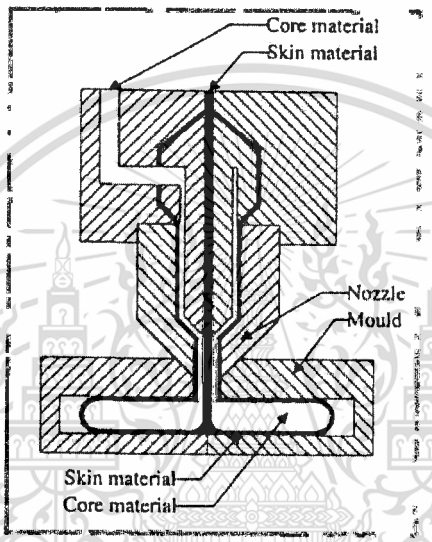

Figure 2.11 Three-channel nozzle technique (Kortex)[20]

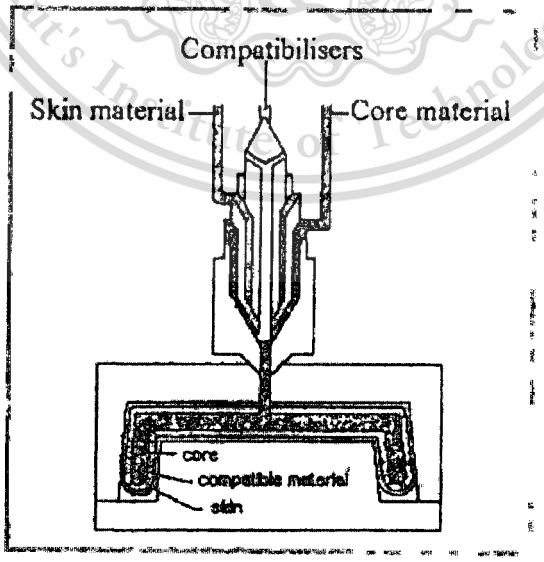

Figure 2.12 Three-channel nozzle technique (Billion)[21]

Therefore the three-channel technique was developed, as depicted in **Figure 2.11** and **2.12**. As seen in **Figure 2.11**, it was based on a three-channel nozzle with an auxiliary channel for the skin in the centre of the gate, which could reach the opposite side of the molding. The injection of skin material to the two surfaces could be regulated possibility was the solution to polymer incompatibility for sandwich injection molding by using the third intermediate layer polymer as a binder adhesive; this process was proposed by the Billion Corporation of France. There were obvious machine-cost disadvantages because the runner system was complex and there must be a third injection unit.

Moreover, Battenfeld had invented the new three-channel co-injection molding machine using the nozzle scheme as shown in **Figure 2.13**.

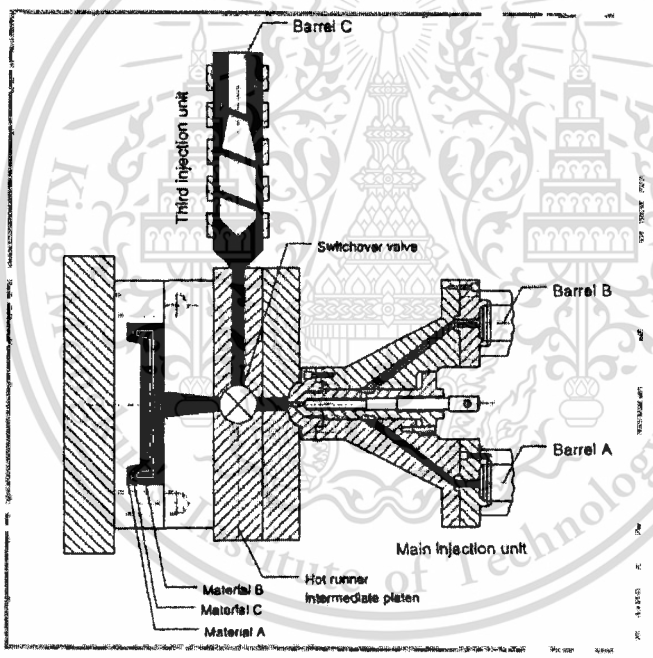

Figure2.13 Three-channel nozzle technique (Battenfeld)[22]

2.6 Process Technology for Co-injection Molding Process [16]

The various techniques for co-injection molding process were investigated. However, those could be divided into two main groups: sequential and simultaneous technique.

2.6.1 Sequential Co-injection Molding Process

It is common knowledge that one-channel nozzle co-injection or sandwich injection molding machines has two cylinders in use. The melts are injected sequentially into the mold through the adjustable designed valve. The first injected melt forms the skin and conceals the core material which is injected afterwards.

2.6.2 Simultaneous Co-injection Moulding Process

The limitations of the sequential co-injection molding process are eliminated by application of the simultaneous phase, which can be produced by injecting skin overlap core materials. The filling of the mold with the two melts is commenced with injection of skin melt material, then core melt is admitted afterwards. Then both melts are injected simultaneously. The duration of simultaneous phase is usually about 5 to 25% of the metering stroke of skin material, dependent on the selected material and the geometry of the molding. When the cavity is nearly filled, the core nozzle switches to shut off the core melt. A small amount of skin melt is then injected into the mold until end of injection stroke to ensure that the core melt is removed and does not contaminate the next cycle.

.

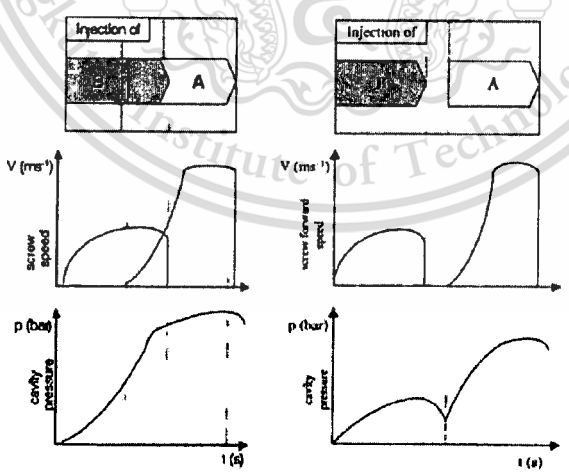

Figure 2.14 Comparison of mold filling of simultaneous (left) and sequential (right) injection molding (Battenfeld operating manual for co- injection molding machine BMT-1100)

Form **Figure 2.14**, these figures show the pressure profiles and screw velocity of the simultaneous and single channel methods. In the sequential method, the period of stagnation after injection of A before injection of B can be clearly seen, resulting in a drop of cavity pressure and a period where there is no movement of material in the screw. These problems from sequential method were solved by using the simultaneous method because it has continued pressure and velocity profiles.

2.7 The Co-injection molding process with Fibres[23]

A sandwich construction consisting of a structurally enhanced and modified fibrous substrate, (i.e., PP, material A) covered by a skin suitable for painting, (i.e., Nylon (PA), material B). This overcomes the conflict of mechanical performance versus cosmetic finish mentioned previously. The relative amounts of skin and the substrate can be varied to different produce different skin-core ratios giving optimum skin thickness or overlap sealing edges. Materials can either be injected simultaneously or sequentially; sequential injection is shown in **Figure 2.15**.

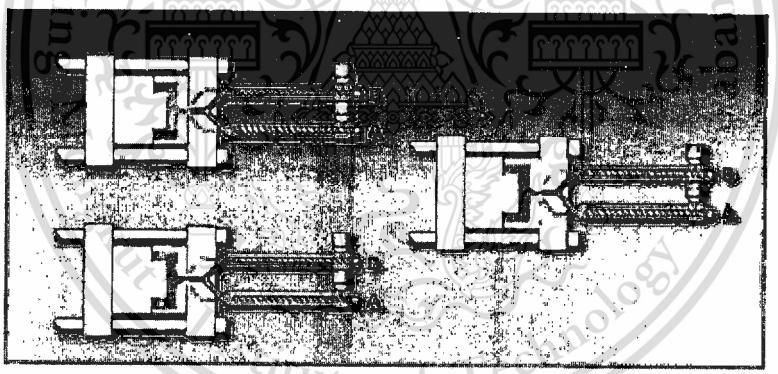

Figure 2.15 Schematic diagram of dual injection (Source: Battenfeld)

The co-injection molding process with fibrous and modified cores and incompatible skins with compatibilisers all have to go through the same fundamental injection molding cycle: these are as follows.

Stage 1 The mold is closed hydraulically, both injection units are charged with polymer, and screws are retracted. The valve is shut.

Stage 2 The valve is opened to the first injection unit, which injects a partial charge of skin (non-flammable) material into the mold.

Stage 3 Next the valve is opened to the second injection unit, which injects core material into the mold, forcing the skin polymer outwards. The mechanism is analogous to blowing up a balloon. So with two polymer charges, provided the conditions of polymer temperature, mold temperature, injection rate and other variables are controlled, the core polymer forces the skin to the edges of the mold (Stage3) laying down a uniform layer as it goes without bursting through.

Stage 4 The full injection pressure of the second injection unit is applied to pack the mold and ensure a good surface finish.

Stage 5 The valve is again opened to the first injection unit and a sufficient amount of skin polymer is injected into the mold cavity to clear the sprue of core polymer. If the small additional charge were not injected, foam structure would be revealed on cutting the sprue from the molding, and residual core polymer in the valve channel would appear in the skin of the next molding, causing a poor surface finish on a subsequent molding part.

Stage 6 In the final stage, the valve unit is closed and full clamp pressure is held for a few seconds. The core polymer cools to give a uniform cellular structure encapsulated with in a thin skin of polymer.

2.8 The influence of Molding Conditions on the dual injection process

It is necessary to understand the influential conditions, such as, injection speeds, melt temperatures, tool temperatures, length of simultaneous phases and compatibiliser on skin and core thickness formation. Injection speed is one of the most effective factors in controlling the process. The effect is quite similar to that of melt temperature. Skin-core melt temperatures play an important role in fibrous skin formations and core penetration. In the case of increasing of skin melt temperature, lower skin viscosities ensures that the skin material flows more easily than the core, lower melt temperatures lead to a higher skin thickness and core breakthrough.

2.9 Examples of 2K moldings

The following components with electrostatic surfaces by incorporating short and long glass/ carbon fibres as well as incorporating compatibilisers into the core material for adhesion are shown as example of this process. **Figure 2.16** shows a Wheel trim (sectioned to show the skin-core structure). **Figure 2.17** and **Figure 2.18** shows the fender mouldings (made by Magna (Exteriors) UK before and after painting on a standard production line.

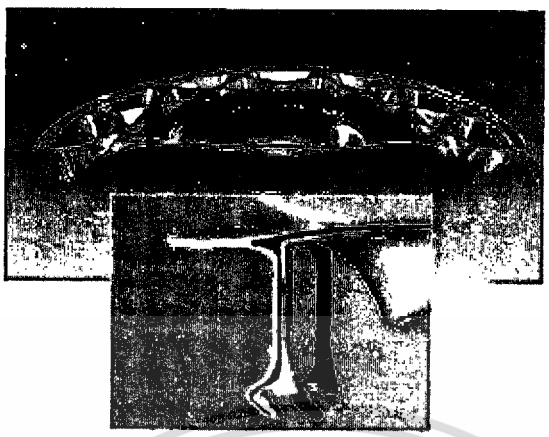

Figure2.16 Wheel trim molding

Figure2.17 The Magna Fender-before in-line painting

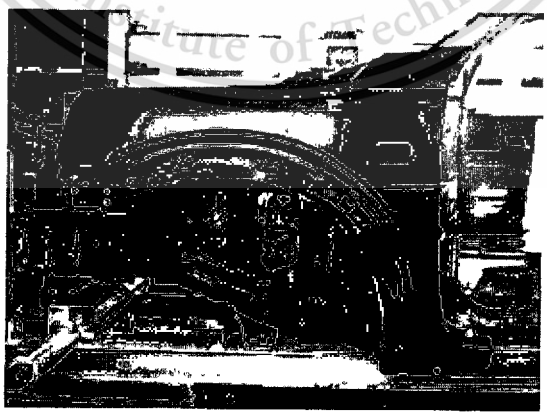

Figure2.18 The Magna Fender-after in-line painting

2.10 Classification of Fluid Behavior

Imagine a fluid, at fixed temperature, placed between two plates that are a small distance apart. Suppose the bottom plate is stationary and the top plate moves with a constant speed (V_x) in the x-direction due to application of a force F as illustrated in **Figure 2.19.** This flow is called steady simple shear flow. The shear stress (τ) acting on the top plate.

$$\tau = \frac{F}{A} \tag{2.1}$$

Figure 2.19 Steady simple shear flow

Where A is the area of the plate. The dimension of shear stress is force per unit area. It has been determined empirically that the shear stress is proportional to the velocity gradient of the fluid, dV_x/dz. That is,

$$\tau_{zx} = \mu \frac{dV_x}{dz} \tag{2.2}$$

The velocity gradient dV_x/dz is called the shear rate and is denoted by $\dot{\gamma}$. It has units of reciprocal seconds. The shear rate is a measure of how fast the layers slide over each other. Therefore,

$$\tau_{zx} = \mu \dot{\gamma} \tag{2.3}$$

The constant of proportionality μ, is called the viscosity of the fluid, η. It relates the shear stress to the rate of deformation of the fluid. From Equation (2.3), this fluid is known as Newtonian type, the viscosity is a property of the fluid and is not altered or changed by the shear rate, $\dot{\gamma}$. For Newtonian fluid, only temperature and pressure has an effect on viscosity.

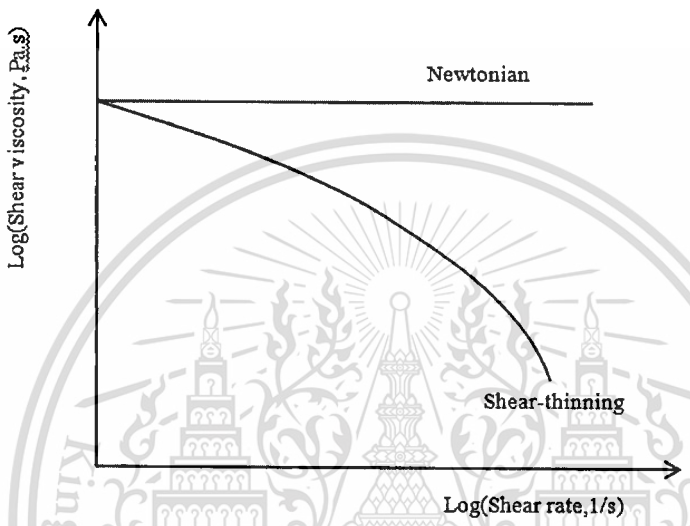

Figure 2.20 Relationship between shear viscosity against shear rate of Newtonian and non-Newtonian fluid (shear thinning)

In polymer melt systems, there is an another fluid system, which is called non- Newtonian. As can be seen in above figure (**Figure 2.20**), the apparent viscosity, η_{app} for a Newtonian fluid is a constant whereas non-Newtonian fluid show a decreasing apparent viscosity with increasing shear rate, sometimes called shear-thinning fluid. Shear-thinning fluid is also called pseudoplastic. Modification of Equation (2.3) is made to allow the viscosity to be a function of shear rate.

Therefore, Equation (2.3) becomes

$$\eta = \eta_0 \dot{\gamma}^{n-1} \tag{2.4}$$

This model is called Power law model.

Where η_0 is the zero-shear viscosity and n is a constant, lie between 0 and 1.

2.11 Viscosity Models for Flow Analysis

Some plots of viscosity against shear rate at the different temperatures are shown in **Figure 2.21**. The curves are typical for materials commonly used in injection molding. The aim of the viscosity model is to match the observed behavior of the material as closely as possible.

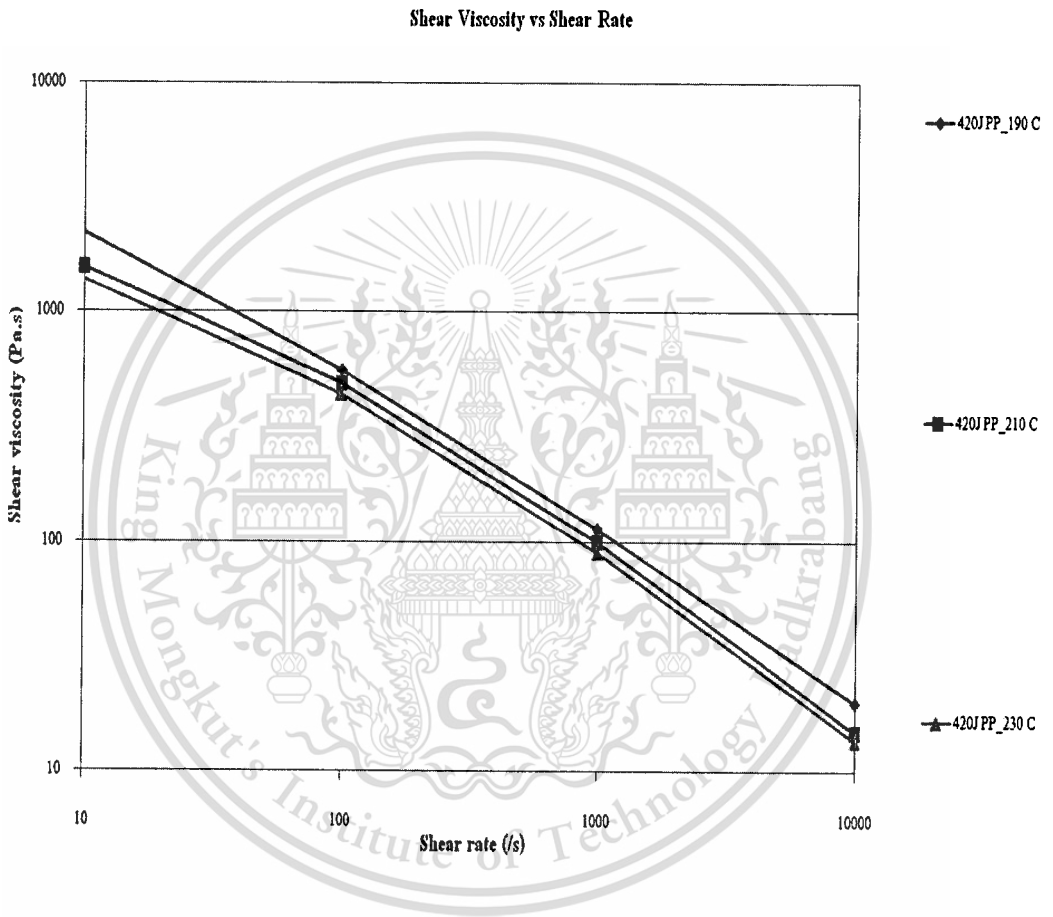

Figure 2.21 Plot of viscosity against shear rate at the various temperatures

2.11.1 Power Law Model

This model has the form:

$$\eta = \eta_0 \dot{\gamma}^{n-1} \tag{2.5}$$

Where η_0 is the zero-shear viscosity and n is a constant, lie between 0 and 1.

Plot of viscosity against shear rate shows power law region on pseudoplastic as show in **Figure 2.2.**

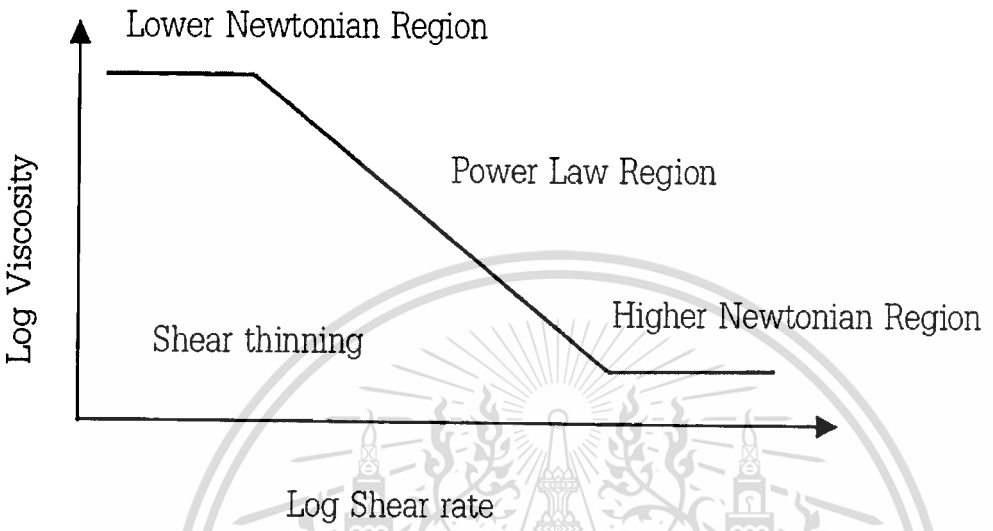

Figure 2.22 The relative of power law region on pseudoplastic [32]

2.11.2 Cross-Exp Model (C-MOLD Filling Stage Model)

To incorporate the dependence of melt viscosity on shear rate, temperature, and pressure, the following 5-constants (n, r*, B, Tb, P), together with the cross-exp model is adequate for simulating the filling stage in injection molding.

$$\eta(T,\dot{\gamma},p)=\frac{\eta_0(T,p)}{1+\left(\frac{\eta_0\dot{\gamma}}{\tau^*}\right)^{1-n}} \tag{2.6}$$

With

$$\eta_0(T,p)=B.\exp\left(\frac{T_b}{T}\right).\exp(\beta p) \tag{2.7}$$

Where n is power law index

τ^* is shear stress of resin at which shear-thinning behavior begins to manifest itself.

T_b is Temperature-sensitivity factor.

B is resin-dependent constant.

β characterises the pressure dependence of η_0.

η_0 is zero-shear viscosity.

2.12 Molecular weight from Zero-Shear viscosity

The viscosity of a polymer is very strongly affected by molecular weight, particularly at low shear rates. The zero-shear viscosity increases with the 3.4 power of the molecular weight.

$$\eta_0 = KM^{3.4} \tag{2.8}$$

Where the constant K depends on the material.

2.13 Flow of The Molten Polymers In Co-injection Molding Process

Fountain flow is basic characteristic of injection molding. It is occurred when the polymer at the melt front moves from the centre line of the stream to the cavity walls. The melt that contact the cold mold wall is frozen because the wall temperature is lower than the melt temperatures. The Fountain flow schematic diagram is shown in **Figure 2.23**.

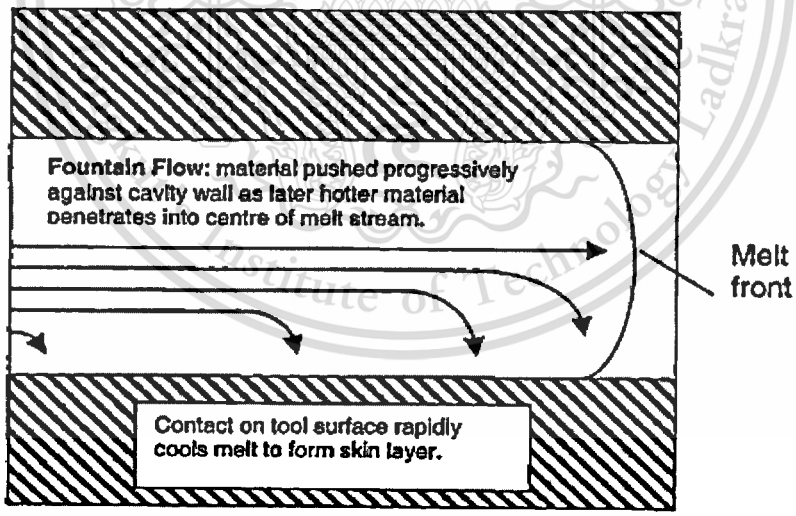

(a)

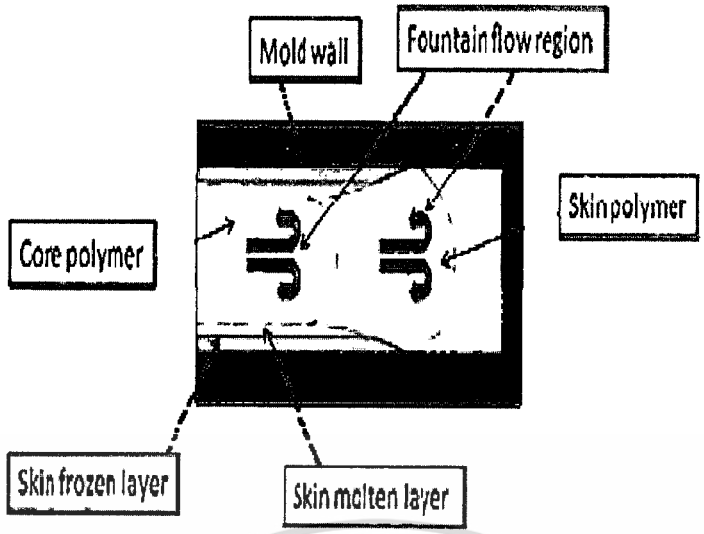

(b)

Figure 2.23 (a) Schematic of fountain Flow, (b) Fountain flow behavior of skin-core structure in the mold

2.14 Material Selection [24]

The selection of raw materials for using as skin and core depends on the properties required of the final molded part. Care has to be taken that the selected materials adhere with each other. Nevertheless, there are several criteria for process molding from which good adhesion skin-core components, can be acquired. Therefore, for good adhesion, the materials should:

- Have approximately the same shrinkage and thermal expansion. A large difference in mold shrinkage and thermal expansion can give sink marks, warpage, and residual stresses.
- Adhesion between the raw materials must be good. This is particularly important when the component is exposed to mechanical load. If adhesion is poor, the core material could easily detach from the skin.
- Each polymer must have the same range of processing temperature.
- Exhibit same degree of bonding at the interface. A good bonding strength is obtained if a certain amount of interdiffusion occurs between the melts. It can be achieved when there is high compatibility or solubility between the melts.

Table 2.1 Compatible and incompatible material combinations

This table shows compatible and incompatible material combinations are available.

	ABS	ASA	EVA	PA6	PA66	PBT	PC	PE-HD	PE-LD	PET	PMMA	POM	PP	PPO.mod.	PS-GP	PS-HI	PVAC	PVC-W	SAN	TPU
ABS	+	+	+			+	+	-	-	+	+	-	-	-	*	*		+	+	+
ASA	+	+	+			+	+	-	-	+	+	-	-	-	*	-		+	+	+
EVA	+	+	+					+	+				+		+	+			+	
PA6				+	+	*	*	*	*			-	*	-	-	-			+	+
PA66				+	+	*	*	*	*			-	-	-	-	-			+	+
PBT	+	+		*	*	+	+	-	-	+	-	-	-	-	-	-		+	+	+
PC	+	+		*	*	+	+	-	-	+		-	-	-	-	-			+	+
PE-HD	-	-	+	*	*	-	-	+	+	-	*	*	-	-	-	-		-	-	-
PE-LD	-	-	+	*	*	-	-	+	+	-	*	*	+	-	*	-		-	-	-
PET	+	+				+	+	-	-	+	-	-		-	-	-				+
PMMA	+	+				-		*	*	-	+		*	-	-	-		+	+	
POM	-	-	-	-	-	-	-	*	*	-		+	-	-	-	-			-	
PP	-	-	+	*	-	-	-	-	+		*	-	+	-	-	-		-	-	-
PPO.mod.	-	-		-	-	-	-	-	-	-	-	-	-	+	+	+		-	*	-
PS-GP	*	*	+	-	-	-	-	-	*	-	-	-	-	+	+	+		-	-	-
PS-HI	*	-	+	-	-	-	-	-	-	-	-	-	-	+	+	+		-	-	-
PVAC																	+			
PVC-W	+	+				+		-	-		+		-	-	-	-		+	+	+
SAN	+	+	+	+	+	+	+	-	-		+	-	-	*	-	-		+	+	+
TPU	+	+		+	+	+	+	-	-	+			-	-	-	-		+	+	+

(-):No adhesion, (*):Poor adhesion, (+):Good adhesion

2.15 The mechanism of adhesion [31]

The interaction, adhesion, between two different materials across an interface may involve either physical or chemical bonding. Chemical bonding consists of direct interlinking between molecules of the two materials, the adhesive and the substrate, by covalent or ionic bonds. Physical bonding may result from mechanical interlocking, or from the forces of physical absorption between adhesive molecules and substrate molecules, or by the penetration of adhesive molecules into the substrate by diffusion. Thus, the mechanism of adhesive action is quite different for various types of adhesives and substrates.

2.15.1 Interdiffusion

Figure 2.25(a) shows the diffusion of free chain ends at the interface between two polymers, which leads to chain entanglements and a rise in the adhesive strength. This effect is employed in some coupling agents used on fibers in thermoplastic matrices. Interdiffusion can also take place in non-polymeric systems, particularly if it is accompanied by a chemical reaction. The adhesive strength is dependent on the nature of the resultant interatomic bonds.

2.15.2 Chemical reaction

Various types of chemical reaction may occur at the interface, either deliberately promoted or inadvertent. These can be represented, as in **Figure 2.25(b)**, by new A-B bonds being formed as a result of interfacial chemical reactions. These bonds may be covalent, ionic, metallic, etc., and in many cases are very strong. There are many examples of the interfacial bond strength being raised by localized chemical reactions, but it is often observed that a progressive reaction occurs which results in the formation of a brittle reaction product.

2.15.3 Electrostatic attraction

If the surfaces carry net electrical charges of opposite sign, as illustrated in **Figure 2.25(d)**, then a sustained adhesive force may result. This effect is utilized in certain fiber treatments, as in the deposition of coupling agents on glass fibers. The surface may exhibit anionic or cationic properties, depending on the oxide in the glass and the pH of the aqueous solution used to apply the coupling agents. Thus, if ionic functional silanes are used, it is expected that the cationic functional groups will be attracted to an anionic surface and vice versa (**Figure 2.25(c)**). Electrostatic forces are unlikely to constitute the major adhesive bond in a composite

and they can readily be reduced, for example by discharging in the presence of a strongly polar solvent, such as water.

2.15.4 Mechanical keying

There may be a contribution to the strength of the interface from the surface roughness of the fibers if good wetting has occurred, as illustrated in **Figure 2.25(e).** The effects are much more significant under shear loading than for decohesion as a result of tensile stressed. Some improved resistance to tensile failure results if re-entrant angles are present and there is an increase in strength under all types of loading as a consequence of the increased area of contact.

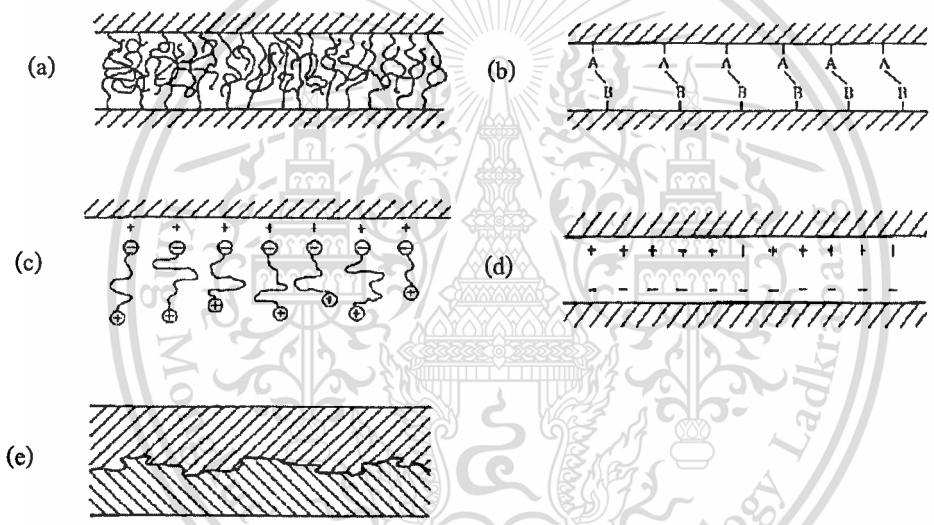

Figure 2.24 Interfacial bonds formed by (a) molecular entanglement following interdiffusion, (b), chemical reaction (c) cationic groups at the end of molecules attracted to an anionic surface, resulting in polymer orientation at the surface, (d) electrostatic attraction and (e) mechanical keying

2.16 Wood

Wood is the secondary xylem of woody plants, which includes trees. Xylem provides mechanical strength and liquid transport and storage of food reserves in a tree [36]. Xylem is produced by the division of vascular cambium, which results in the thickening of the tree. The tree grows higher due to the apical meristem. Trees can either be gymnosperms (softwoods) or angiosperms (hardwoods). These two classifications contain large anatomical differences. Other

variations can also occur between species and even within species depending on growing conditions. Softwoods structure is composed primarily of one cell type, the longitudinal tracheid. Longitudinal tracheid structure is simple when compared to the structure of hardwoods. Softwood fibers range in length from 3-4mm. Hardwoods' complex structure is primarily made up of 4 major cell types: vessel elements, fiber tracheids, longitudinal parenchyma, and ray parenchyma. The amount of each depends on species and growing conditions. The fiber length of hardwoods is much smaller than softwoods, at less than 1mm [38]. Both softwoods and hardwoods are chemically made up of cellulose, hemicellulose, lignin, and minor amounts (5-10% by weight) of extractives (Table 1.1) [36]. Cellulose chains are connected through hydrogen bonding into linear microfibrils made up of crystalline and non-crystalline regions. Hemicellulose is interdispersed between adjacent microfibrils and lignin cements it all together to help form different distinct layers of the cell wall [36].

Table 2.2 Chemical composition of both softwoods and hardwoods by weight percent

Tree type	Cellulose(%)	Hemicellulose(%)	Lignin(%)
Hardwood	40-44	15-35	18-25
Softwood	40-44	20-32	25-35

2.16.1 Cellulose [33]

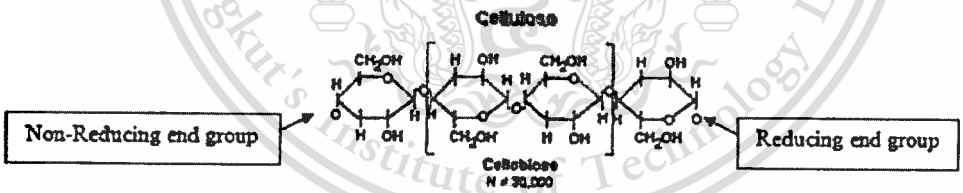

Figure 2.25 Chemical structure of Cellulose

Cellulose $[C_6(H_2O)_5]_n$ provides wood's strength and comprise approximately between 40-50 wt% of dry wood. Chemically cellulose is a high-molecular-weight (10^6 or more) linear polymer of β-(1 4)-D-glucopyranose units in the $^4C_1$ conformation. The basic repeating unit of the cellulose polymer consists of two glucose anhydride units, called a cellobiose unit. Glucose anhydride is formed via the removal of water from each glucose unit. This is polymerized into long cellulose chains that contain 5000-10000 glucose units. The fully equatorial conformation of β-linked glucopyranose residues stabilizes the chair structure,

minimizing flexibility. Each D-anhydroglucopyranose unit possesses hydroxyl groups at C2, C3, and C6 positions, capable of undergoing the typical reactions known for primary and secondary alcohols. The molecular structure of cellulose gives it, its characteristics properties: hydrophylicity, chirality, degradability, and broad chemical variability initiated by the high donor reactivity of hydroxyl groups. Cellulose has a strong tendency to form intra- and inter-molecular hydrogen bonds by the hydroxyl groups on these linear cellulose chains, which stiffen the straight chain and promote aggregation into a crystalline structure and give cellulose a multitude of partially crystalline fiber structures and morphologies.

The crystalline structure resists thermal decomposition better than hemicelluloses. Besides this the presence of crystalline cellulose, with regions of less order and the size of the elementary fibrils work together to produce interesting combination of contrary properties such as stiffness and rigidity on one side and flexibility on the other. Crystalline cellulose has very limited accessibility to water and chemicals thus attack by chemicals are primarily expected to occur at the amorphous cellulose and crystalline surface. Cellulose degradation occurs at 240-350 °C to produce anhydrocellulose and levoglucosan [34]. Levoglucosan is produced when the glucosan radical is generated without the bridging oxygen from the preceding monomer unit.

2.16.2 Hemicellulose[33]

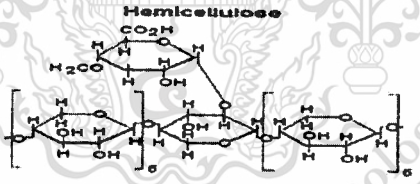

Figure 2.26 Chemical structure of Hemicellulose

Hemicellulose also called polyose constitute about 25-35% by mass of dry wood. Hemicellulose $[C_5(H_2O)_4]_n$ or $[C_6(H_2O)_5]_n$ is a heteropolysaccharide made up of monosaccharide such as glucose, mannose, galactose, xylose, arabinose,4-O-methyl glucuronic acid and galacturonic acid residues and unlike cellulose hemicellulose have a lower degree of polymerization (between 50-300) with some containing side groups on the chain molecules and are essentially amorphous. The types of hemicellulose found in wood depend on the type of wood and they vary in structure and amount.

In soft wood the main types of hemicellulose present are galactoglucomannans (10-15 wt%) and arabinoglucoronoxylan (7-10 wt%) while in hardwood it's the partially

acetylated glucuronoxylan (20-35 wt%) and a small percentage of galactomannan (2-5 wt%) in hardwood. Xylan is different from glucomannan in the sense that it contains acidic groups (glucuronic acid) and has a molecular structure similar to cellulose when their side branches are removed from xylan. This makes xylan combine with cellulose in more ordered structure after kraft pulping Glucomannan is more sensitive to kraft cooking conditions than xylan. Hemicellulose in hardwood pulp are dominated by xylan however in soft wood kraft pulps the amount of xylan present becomes almost the same as that of glucomannan though glucomannan is higher in content in softwood due to its chemical resistant nature.

2.16.3 Lignin [33]

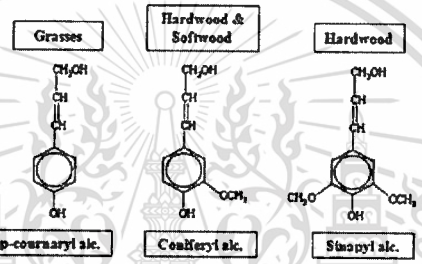

Figure 2.27 Chemical structure of lignin monomers

Lignin $(C_{10}H_{12}O_4)_n$ is the third major wood component. In soft wood, it accounts for 25%-35% of the mass while in hardwood it accounts for 18%-25% by mass of hardwood [35]. Structurally Lignin is a three-dimensional, highly branched, polyphenolic substance that consists of an irregular array of variously bonded "hydroxy-" and "methoxy-"substituted phenylpropane units. Lignin is an amorphous cross-link resin with no exact structure, functionally serving as a binder for the agglomeration of fibrous cellulosic components while also serving as a shield against rapid microbial or fungal destruction of the cellulosic fibers. The p-coumeryl, coniferyl and sinapyl structures are exhibited by these three general phenyl propane units, which undergo radical dimerization and further oligomerisation, eventually polymerize and cross linking to form lignin. Softwood mostly contains guaiacyl lignin formed from the polymerization of a higher fraction of coniferyl phenyl propane units. In hardwood the type of lignin found is the guaiacyl-syringyl a copolymer of both the coniferyl and synapyl phenyl propane units where the fraction of synapyl units is higher than that in soft wood lignin between individual units. This is due to the fact that the radical reactions that results in lignin formation are nonselective random condensations [34]. In terms of bond linkages between units, ether bonds predominate among lignin units whilst in cellulose and hemicellulose the acetyl functional group

predominates. Besides this the carbon-to-carbon linkages also exist in lignin. Lignin is linked to the polysaccharides by covalent bonds. Lignin isolation from the polysaccharides results in a modified and partially degraded product. The chemical and physical properties of lignin differ depending on the extraction or isolation method used [34].

2.17 Previous Mold Filling Studies of Co-injection Molding Process

Several investigations dealing with sandwich molding has been published. Almost all deal with the one-channel technique. A brief review on these studies is given in the following section.

White and Dee [25] studied mold filling in thin rectangular plates. They found that the skin should have a significantly lower viscosity than the core to obtain a good skin-core structure.

A relatively investigation was performed by Young et al.[26]. Six polymers were studied. These polymers were two polystyrenes, two high-density polyethylenes, a low-density polyethylene, and a polypropylene. Their viscosities were measured as a function of shear stress. The ratio of zero shear viscosities was determined from these data measurements and varied between 0.04 to 24.0 (depending on the material that formed the skin). The process used a screw extruder and a ram injection molding machine. An adjustable valve regulated the sequence of the melts entering the mold. The mold was a square plate with a gate positioned centrally on one of the long sides. It was equipped with a glass window so that mold filling could be observed. They found that the most uniform skin thickness occurred when the ratio of zero shear viscosities was between 1.5 and 2.0.

Mold filling studies on circular plates, diameter 180 mm, thickness 3 mm, gated at the centre, were also made by Schlatter et al. [27]. Studies were performed with the mono sandwich technique on two polystyrene (PS) melts, one with a slightly higher viscosity. The parameters investigated were flow rate, melt temperature, and volume ratio skin/core. The core was colored with a masterbatch for identification. The position of the interface was measured by cutting the plates along the radius and measuring layer thickness with a microscope. They found that when the core injection rate increased a lower skin thickness was obtained. Skin temperature also had some effect. And when the skin temperature was increased, a slightly thinner skin was obtained.

Donovan et al. [28] also studied mold filling. They used a two-shot nozzle one polymer flowing axially through a cylindrical passage at the centre of the nozzle and the other surrounding the first polymer. Different mold geometries were studied, such as end-gated plaque molds, centre-gated disc molds, and in some cases also telephone housing and handle molds. A variety of colored acrylonitrile-butadienestyrene (ABS) molding compounds were used, including scrap

ABS. Mold filling simulation was performed with a computer program described by Lord [35]. Interface shape was measured for plaque and disc molds and compared with the simulation results. Skin thickness was measured by sectioning the parts and using an optical comparator attached to a microscope. Typical results for the disc mold were obtained with 52% and 62% core material by volume. In general there was a good agreement between experiments and the simulations.

Somnuk and Smith [29] using a Battenfeld co-injection machine performed mold filling studies with the two-channel technique. The dimensions of the injected plates were 100 x 75 x4 mm. Four grades of polypropylene with differing viscosities were studied. Viscosity data was obtained from the material supplier and the ratio of viscosity varied between 0.54 to 1.83, measured at a shear rate of 10^3 s^{-1}. Mold filling was studied with a mold equipped with a Pyrex-glass window. Optimum mold filling was obtained when the viscosity ratio between skin/core was 0.8-1.8. They claimed that, at approximately equal viscosity, good mold filling results were obtained by letting the duration of the simultaneous injection period correspond to almost 95% of the injection time for the skin. It was also found that by changing the skin/core volume ratio and their relative velocity a better skin core morphology could be obtained.

Lanvers et al.[30] performed extensive mold-filling studies with co-injection molding machine at the IKV in Aachen, Germany. The Mold filling was examined starting from the viscosity ratios between skin and the core. A relatively large number of materials were determined, such as PP, PS, HDPE, PBT, and PA 66, and variations of these, with and without filler. By cutting thin injection molded plates along the flow direction, the shape of the interface between the melts at the flow front was studied. They found that the interface structure of the component had in all cases a parabolic shape. A more sharp-angled, wedge-shaped profile was obtained if the core had a higher viscosity than the skin, a blunter profile was obtained if the core had a lower viscosity than the skin.

Rungseesantivanon [16] reported adhesion levels and minimum skin could be improve when simultaneous injection times were increased. The simultaneous times were discovered to have a non-linear correlation to skin/core viscosity ratios. At the beginning of the gate area, the thickness of skin layers were thinnest and increased with length of flow path.

CHAPTER 3

EXPERIMENTAL PROCEDURES

3.1 Material

3.1.1 Polypropylene

Four grades of polypropylene (HP420J, HP740H, HP500N and P440J) were used in this study. The commercial name of (HP420J, HP500N, HP740H) is Moplen and supplied by Basell Service Company but EL-Pro P440J is originated by The Siam Cement Group (SCG). These polypropylenes was different melt flow rate (MFR) because this investigation was focused on the major and minor effects of skin-core formation by various molding parameters such as skin-core viscosity ratios, injection speeds, volume ratios and temperatures. The characteristics and technical data of polypropylene used in this study are shown in **Table 3.1.**

Table3.1 The characteristics and technical data of polypropylene (A) HP420J, (B) HP740H, (C) HP500N, (D) P440J

(A)

Name	Moplen
Grade	HP420J
Resin type of Polypropylene	Homopolymer
Description	Moplen HP420J is a polypropylene homopolymer manufactured using the Spheripol process. It is particularly suitable for BOPP, with potential end use applications in general purpose packaging, lamination film and adhesive tape.
Density Specific Gravity	0.90 g/cm^3
Melt flow rate	3 g/10 min
Tensile Strength at Yield	32 Mpa
Flexural Modulus	1350 MPa

(B)

Name	Moplen
Grade	HP740H
Resin type of Polypropylene	Homopolymer
Description	Moplen HP740H is a polypropylene homopolymer. With its good stiffness and top load strength, this grade is especially suitable for solid phase pressure thermoforming process. Potential end use products include drinking, margarine, noodle and dairy cups, etc.
Density Specific Gravity	0.90 g/cm³
Melt flow rate	2.1 g/10 min
Tensile Strength @ Yield	36 MPa
Flexural Modulus	1750 MPa

(C)

Name	Moplen
Grade	HP500N
Resin type of Polypropylene	Homopolymer
Description	Moplen HP500N is a homopolymer used for general purpose injection moulding applications. It exhibits good flow and stiffness. Moplen HP500N is suitable for food contact.
Density Specific Gravity	0.90 g/cm³
Melt flow rate	12g/10 min
Tensile Strength at Yield	35 MPa

(D)

Name	EL-Pro
Grade	P440J
Resin type of Polypropylene	Comopolymer
Description	EL-Pro P440J is an impact copolymer polypropylene resin suitable for injection molding process. This resin is recommended for product that requires high impact strength with good process

	ability.
Density Specific Gravity	0.91 g/cm³
Melt flow rate	5g/10 min
Tensile Strength @ Yield	26.48 MPa

3.1.2 Wood flour

Wood flour from ironwood obtained from Udornpattana Factory in Pathumthani Province of Thailand.

3.1.3 The compatibilizer

A Maleic anhydride grafted polypropylene or Compoline CO/PP C55 obtained from Behn Meyer Chemical Co.Ltd. The melt flow rate is 2.5 g/10 min.

3.2. Equipment

3.2.1 Co-injection molding machine

Initially, Co-injection molding machine was designed by CAD/CAE software. Plungers that transmitted the power from hydraulic power unit pressed the melts in the hot cylinders. Double gear pump was chosen to separate the operation of hydraulic cylinders. The velocities each plunger was controlled by flow control valves. Heaters covered two hot cylinders. The temperatures in cylinders were controlled by temperature controller. Four sensors were connected in hydraulic cylinders to vary the volume in the experiments. Co-injecion molding machine is shown in **Figure3.1.**

In **Figure3.2** show the drawing of polymer flow path from CAD/CAE simulation software, which skin-core polymer was injected at the same gate. Plungers from the left hand side and right hand side injected the skin and core polymer melt to the transparency acrylic mold, respectively to make sandwich specimen.

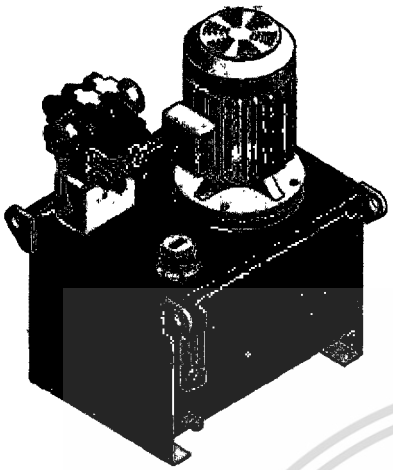

(a)

(b)

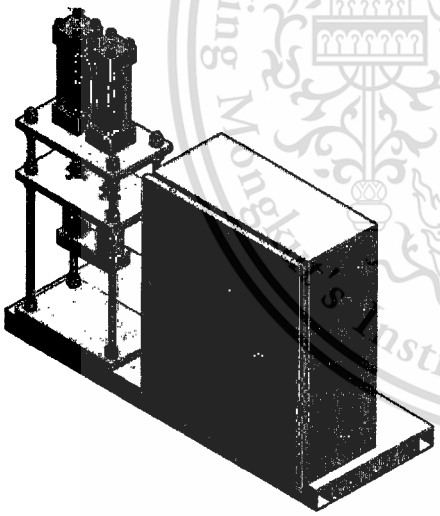

(c)

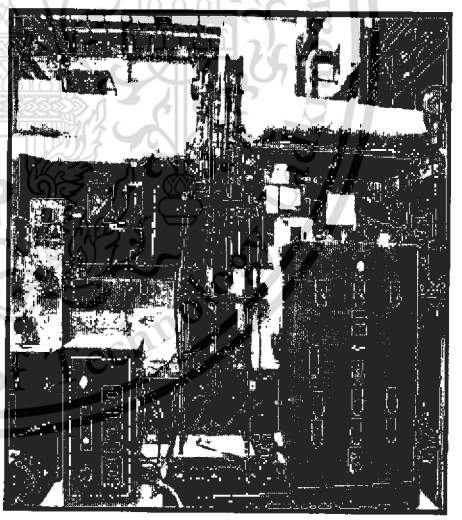

(d)

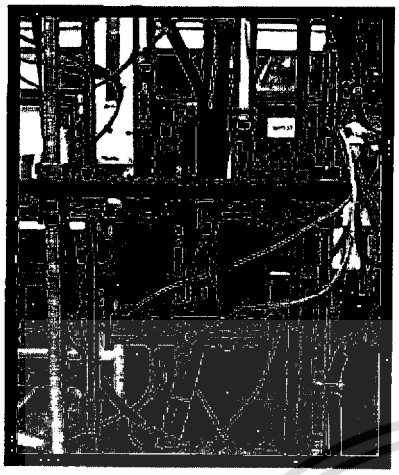

(e)

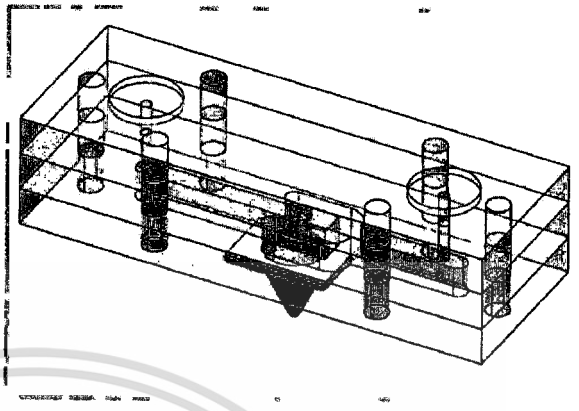

(f)

Figure 3.1 (a),(b) Hydraulic power unit with solenoid valves, (c),(d) Co-injection molding machine, (e) Two Hot barrels, (f) The polymer flow path from CAD/CAE simulation software

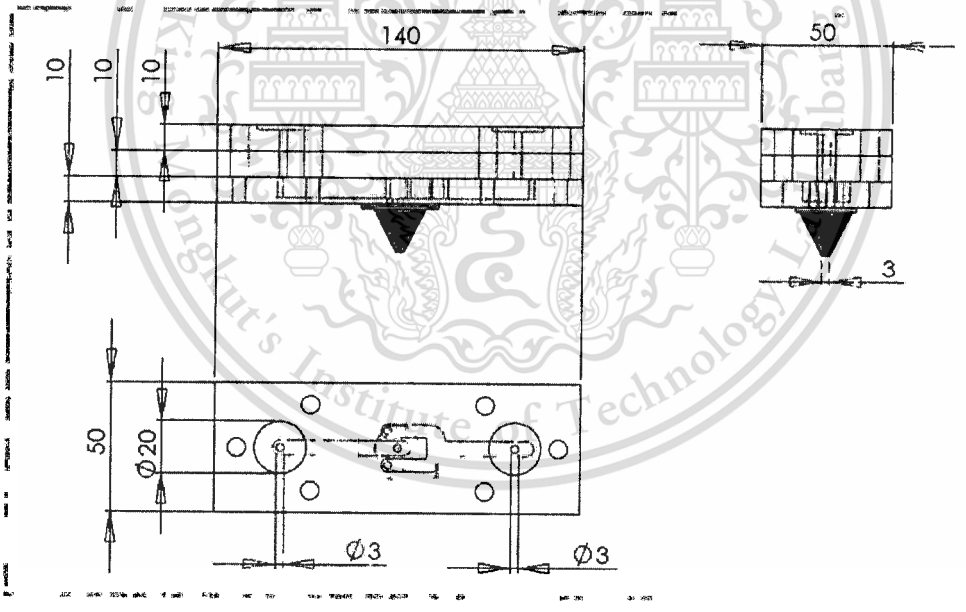

Figure 3.2 The drawing of polymer flow path from CAD/CAE simulation software

3.2.2 Soft tooling (transparency acrylic mold)

In **Figure3.3**, the acrylic mold was designed to investigate the flow behavior and find the optimum condition. A cavity in the mold was a rectangular plate 50x100 x3 (mm). The polymers of two hot cylinders were injected into the mold at the same gate. This system was designed to operate with sequential injection molding. Four grades of polypropylene (HP700H, HP420J, HP500N, and P440J) and wood plastic composite were used in this investigation.

Figure 3.3 Soft tooling (transparency acrylic mold) with rectangular shape

3.3. Process

The overall experimental procedures in this work were divided into two processes as show in **Figure 3.4** and **Figure 3.5.**

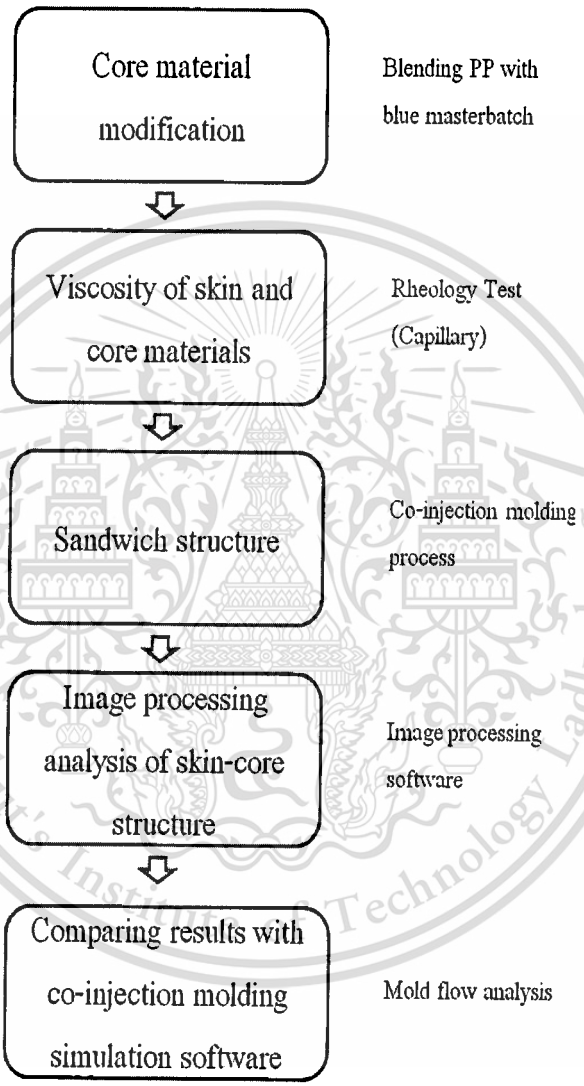

Figure 3.4 Overall experimental procedures of first process

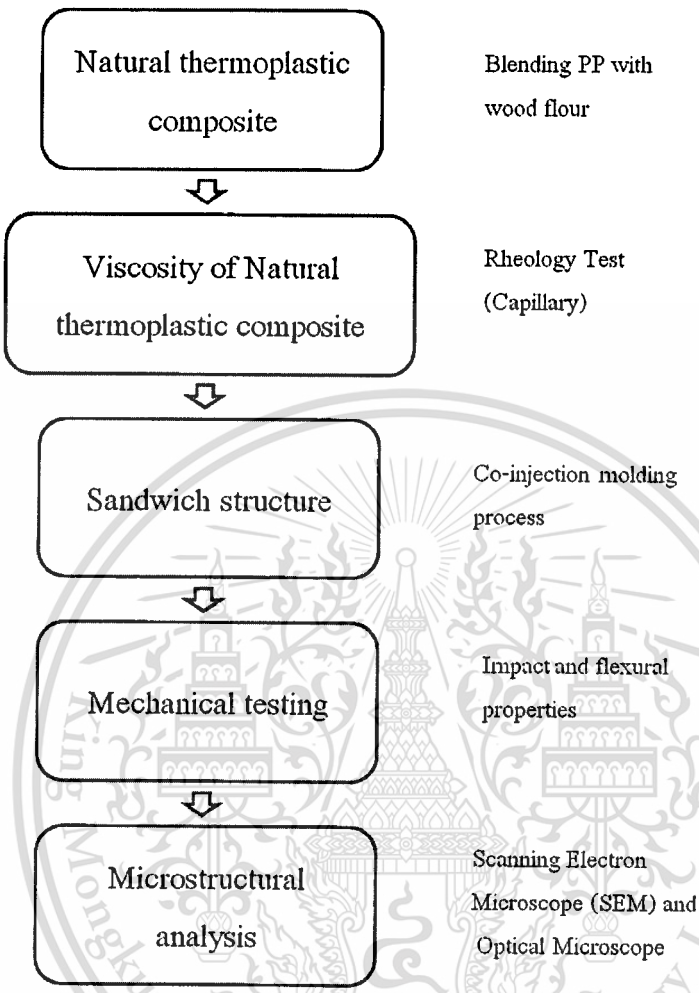

Figure 3.5 Overall experimental procedures of second process

First process, the single screw extruder **(see Figure3.6)** was used in blend polypropylene with blue masterbatch at 5 wt%. The rotation frequency was set at 60 rpm and temperature was 210 °C. The extruded plastic rod were immediately quenched in the water and cut into pellets. Polypropylene mixed with blue masterbatch was chosen to inject the core because skin-core structure could be clearly divided and easily observed. Pure and blue polypropylene were fed to the co-injection molding machine to make sandwich structure. In **Figure 3.7**, cross-section of work piece was obtained by cutting along A-A side. The image processing software (see **Figure 3.8**) was used in measure the profiles of skin-core structures.

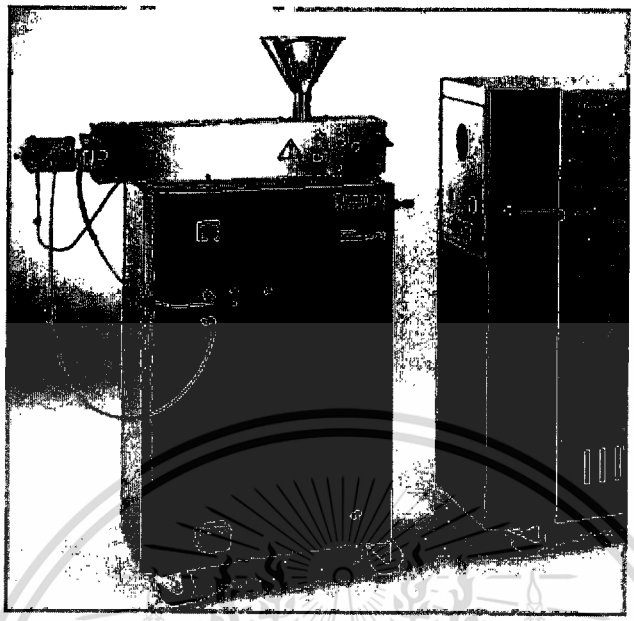

Figure 3.6 The single screw extruder

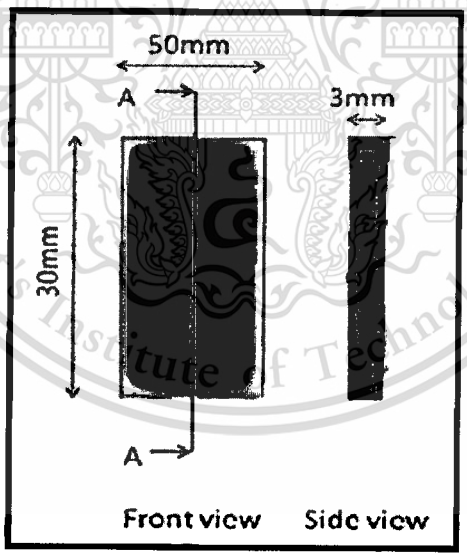

Figure 3.7 Skin-core structure form Co-injection molding machine

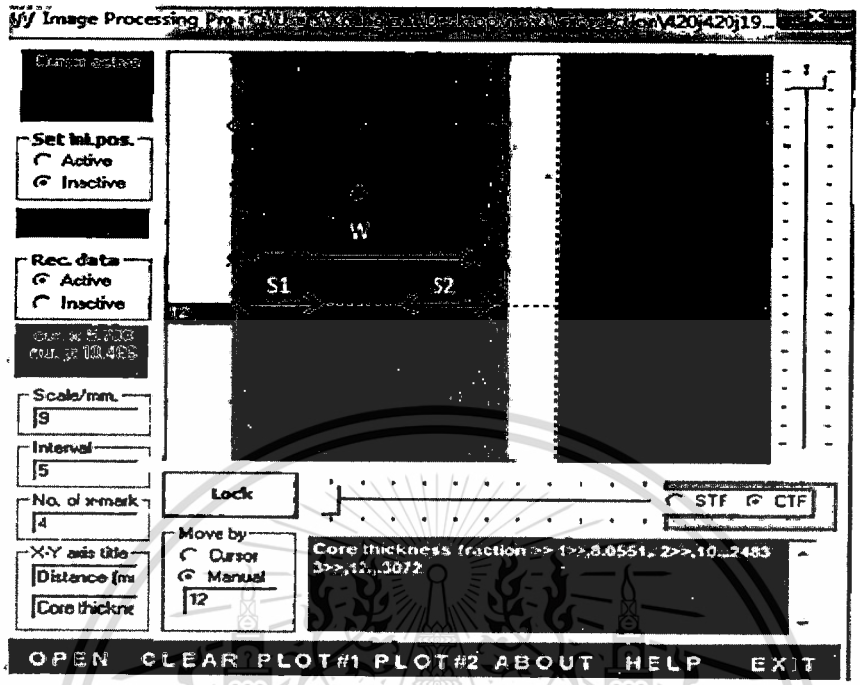

Figure 3.8 Image processing with skin-core structure

Generally, the skin-core thickness fractions were obtained using optical microscope. The disadvantage of this method was taking long time. Therefore, the image processing software was used. The cross section of sandwich specimen was scanned and loaded to software then user moved cursor on the location of skin and core layers.

The measurements were carried out to obtain skin thickness fraction (*STF*) and core thickness fraction (*CTF*). It is can be calculated as follows.

Skin thickness fraction (STF)

$$STF = \frac{S_1 + S_2}{W}$$

core thickness fraction (CTF)

$$CTF = \frac{W - (S_1 + S_2)}{W}$$

Where, W = total thickness (mm)

S_1, S_2 = skin thickness

The plastic injection molding simulation software was used to compare with the experiment result is shown in **Figure 3.9**.

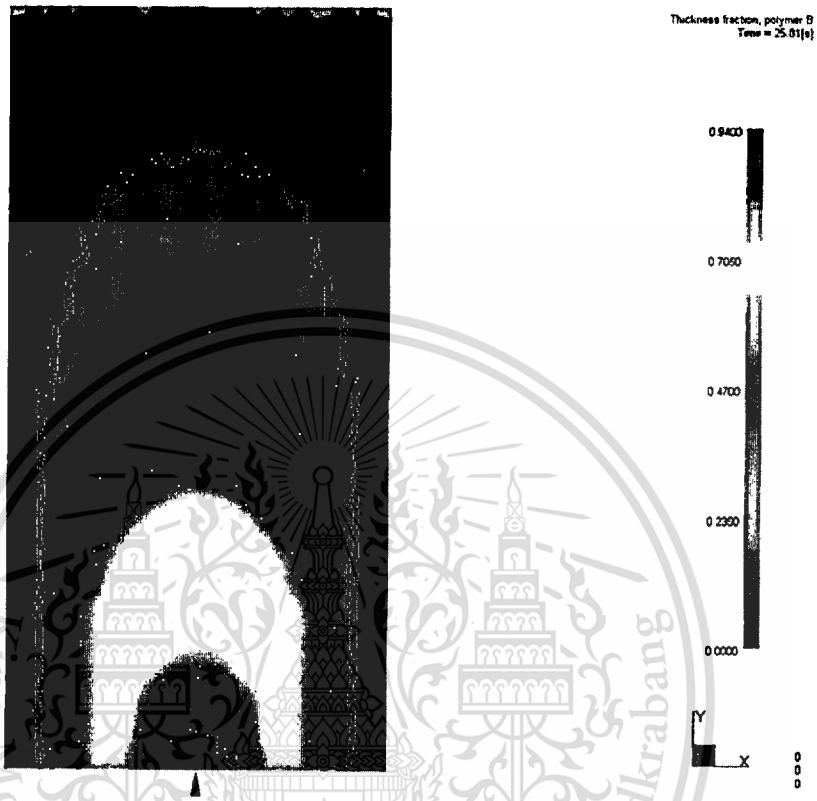

Figure 3.9 The plastic injection molding simulation software

Second process, wood flour from ironwood obtained from wood industry is shown in **Figure 3.10**. The vacuum oven from memmert (**Figure 3.11**) was used to reduced moisture in wood flour. Dry wood flour, polypropylene and PP-g-MA 5wt% was mixed with by using the twin screw extruder (**Figure 3.12**) to make a natural thermoplastic composite. The extruded wood plastic composite rod were immediately quenched in the air and cut into pellets (**Figure 3.13**). Pure polypropylene and wood plastic composite were fed to the co-injection molding machine to make sandwich specimens. These specimen were examined the mechanical and rheology properties. To investigate the morphology of the specimens, their cross-sections were examined with a Scanning Electron Microscope (SEM) and Optical Microscope.

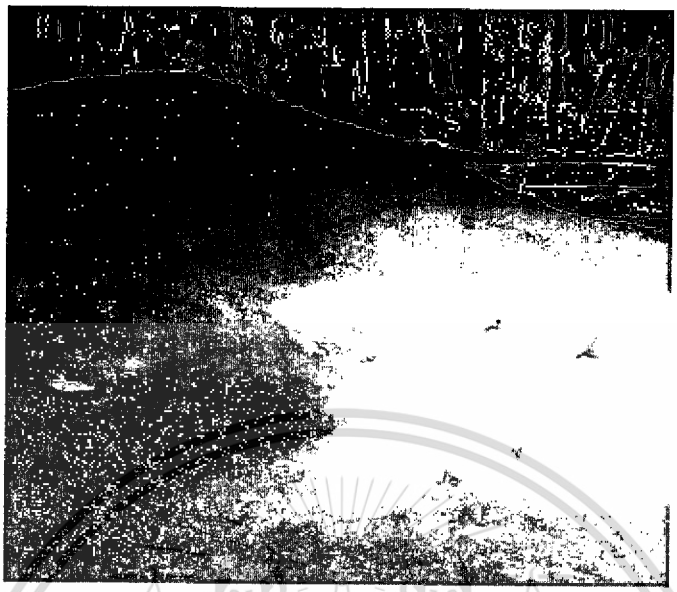

Figure 3.10 Wood flour

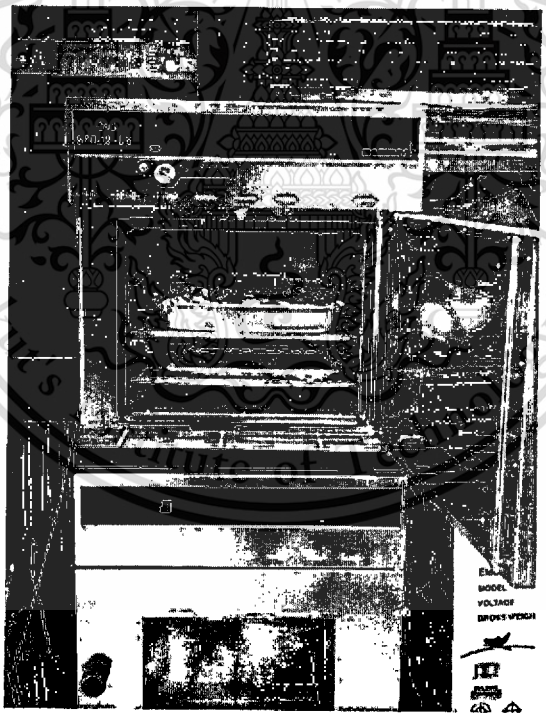

Figure 3.11 The vacuum oven

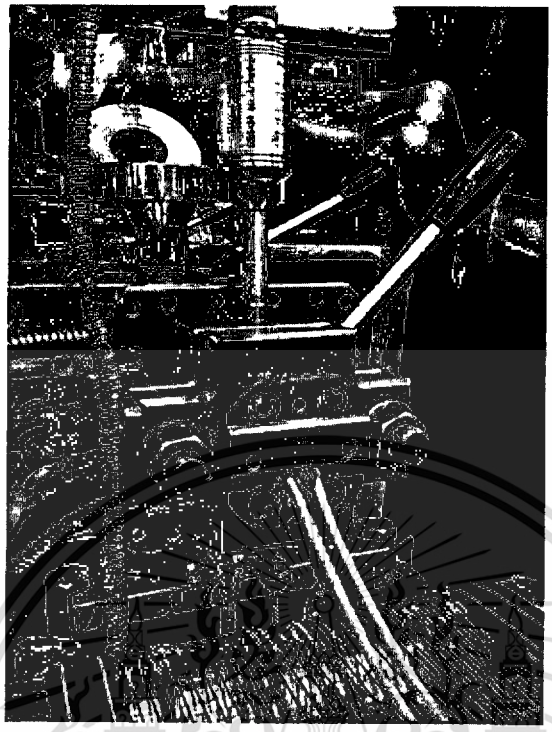

Figure 3.12 The twin screw extruder

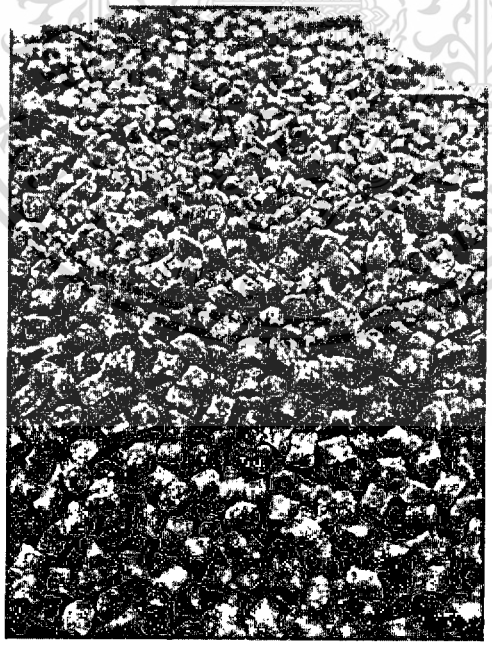

Figure 3.13 Wood plastic composite

3.4. Experiment

3.4.1 Effect of skin-core volume fractions on sandwich structure

Firstly, the machine control setting are shown in **Table 3.2** and Skin-core volume fractions of polypropylene (HP420J) were varied to find optimum condition as shown in **Table 3.3**. Avoid the core breakthrough.

Table 3.2 The molding conditions

Skin melt temperature (A barrel)	210 °C
Core melt temperature (B barrel)	210 °C
Velocity of skin	5.86 mm/s
Velocity of core	5.86 mm/s

Table 3.3 Skin-core volume fractions

No.	Skin material (%)	Core material (%)	Volume fractions (skin/core)
1	74.28	25.72	2.89
2	60	40	1.50
3	48.57	51.43	0.94
4	42.85	57.15	0.75

3.4.2 Effect of skin injection speeds on sandwich structure

As show in **Table 3.4**, the skin-core temperatures of polypropylene (HP420J) were set the same as **3.4.1 Effect of skin-core volume fractions**. The skin-core volume proportion was set at optimum condition 48.57% and 51.43%, respectively. The skin injection speeds were adjusted as show in **Table 3.5** to understand the behavior of skin injection speeds on sandwich structure.

Table3.4 The molding conditions

Skin melt temperature (A barrel)	210 °C
Core melt temperature (B barrel)	210 °C
Skin material	48.57 %
Core material	51.43 %

Table3.5 Skin-core injection speeds

No.	Skin injection speeds (mm/s)	Core injection speeds (mm/s)
1	2.45	5.86
2	5.86	5.86

3	11.43	5.86

3.4.3 Effect of core injection speeds on sandwich structure

As show in **Table 3.6**, the skin-core temperatures of polypropylene (HP420J) were set the same as **3.4.1 Effect of skin-core volume fractions**. The skin-core volume proportion was set at optimum condition 48.57% and 51.43%, respectively. The core injection speeds were adjusted as show in **Table 3.7** to understand the behavior of core injection speeds on sandwich structure.

Table3.6 The molding conditions

Skin melt temperature (A barrel)	210°C
Core melt temperature (B barrel)	210°C
Skin material	48.57%
Core material	51.43 %

Table3.7 Skin-core injection speeds

No.	Skin injection speeds (mm/s)	Core injection speeds (mm/s)
1	5.86	2.45
2	5.86	5.86
3	5.86	11.43

3.4.4 Effect of skin temperatures on sandwich structure

As show in **Table 3.8**, the skin-core injection speeds of polypropylene (HP420J) were set the same as **3.4.1 Effect of skin-core volume fractions**. The skin-core volume proportion was set at optimum condition 48.57% and 51.43%, respectively. The skin temperatures were varied as show in **Table 3.9** to understand the behavior of skin temperatures on sandwich structure.

Table3.8 The molding conditions

Velocity of skin	5.86 mm/s
Velocity of core	5.86 mm/s
Skin material	48.57 %
Core material	51.43 %

Table3.9 Skin-core temperatures

No.	Skin temperatures (°C)	Core temperatures(°C)	Viscosity Ratios (skin/core)
1	190	210	1.132
2	210	210	1
3	230	210	0.896

3.4.5 Effect of core temperatures on sandwich structure

As show in **Table 3.10**, the skin-core injection speeds of polypropylene (HP420J) were set the same as **3.4.1 Effect of skin-core volume fractions**. The skin-core volume proportion was set at optimum condition 48.57% and 51.43%, respectively. The core temperatures were varied as show in **Table 3.11** to understand the behavior of core temperatures on sandwich structure.

Table 3.10 The molding conditions

Velocity of skin	5.86 mm/s
Velocity of core	5.86 mm/s
Skin material	48.57 %
Core material	51.43 %

Table3.11 Skin-core temperatures

No.	Skin temperatures (°C)	Core temperatures (°C)	Viscosity Ratios (skin/core)
1	210	190	0.883
2	210	210	1
3	210	230	1.116

3.4.6 Effect of skin viscosities on sandwich structure

As show in **Table 3.12**, the skin-core injection speeds and temperatures were set the same as **3.4.1 Effect of skin-core volume fractions**. The skin-core volume proportion was set at optimum condition 48.57% and 51.43%, respectively. The skin viscosities were varied as show in **Table 3.13** to understand the behavior of skin viscosities on sandwich structure.

Table 3.12 The molding conditions

Velocity of skin	5.86 mm/s
Velocity of core	5.86 mm/s
Skin material	48.57 %
Core material	51.43 %
Skin temperature	210 °C
Core temperature	210 °C

Table 3.13 Skin-core viscosities

No.	Skin viscosities(Pa-s) (Grade of PP)	Core viscosities (Pa-s) (Grade of PP)
1	110.476 (HP740H)	99.586 (HP420J)
2	99.586 (HP420J)	99.586 (HP420J)
3	87.824 (P440J)	99.586 (HP420J)
4	68.335 (HP500N)	99.586 (HP420J)

3.4.7 Effect of core viscosities on sandwich structure

As show in **Table3.14**, the skin-core injection speeds and temperatures were set the same as **3.4.1 Effect of skin-core volume fractions**. The skin-core volume proportion was set at optimum condition 48.57% and 51.43%, respectively. The core viscosities were varied as show in **Table3.15** to understand the behavior of core viscosities on sandwich structure.

Table3.14 The molding conditions

Velocity of skin	5.86 mm/s
Velocity of core	5.86 mm/s
Skin material	48.57 %
Core material	51.43 %
Skin temperature	210 °C
Core temperature	210 °C

Table3.15 Skin-core viscosities

No.	Skin viscosities(Pa-s) (Grade of PP)	Core viscosities (Pa-s) (Grade of PP)
1	99.586 (HP420J)	110.476 (HP740H)
2	99.586 (HP420J)	99.586 (HP420J)
3	99.586 (HP420J)	87.824 (P440J)
4	99.586 (HP420J)	68.335 (HP500N)

3.4.8 Effect of wood plastic composite contents on sandwich structure

As show in **Table 3.16**, the skin-core injection speeds of polypropylene (HP420J) and natural thermoplastic composite were set the same as **3.4.1 Effect of skin-core volume fractions**. The skin-core volume proportion was set at optimum condition 48.57% and 51.43%, respectively. Wood plastic composite (wood flour contents 10wt%, 20 wt% and 30wt%) were investigated on sandwich structure as show in **Table 3.17**.

Table 3.16 The molding conditions

Skin melt temperature (A barrel)	210 °C
Core melt temperature (B barrel)	210 °C
Velocity of skin	5.86 mm/s
Velocity of core	5.86 mm/s

Table 3.17 Skin-core viscosity ratio of wood plastic composite

No.	Skin material	Core material	Viscosity ratios (skin/core)
1	Pure polypropylene (HP420J)	Wood plastic composite(10%)	1.44
2	Pure polypropylene (HP420J)	Wood plastic composite(20%)	1.31
3	Pure polypropylene (HP420J)	Wood plastic composite(30%)	1.13

3.5. Properties Testing

3.5.1 Sieve analysis

The analytical sieve shakers of the series AS 200 (**Figure 3.14**) were used in research to classify particle sizes of wood flour.

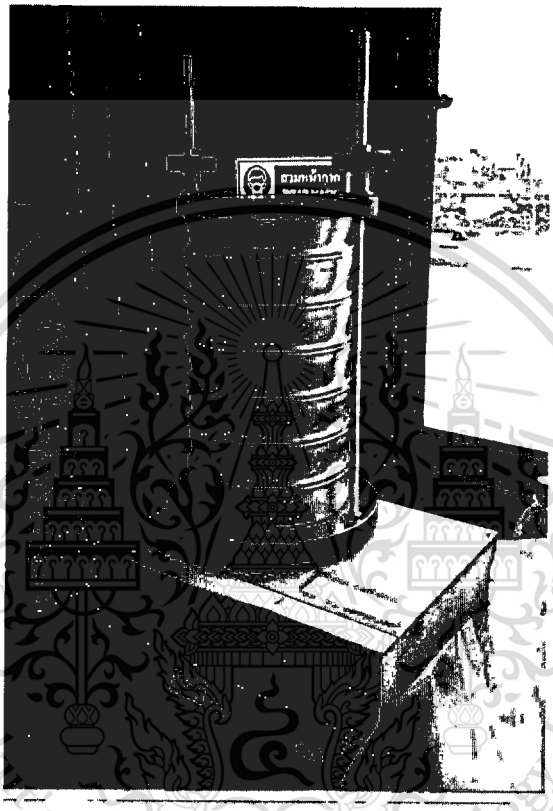

Figure 3.14 Retsch Sieve Shakers AS 200

3.5.2 Flexural Stress

In **figure3.15**, A Universal Testing Machine (Model 55R4502 S/N H3342, Instron Co.) was used to obtain the flexural properties of the specimen at room temperature. This specimen was prepared to measure flexural stress with standard ASTM D790-03 with a test span of 48mm as shown in **Figure 3.16**. All measurements were performed for five specimens and averaged to obtain the final results. The maximum stress in the outer surface of test specimen occurred at the midpoint when a sandwich structure was tested in flexure as a simple beam supported at two points and loaded at the midpoint. The flexural stress of elasticity for each specimen is calculated by the following equations.

$$\sigma_f = 3PL/2bd^2$$

Where: σ_f = Stress in the outer fibers at midpoint (MPa)

P = Load at given point on the load-deflection curve (N)

L = Support span (mm)

b = Width of beam tested (mm)

d = Depth of beam tested (mm)

Figure 3.15 A Universal Testing Machine (Model 55R4502 S/N H3342, Instron Co.)

Figure 3.16 Flexural testing

The sandwich specimens used in this investigation were set the same as **3.4.8 Effect of wood plastic composite on sandwich structure**. Wood plastic composite (wood flour contents 10wt%, 20 wt% and 30wt%) were investigated.

3.5.3 Notched Izod Impact strength

Izod impact tester was selected to measure notched impact strength as shown in **Figure3.17**. This investigation is focus on relation between notched impact strength and profile of sandwich structure. Five pieces of sandwich specimens were cut perpendicular with flow direction and notched before impact tester (**Figure 3.18**). The digital display showed the total energy absorbed during impact. All data were performed for five specimens and averaged to obtain the results.

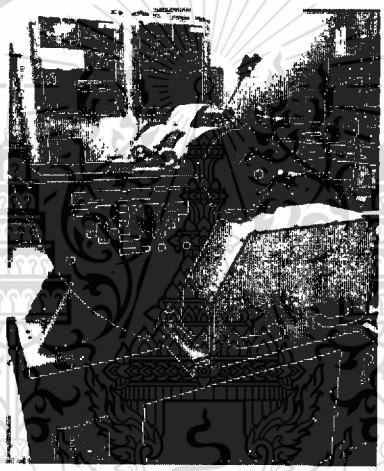

Figure 3.17 Izod impact tester

Figure 3.18 Notched impact specimens

Analysis of impact strength on sandwich structure using this equation.

$$I_{total} = (I_{core} * CTF) + (I_{skin} * STF)$$

Where: I_{total} = Total impact strength

I_{core} = Core impact strength

I_{skin} = Skin impact strength

CTF= Core thickness fraction

STF = Skin thickness fraction

The sandwich specimens used in this investigation were set the same as **3.4.8 Effect of wood plastic composite on sandwich structure**. Wood plastic composite (wood flour contents 10wt%, 20 wt% and 30wt%) were investigated.

3.5.4 Moisture content

The moisture contents in wood plastic composite were examined by Moisture Analyzer HX204 is shown in **Figure 3.19**. This experiment measured moisture of wood plastic composite before and after using vacuum oven.

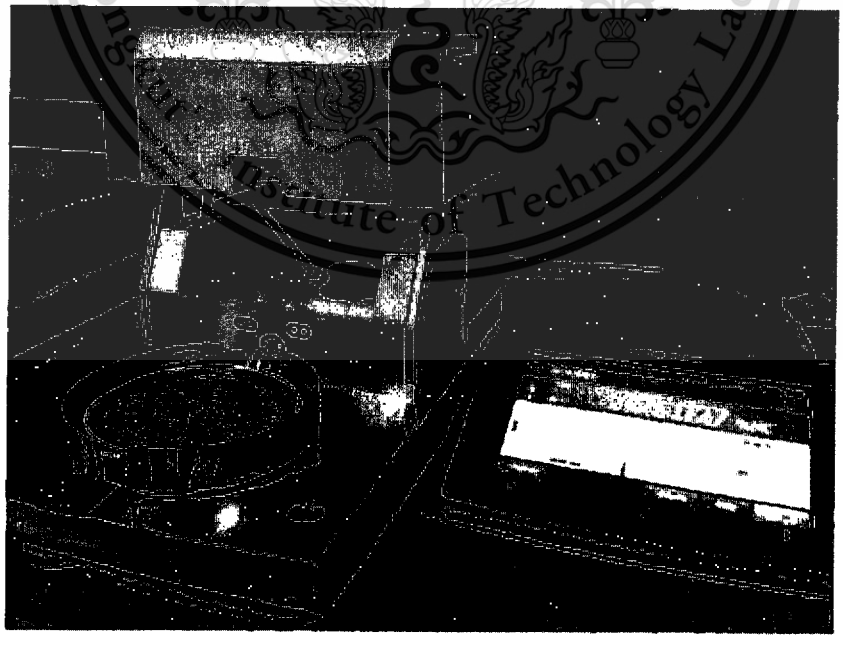

Figure 3.19 Moisture Analyzer HX204

3.5.5 Microstructure

3.5.5.1 Scanning Electron Microscopy (SEM)

Scanning Electron Microscopy (SEM) JEOL JSM-5410 in **Figure 3.20** examined the fracture surface of the specimens. This experiment was prepared by fracture in liquid nitrogen. The samples were spotted with gold to make them conducting by using JEOL JFC-1200 fine coating in **Figure 3.21**. The observed area is top, middle and bottom area of specimen that is shown in **Figure 3.22**.

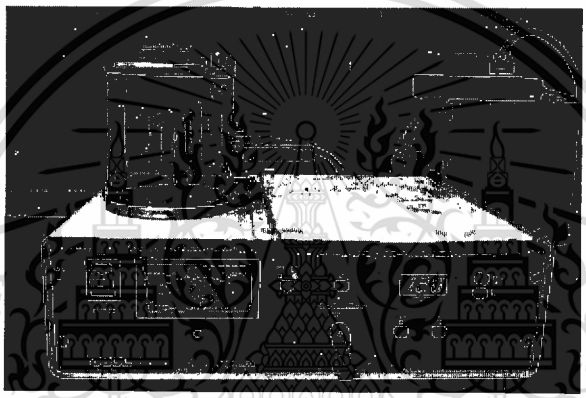

Figure 3.20 Fine coating JEOL JFC-1200

Figure3.21 Scanning electron microscopy (SEM) JEOL JSM-5410

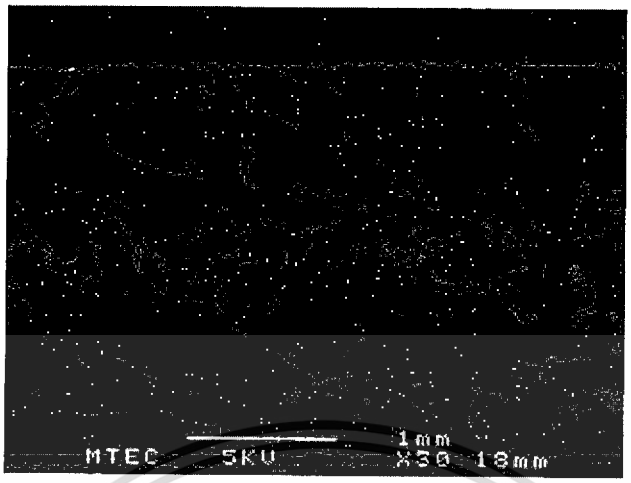

Figure 3.22 Observed area of Scanning Electron Microscope

3.5.5.2 Optical Microscope

The Optical Microscope (**Figure 3.23**) was used to observe the microstructures of the specimen with magnification of 50x and 100x.

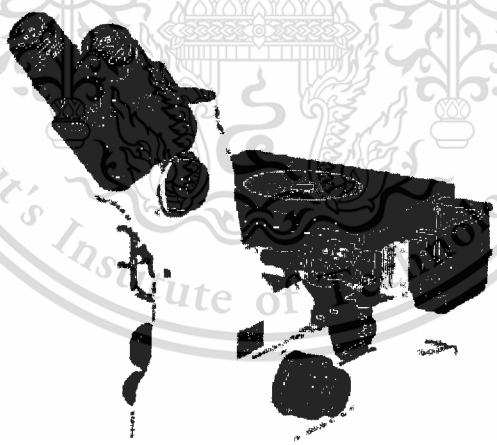

Figure 3.23 Optical Microscope

3.5.6 Rheological Properties

3.5.6.1 Capillary rheometer test

The Bohlin instrument capillary rheometer model RH2000 **(Figure 3.24)** was used to understand the rheology properties of materials. The sample for testing was loaded inside the barrel of the extrusion assembly and forced down into the capillary using a plunger. The melt was extruded through the capillary at predetermined plunger speeds. The measurements were carried out the viscosities at different melt flow rates and temperatures.

Figure 3.24 Capillary rheometer model RH2000

The shear viscosity (η) was calculated using this equation.

$$\eta = \tau / \dot{\gamma}$$

$$\tau_w = \frac{RP_c}{2L}$$

$$\dot{\gamma} = \frac{4Q}{\pi R^3}$$

Where: τ_w = wall shear stress

$\dot{\gamma}_w$ = wall shear strain

R = Diameter of capillary die

L = Length of capillary die

P_c = Pressure

Q = Flow volume

Moreover, the rheological measurement with orifice die can be calculated extensional viscosity (η_ε) using the equation.

$$\eta_\varepsilon = \sigma / \varepsilon^{\bullet}$$

$$\sigma_w = \frac{3(n+1)P_0}{8}$$

$$\varepsilon_w^{\bullet} = \frac{4\eta \dot{\gamma}^2}{3(n+1)P_0}$$

Where: σ_w = wall shear stress

$\varepsilon_w^{\bullet}$ = wall shear strain

Analysis of the relationship between chemical structure and flow properties of polymer was used two parameter including Newtonian viscosity and power law index from two mathematic models.

Cross model $$\eta = \frac{\eta_0}{1+\left(\eta_0 \dot{\gamma}/\tau^{\bullet}\right)^{1-n}}$$

Power law model $$\eta = K\dot{\gamma}^{n-1}$$

Where: $\dot{\gamma}$ = shear rate

η = shear viscosity

η_0 = Newtonian viscosity

$\tau^{\bullet}$ = stress at non-Newtonian point

K = constant

3.5.6.2 Melt flow index test (MFI)

Melt flow index (MFI) is defined as the weight of the polymers in grams extruded in 10 min through capillary of specific dimensions by pressure applied through dead weight via piston. The measurements of melt flow index were carried out using Lloyd Instrument model Davenport MFI-10 (**Figure 3.25**) with standard ASTM D 1238. The melt flow index is experiment at temperature 230. The sample for testing is including pure polypropylene (HP420J, HP740H, HP500N and P440J) and wood plastic composite (PP HP500N mixed wood flour contents 10wt%, 20wt% and 30wt%). Cut off time is setting about 30 second and pre-heat is 3 minutes. The measure of melt flow index (MFI) helps to determine how easily the molten polypropylene or composite will flow during processing. Polypropylene or composite with higher MFR will fill the plastic mold more easily during the injection.

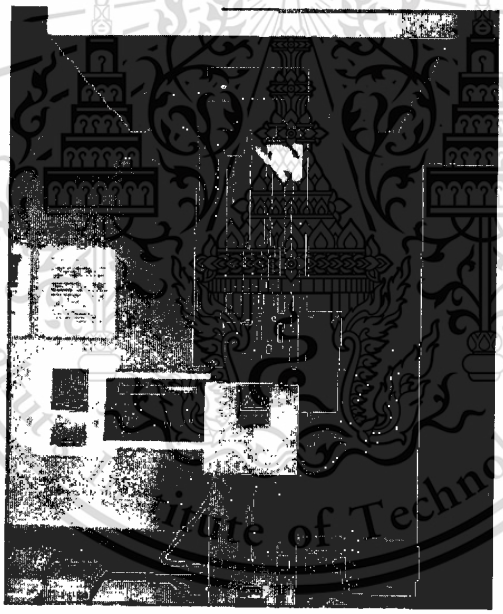

Figure 3.25 Davenport MFI-10 melt flow indexer

CHAPTER 4

RESULTS AND DISCUSSION

4.1 Processing Condition

4.1.1 Effect of molding parameters on Co-injection molding compare with Plastic injection molding simulation software

4.1.1.1 Effect of skin-core volume fractions

From experiment, decreasing skin-core volume proportions lead to high core thickness fractions but a large number of decreasing skin-core volume proportions conduce to core breakthrough as show in Volume faction at 0.75 of **Figure 4.1** and **Figure 4.2**. The results show high skin thickness fractions were obtained when skin-core volume proportions were increased. The optimum condition of this experiment is volume fraction 0.94 (Skin volume is 48.57%, core volume is 51.43%).

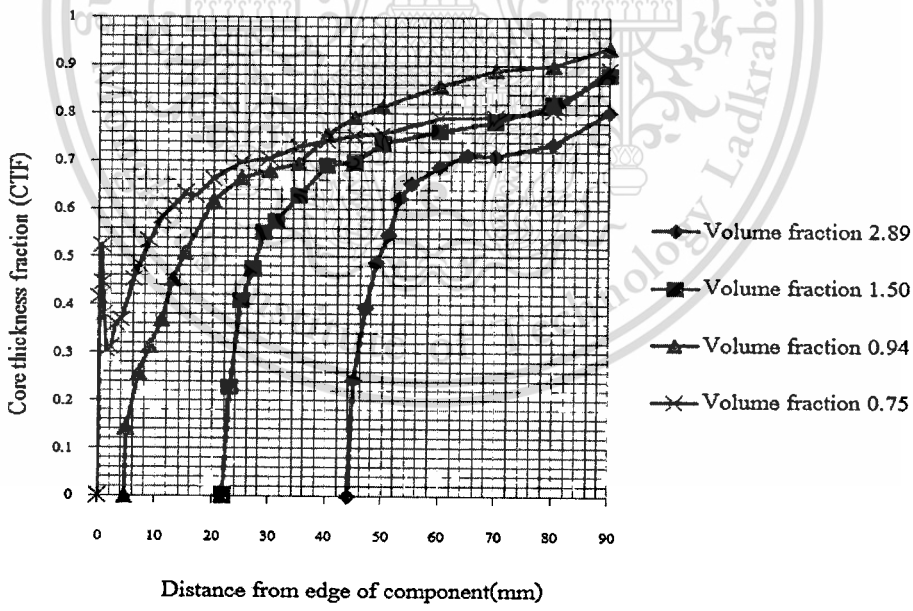

Figure 4.1 Relationship between core thickness fraction and skin-core volume fractions from experiment

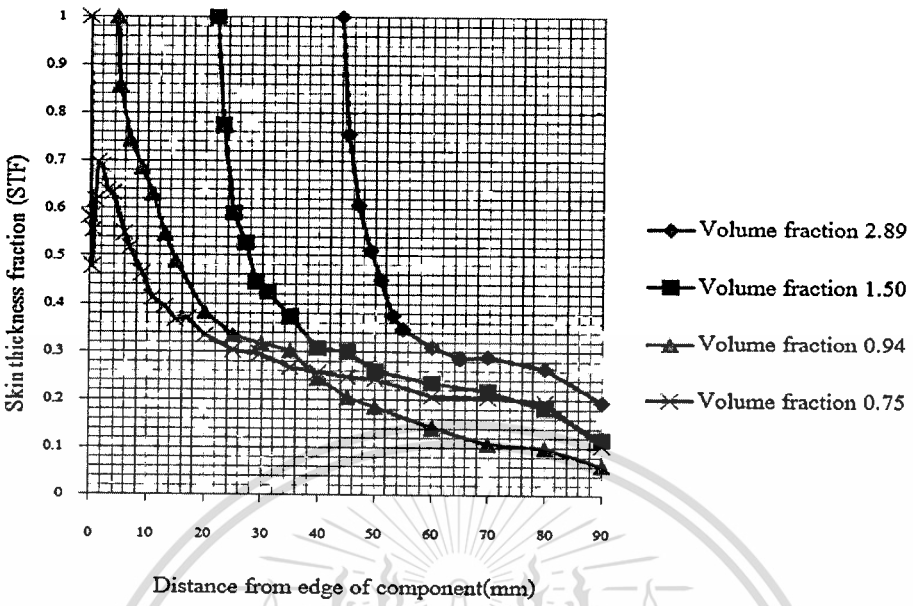

Figure 4.2 Relationship between skin thickness fraction and skin-core volume fractions from experiment

4.1.1.2 Effect of skin injection speeds

From **Figure 4.3** and **Figure 4.4,** the relative comparison between experimental and simulated results show similar trend but the profile of skin-core structures from simulation was different. Increasing skin injection speeds lead to low core thickness fractions because higher skin injection speed will have the less time to solidify and rheological properties testing show at high shear rate conduce to low viscosity. On the other hand, increasing skin injection speeds lead to high skin thickness fractions is shown in **Figure 4.5** and **Figure 4.6**.

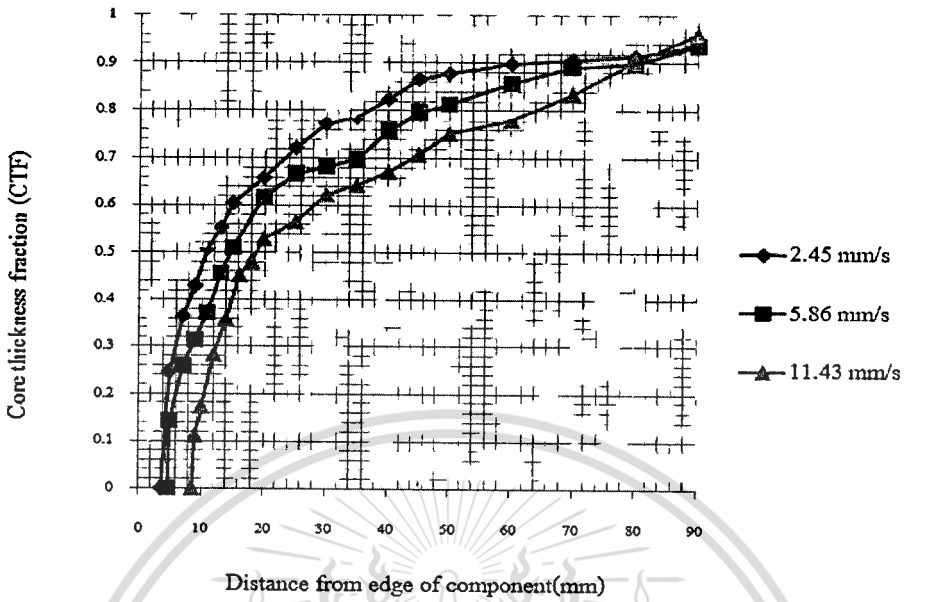

Figure 4.3 Relationship between core thickness fraction and skin injection speeds from experiment

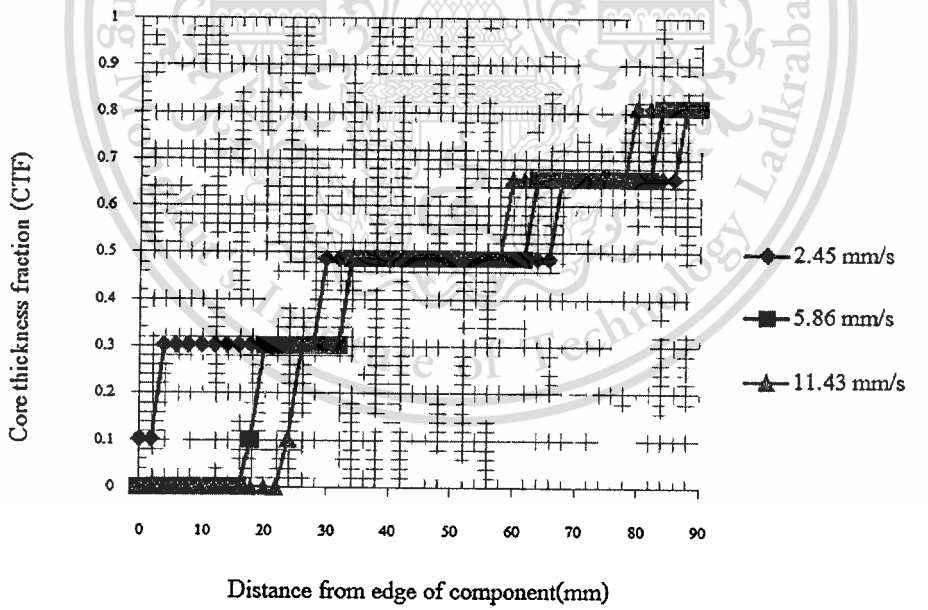

Figure 4.4 Relationship between core thickness fraction and skin injection speeds from Plastic injection molding simulation software

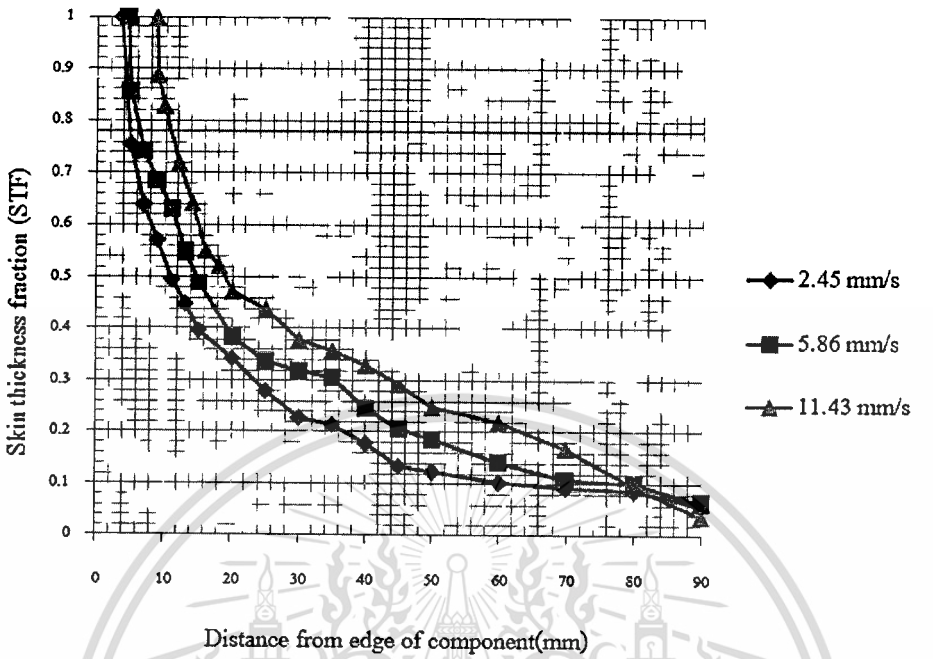

Figure 4.5 Relationship between skin thickness fraction and skin injection speeds from experiment

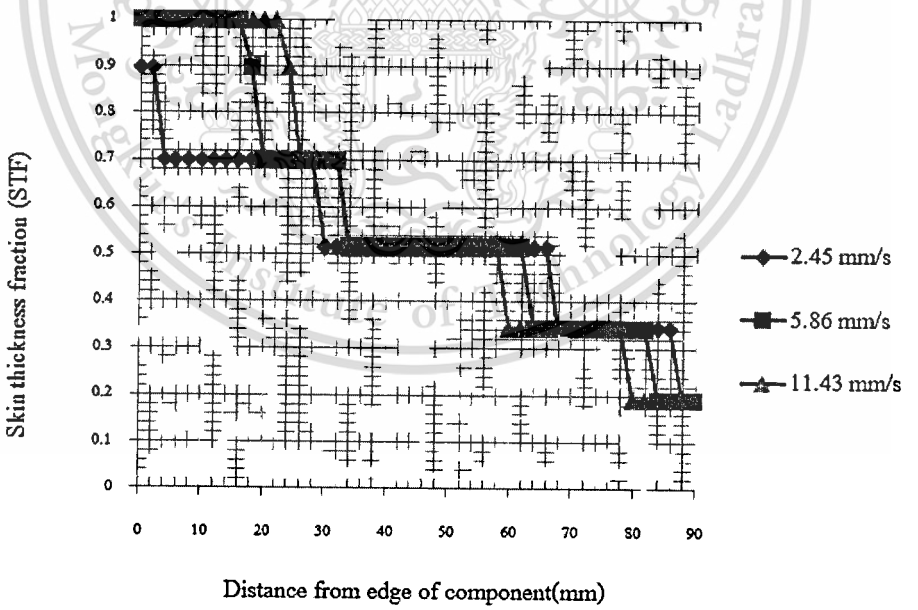

Figure 4.6 Relationship between skin thickness fraction and skin injection speeds from Plastic injection molding simulation software

4.1.1.3 Effect of core injection speeds

From **Figure 4.7**, increasing core injection speeds lead to high core thickness fractions because higher injection speed conduce to low viscosity confirm to rheological properties testing show at high shear rate lead to low viscosity. On the other hand, increasing skin injection speeds lead to low skin thickness fractions is shown in **Figure 4.9.** Unfortunately, the plastic injection molding simulation software could not simulate the correct results as show in **Figure 4.8** and **Figure 4.10**.

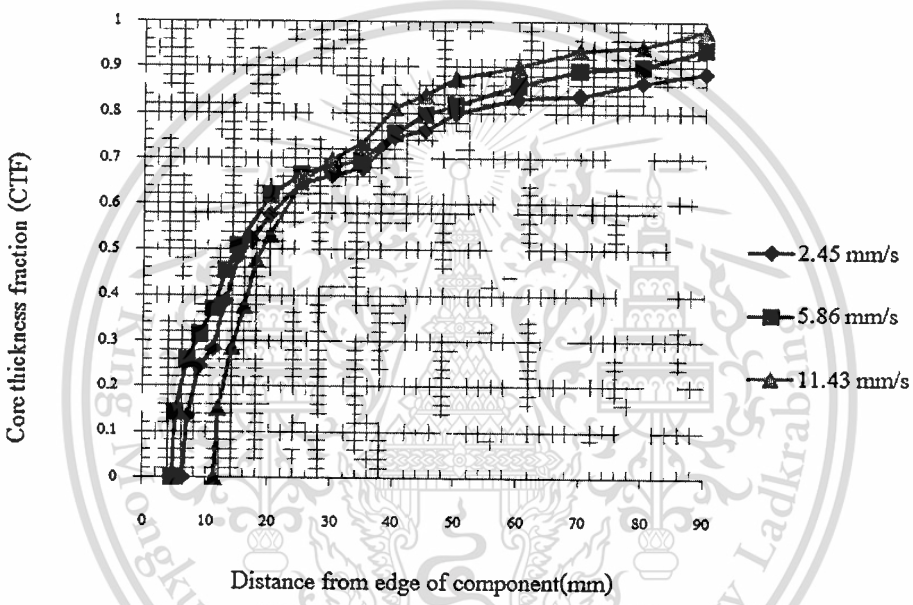

Figure 4.7 Relationship between core thickness fraction and core injection speeds from experiment

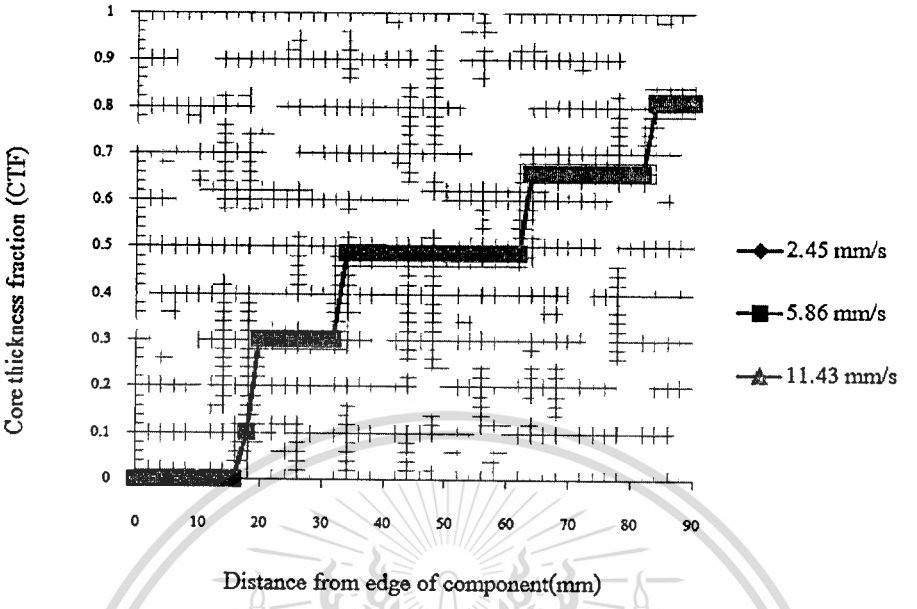

Figure 4.8 Relationship between core thickness fraction and core injection speeds from Plastic injection molding simulation software

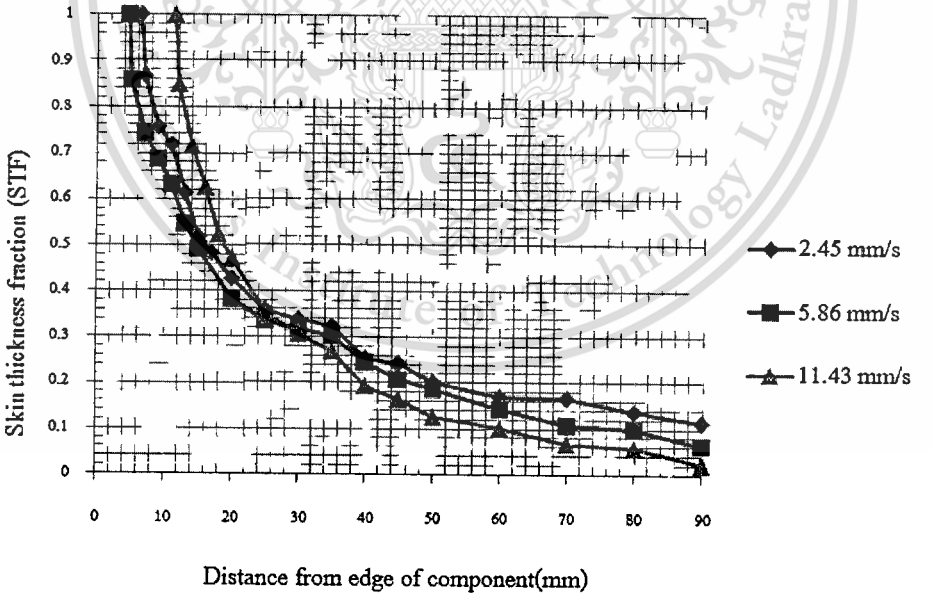

Figure 4.9 Relationship between skin thickness fraction and core injection speeds from experiment

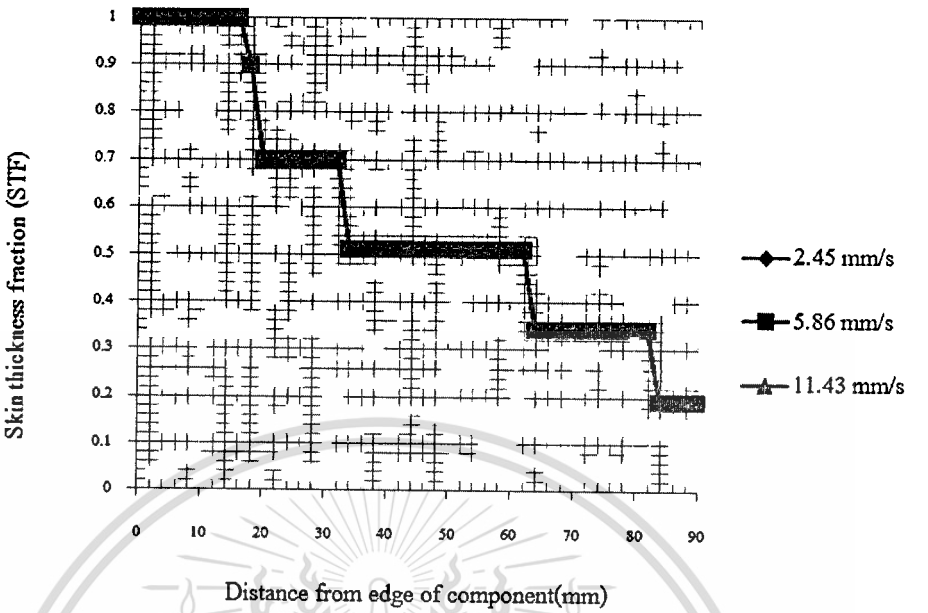

Figure 4.10 Relationship between skin thickness fraction and core injection speeds from Plastic injection molding simulation software

4.1.1.4 Effect of skin temperatures

From **Figure 4.11** and **Figure 4.12**, the relative comparison between experimental and simulated results show similar trend but the profile of skin-core structures from simulation was different. Increasing skin temperatures lead to low core thickness fractions because higher skin temperature conduce to low viscosity. On the other hand, increasing skin temperature lead to high skin thickness fractions is shown in **Figure 4.13** and **Figure 4.14.** These are consistent with Cross-Exp Model (C-MOLD Filling Stage Model) in Chapter2.

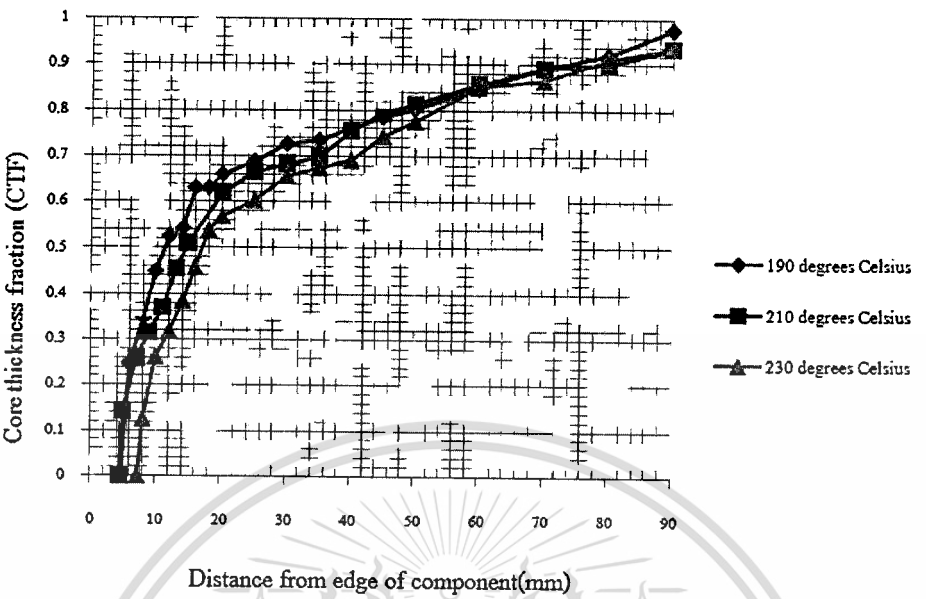

Figure 4.11 Relationship between core thickness fraction and skin temperatures from experiment

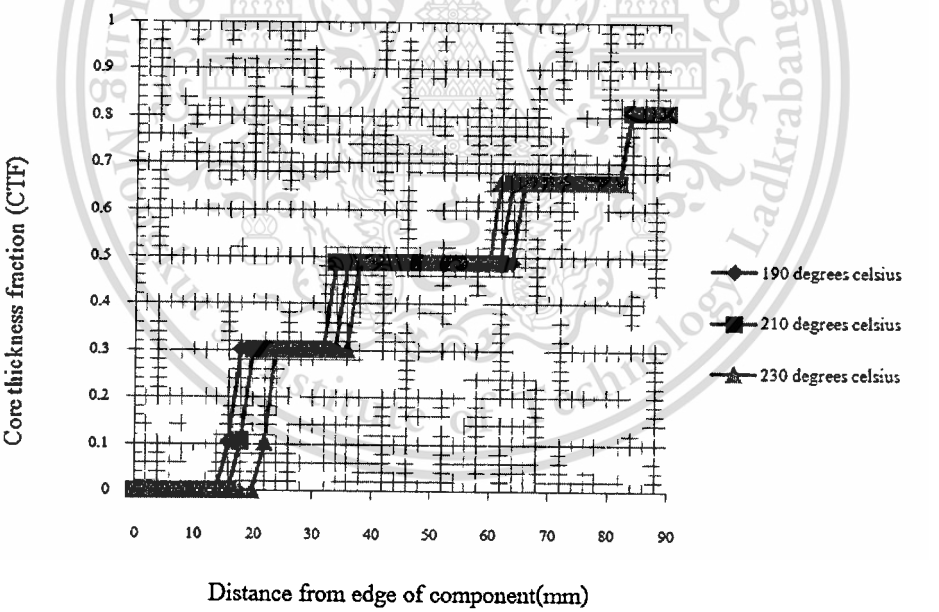

Figure 4.12 Relationship between core thickness fraction and skin temperatures from Moldflow

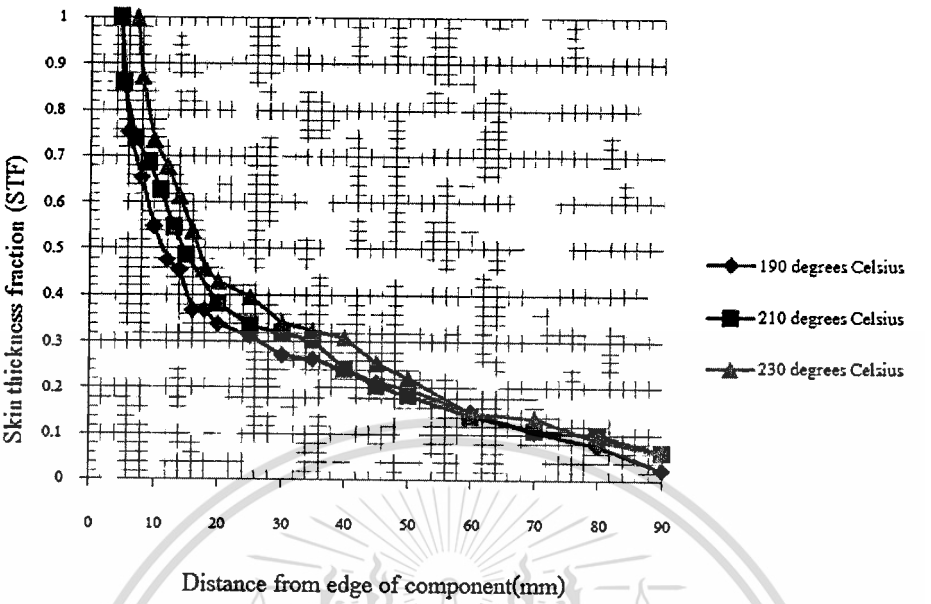

Figure 4.13 Relationship between skin thickness fraction and skin temperatures from experiment

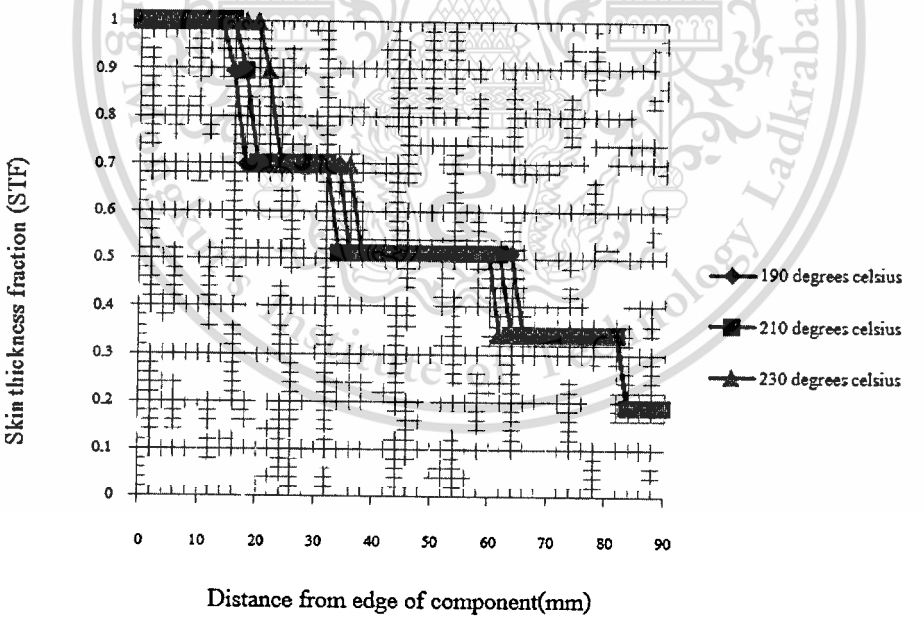

Figure 4.14 Relationship between skin thickness fraction and skin temperatures from Plastic injection molding simulation software

.

4.1.1.5 Effect of core temperatures

From **Figure 4.15** and **Figure 4.16,** the relative comparison between experimental and simulated results show similar trend but the profile of skin-core structures from simulation was different. Increasing core temperatures lead to high core thickness fractions because higher core temperatures conduce to low viscosity. On the other hand, increasing core temperature lead to low skin thickness fractions is shown in **Figure 4.17** and **Figure 4.18.** These are consistent with Cross-Exp Model (C-MOLD Filling Stage Model) in Chapter2.

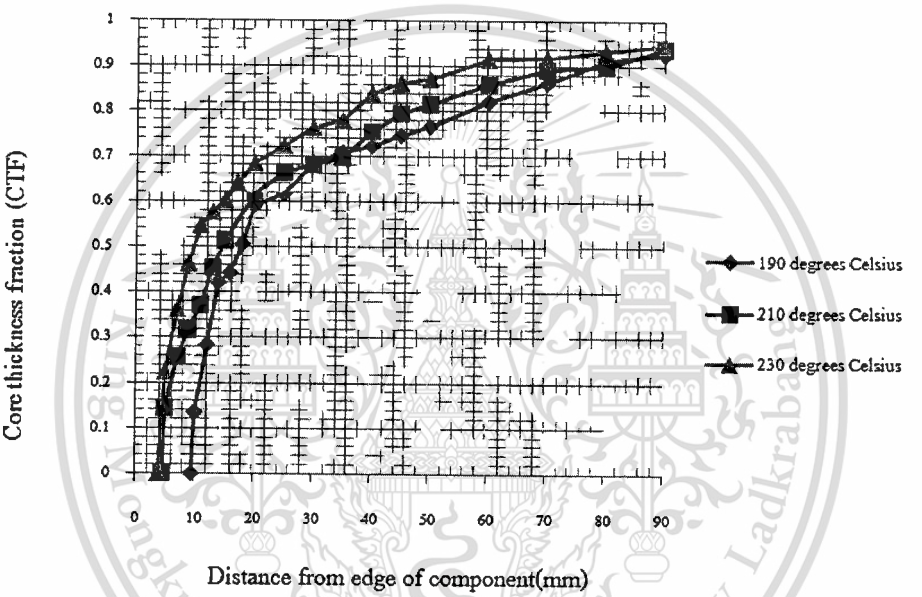

Figure 4.15 Relationship between core thickness fraction and core temperatures from experiment

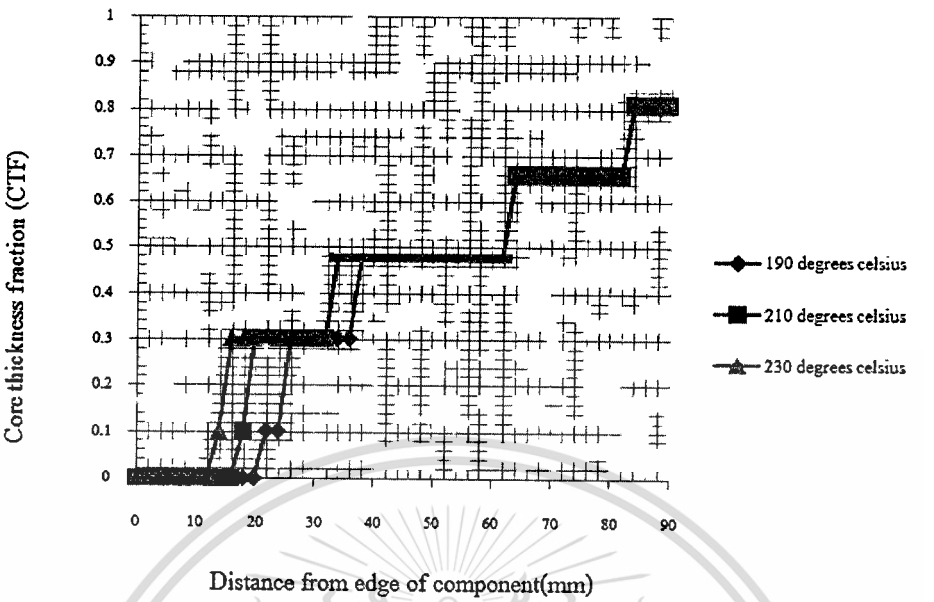

Figure 4.16 Relationship between core thickness fraction and core temperatures from Plastic injection molding simulation software

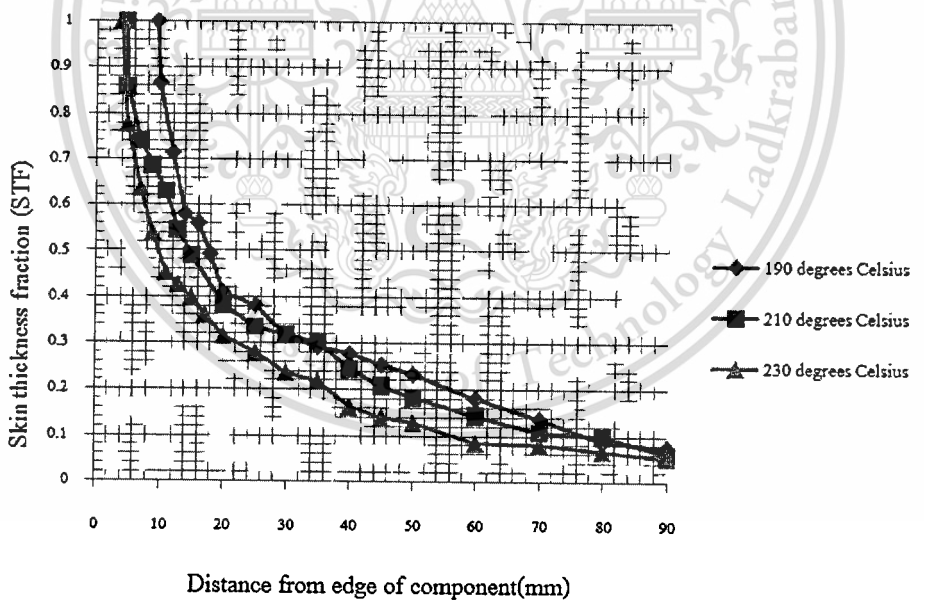

Figure 4.17 Relationship between skin thickness fraction and core temperatures from experiment

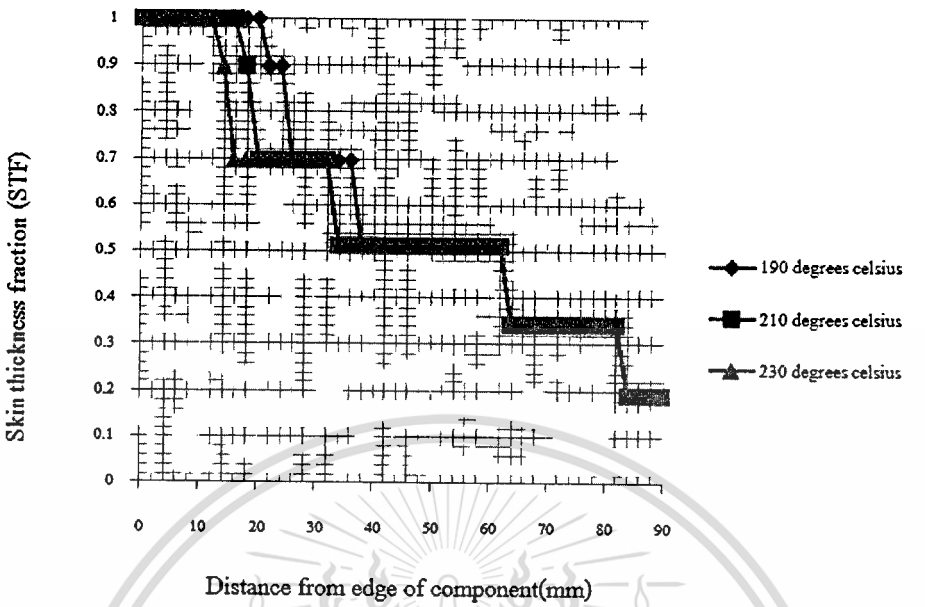

Figure 4.18 Relationship between skin thickness fraction and core temperatures from Plastic injection molding simulation software

4.1.1.6 Effect of skin viscosities

From **Figure 4.19** and **Figure 4.20**, the relative comparison between experimental and simulated results show similar trend but the profile of skin-core structures from simulation was different. Increasing skin viscosities lead to high core thickness fractions and shapes of core penetration tend to be more round than low skin viscosities. On the other hand, increasing skin viscosity lead to low skin thickness fractions is shown in **Figure 4.21** and **Figure 4.22.** These results show viscosities play important role in the profile of skin-core structures.

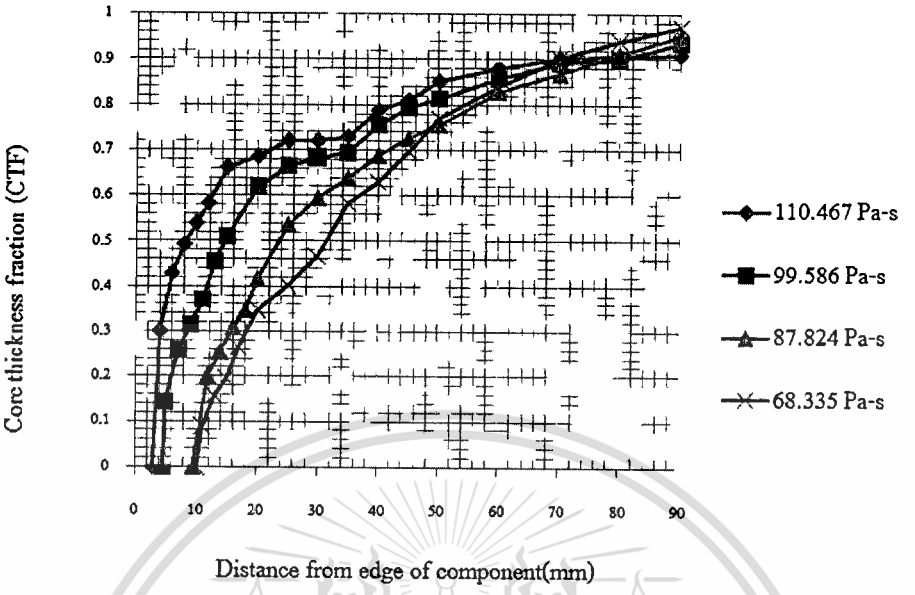

Figure 4.19 Relationship between core thickness fraction and skin viscosities from experiment

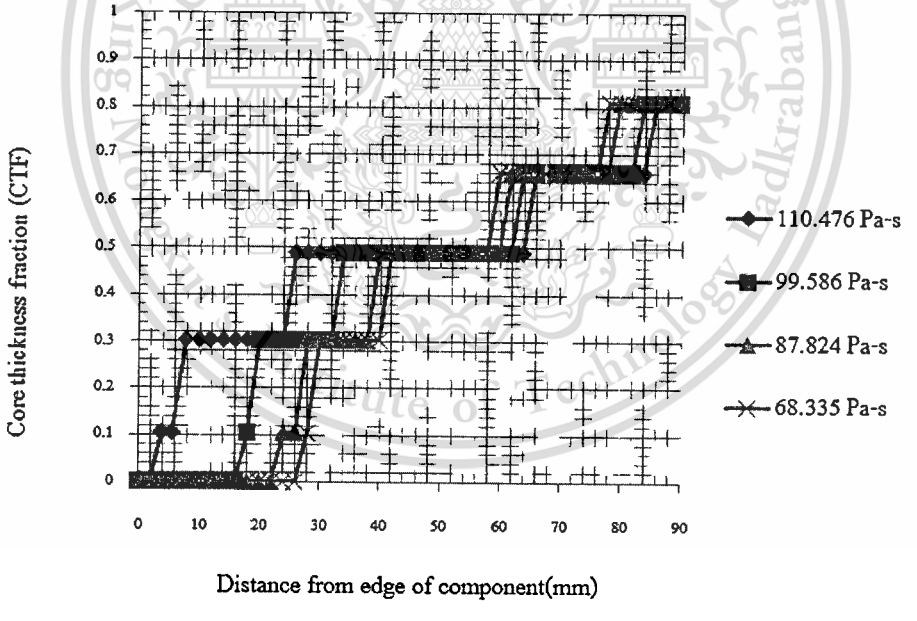

Figure 4.20 Relationship between core thickness fraction and skin viscosities from Plastic injection molding simulation software

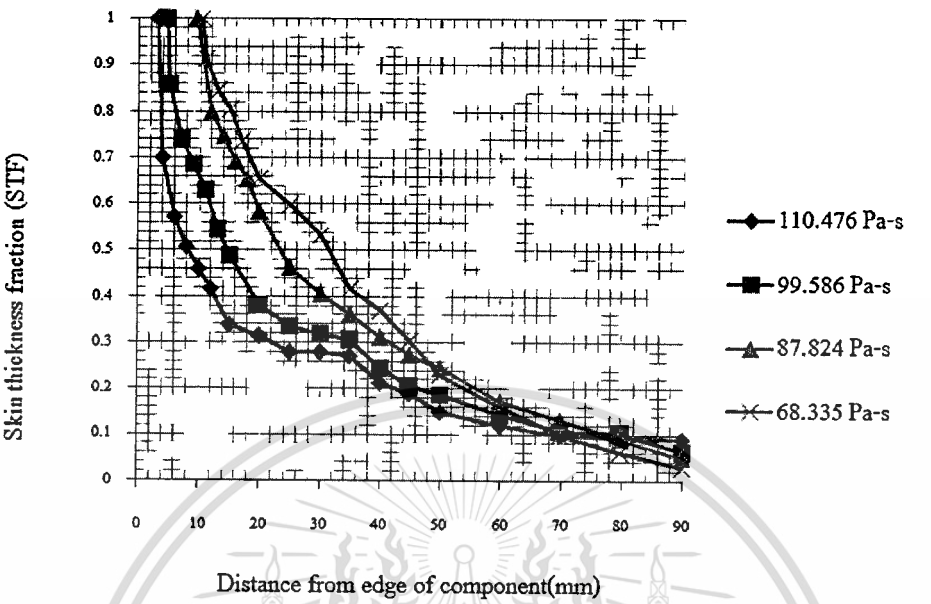

Figure 4.21 Relationship between skin thickness fraction and skin viscosities from experiment

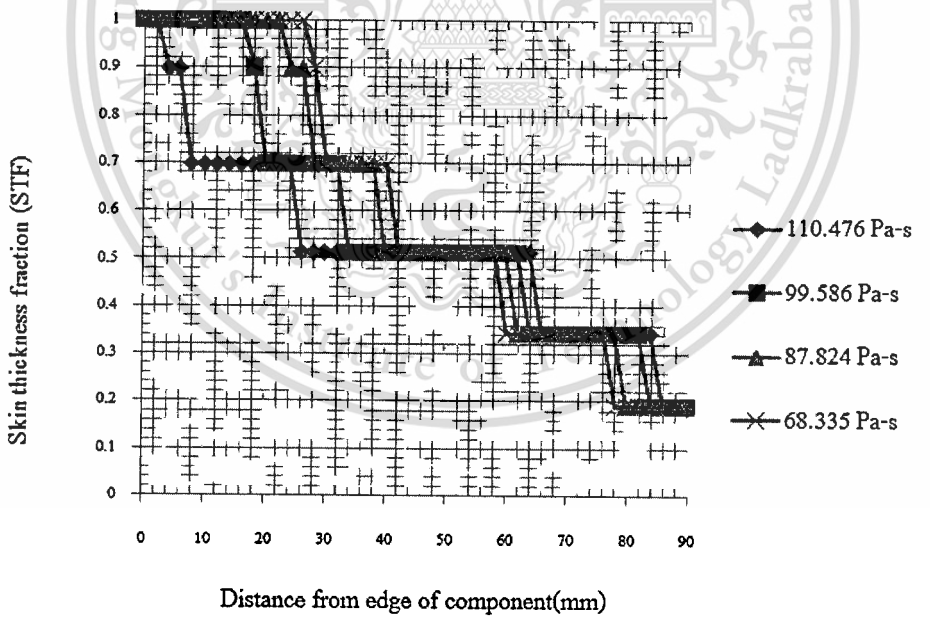

Figure 4.22 Relationship between skin thickness fraction and skin viscosities from Plastic injection molding simulation software

4.1.1.7 Effect of core viscosities

From **Figure 4.23** and **Figure 4.24**, the relative comparison between experimental and simulated results show similar trend but the profile of skin-core structures from simulation was different. Decreasing core viscosities lead to high core thickness fractions at the beginning of edge component then core thickness fractions were slightly increased. Moreover, the shapes of core penetration tend to be more round than high core viscosities. On the other hand, decreasing core viscosity lead to low skin thickness fractions is shown in **Figure 4.25** and **Figure 4.26.** Higher viscosity ratios (η_{skin}/η_{core}) will lead to a core breakthrough.

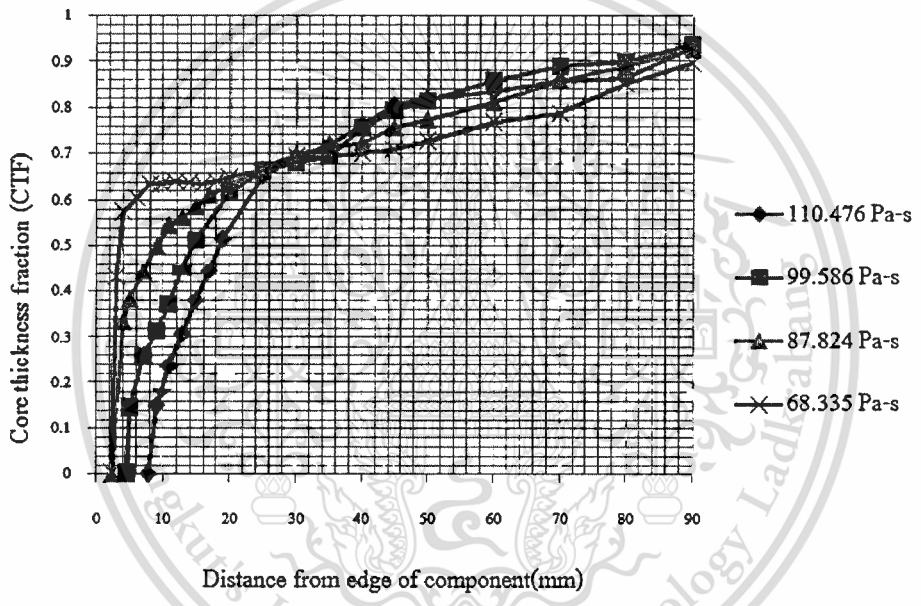

Figure 4.23 Relationship between core thickness fraction and core viscosities from experiment

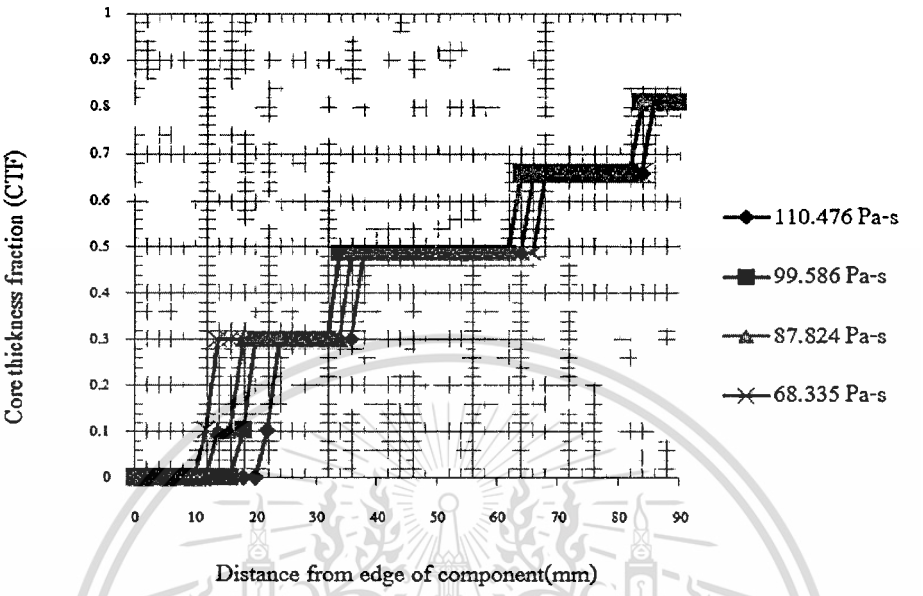

Figure 4.24 Relationship between core thickness fraction and core viscosities from Plastic injection molding simulation software

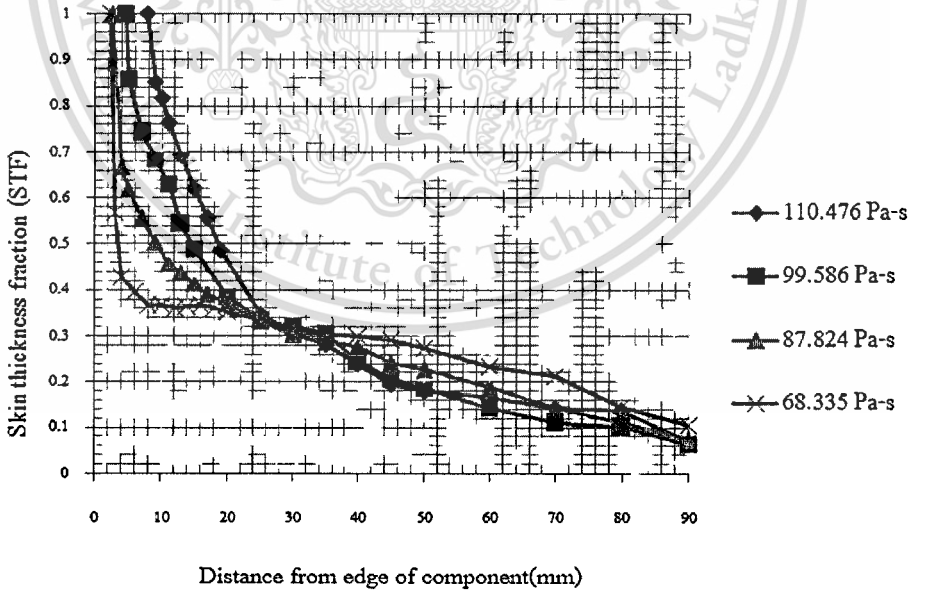

Figure 4.25 Relationship between skin thickness fraction and core viscosities from experiment

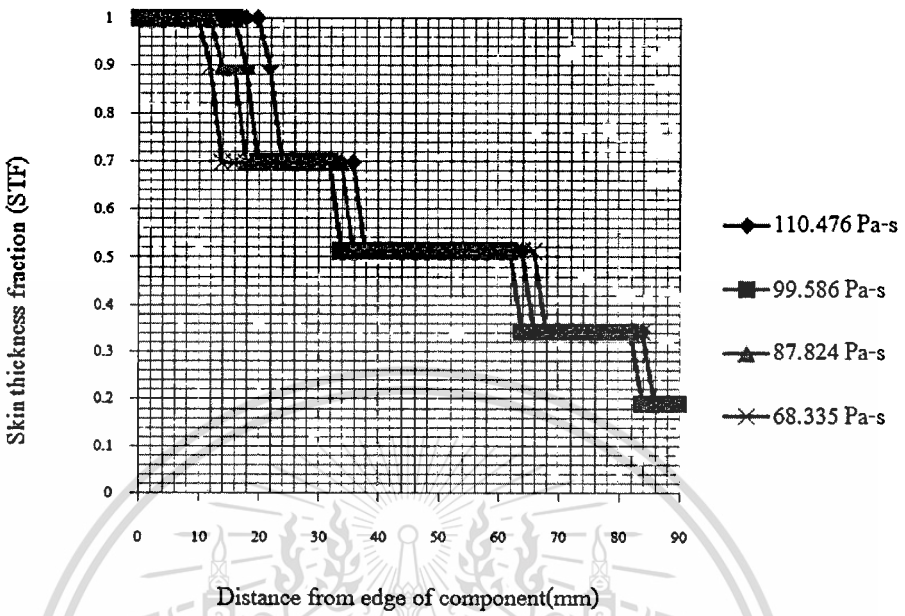

Figure 4.26 Relationship between skin thickness fraction and core viscosities from Plastic injection molding simulation software

4.1.1.8 Effect of wood plastic composite contents on sandwich structure (Skin: PP HP420J, Core: wood composite)

From **Figure 4.27** and **Figure 4.28**, increasing wood flour contents in core structure lead to low core thickness fractions at the beginning of edge component then core thickness fractions were highly increased. Moreover, the shapes of core penetration at high wood contents tend to be sharper than low wood flour content. On the other hand, increasing wood flour contents lead to high skin thickness fractions. These are consistent with (Cross-Exp Model (C-MOLD Filling Stage Model)) and Molecular weight from Zero-Shear viscosity in Chapter2. The relation with high wood contents conduces to high viscosity.

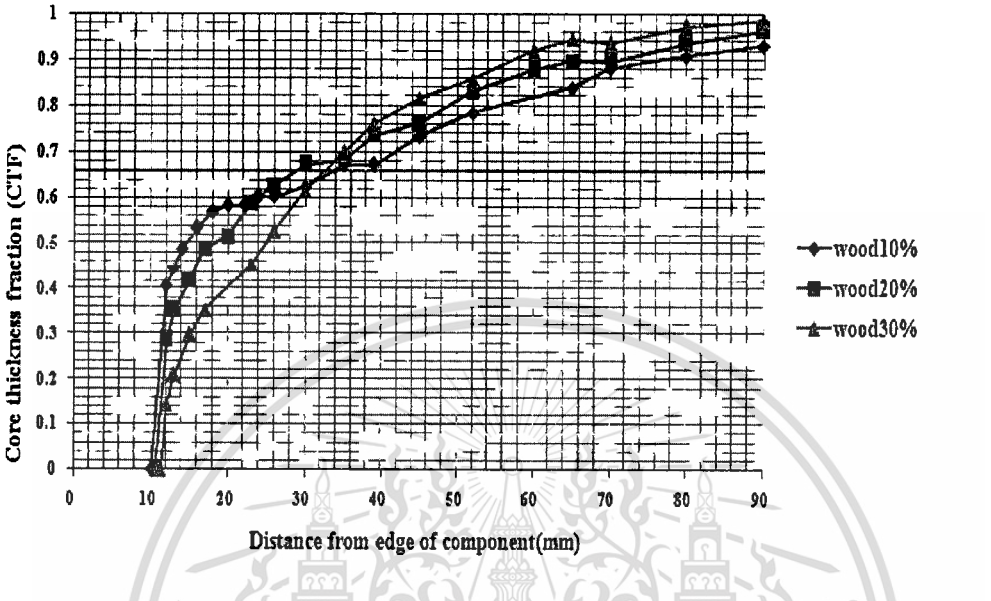

Figure 4.27 Relationship between core thickness fraction and wood plastic composite content from experiment

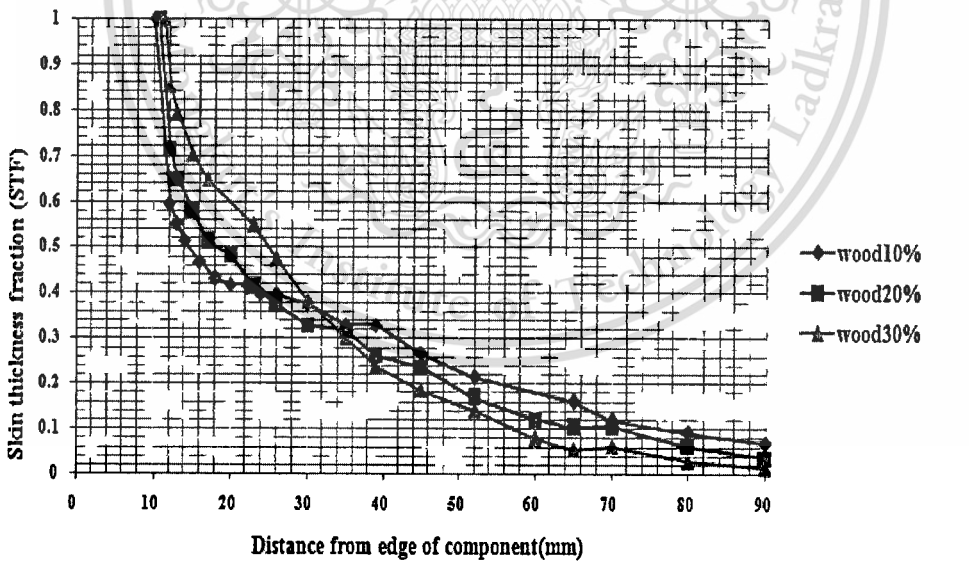

Figure 4.28 Relationship between skin thickness fraction and wood plastic composite content from experiment

In this section, the correlation between the viscosity ratios (η_A / η_B) and the skin to core injection speed (VA/VB) were investigated. Polypropylenes (PP) were used as skin and core material. The skin and core material were investigated by changing the viscosity ratios of skin to core. Afterwards, the optimum conditions for each combination were recorded. The relationship between skin/core viscosity ratios and skin/core injection speed ratios was found to be a linear trend as in **Figure 4.29**.

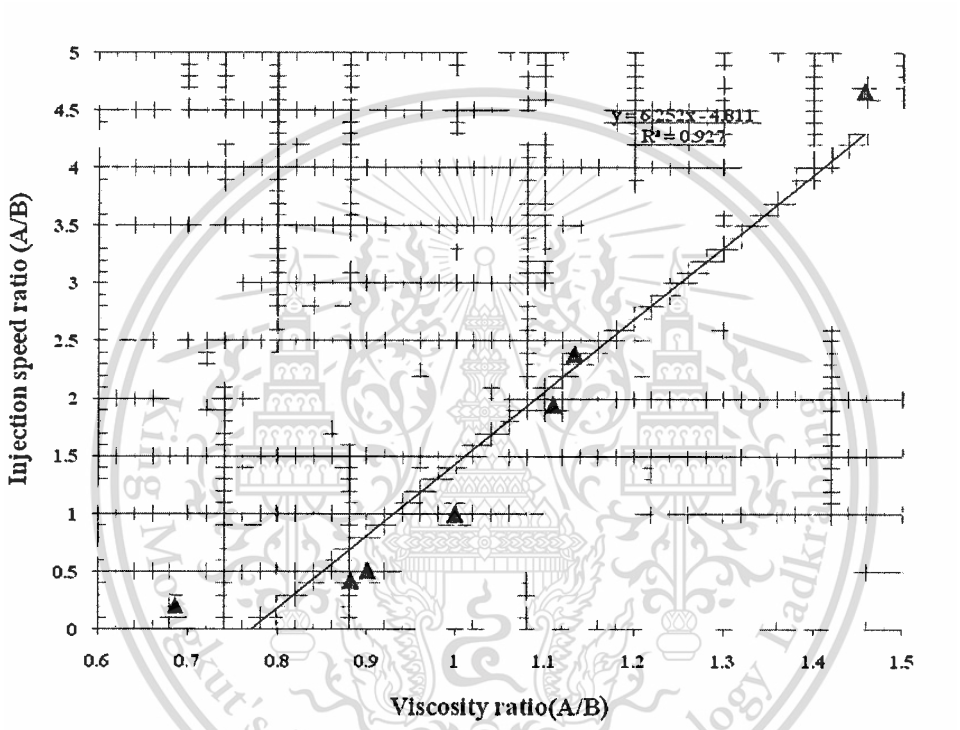

Figure 4.29 Relationship between skin/core viscosity and injection speed ratios

The correlation between η_A / η_B and VA/VB is y=6.252x-4.811

Where x is skin/core viscosity ratios.

y is skin/core injection speed ratios.

R^2 = 92.7%, which mean 92.7 of data are applicable.

4.2 Rheological Properties testing

4.2.1 Effect of pure polypropylene and wood plastic composite on Melt flow index testing

The melt flow index of pure polypropylene (HP420J, HP740H, HP500N and P440J) and wood plastic composite (PP HP500N mixed wood flour content 10 wt%, wood flour,20 wt% and wood flour and 30 wt%) are shown in **Table 4.1**. The melt flow index was decrease when increasing wood flour contents. Because polypropylene was melt first and the characteristic of wood fiber was against the flow. Thus, melt flow index was decrease.

Table 4.1 Melt flow index values of material at 230 °C

Sample	MFI(g/10min)
Polypropylene (HP740H)	2.1
Polypropylene (HP420J)	3
Polypropylene (P440J)	5
Polypropylene (HP500N)	12
PP HP500N with 10 wt% wood flour	10.84
PP HP500N with 20 wt% wood flour	9.42
PP HP500N with 30 wt% wood flour	7.53

4.2.2 Effect of pure polypropylene and wood plastic composite on Capillary rheometer testing

4.2.2.1 Effect of temperatures

From the **Figure 4.30**, it is clear that shear viscosities decreases with increasing temperatures. This was due to the accelerated molecular motion at higher temperature due to the availability of greater free volume and also due to the decreasing entanglement density and weaker intermolecular interactions at higher temperature.

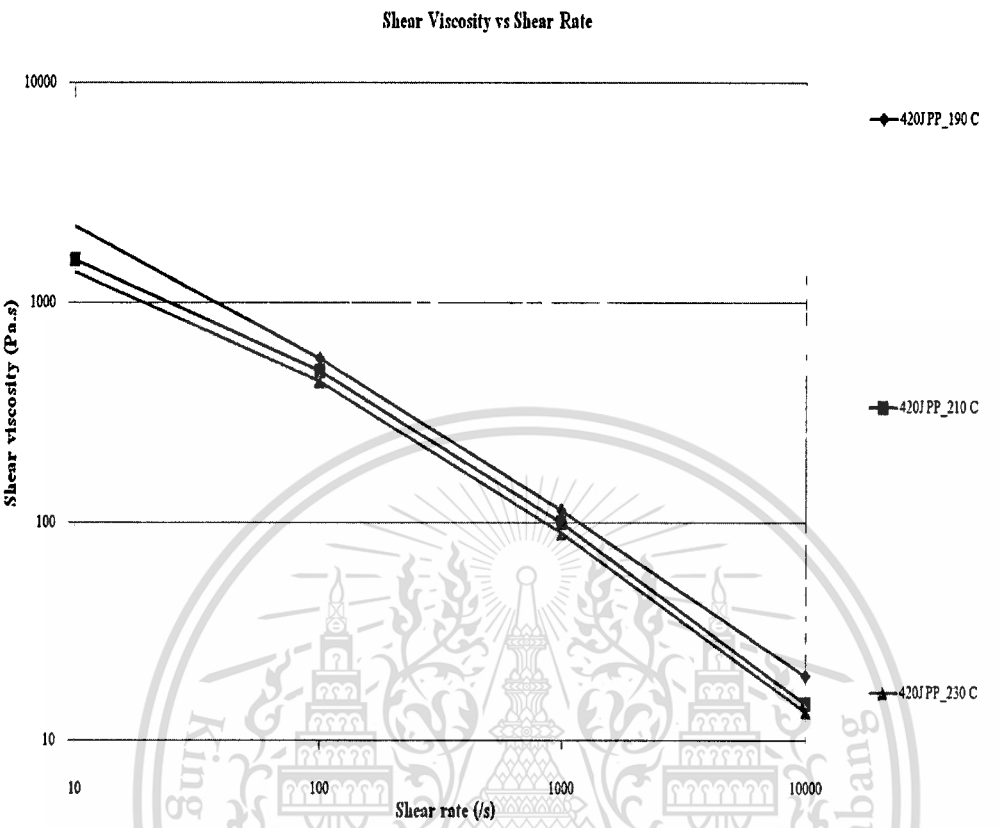

Figure 4.30 Plots of viscosities against shear rates by various temperatures

4.2.2.2 Effect of viscosities

The overall results show injection speed and viscosity are the major factor and the melt temperature is the minor factor for controlling the profile of co-injection process. Skin-core viscosities play important role on the sandwich structures. The viscosity changes with temperature and injection speed as show in **Figure 4.31**.

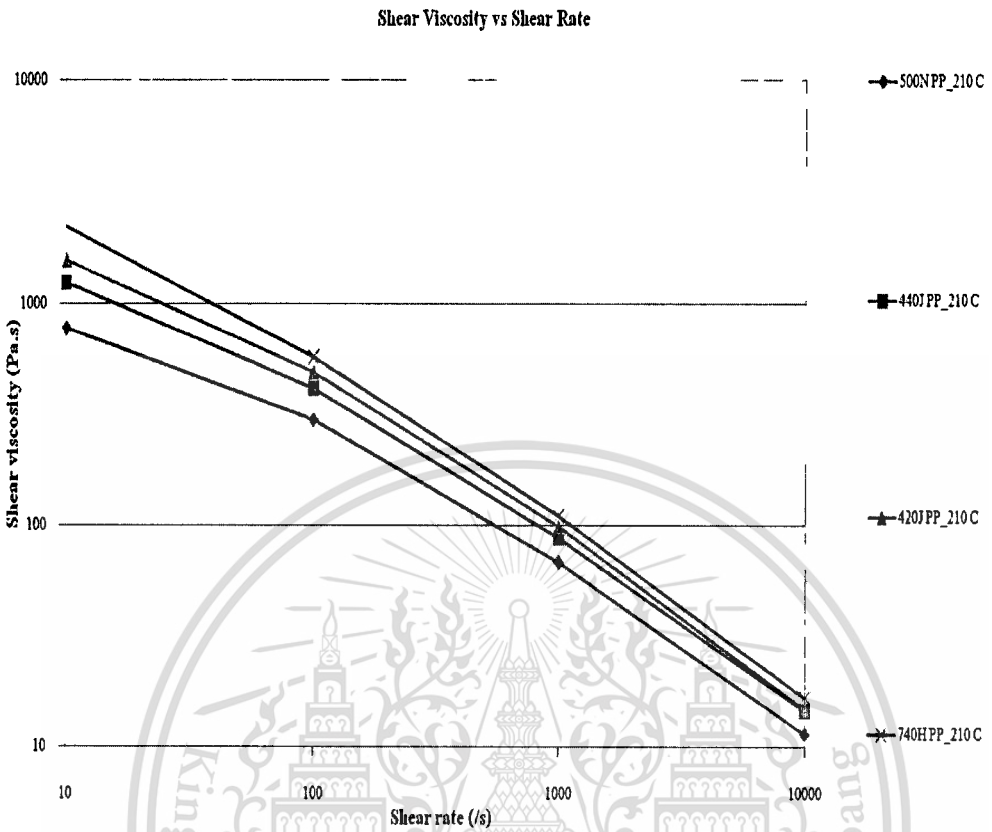

Figure 4.31 Plots of viscosities against shear rates at the various viscosities

4.2.2.3 Effect of wood contents on wood plastic composite

Figure 4.32 shows the variation of shear rates between 20 and 10000 (1/s). It is clear from the figure that the shear viscosities increased with increasing wood flour contents. The increasing of wood flour contents were effect to the shear viscosity because of the rapidly increasing collisions between particles as they become packed more closely to each other. In Chapter2 (Cross-Exp Model (C-MOLD Filling Stage Model)) and Molecular weight from Zero-Shear viscosity show the relation with high wood contents conduce to high viscosity.

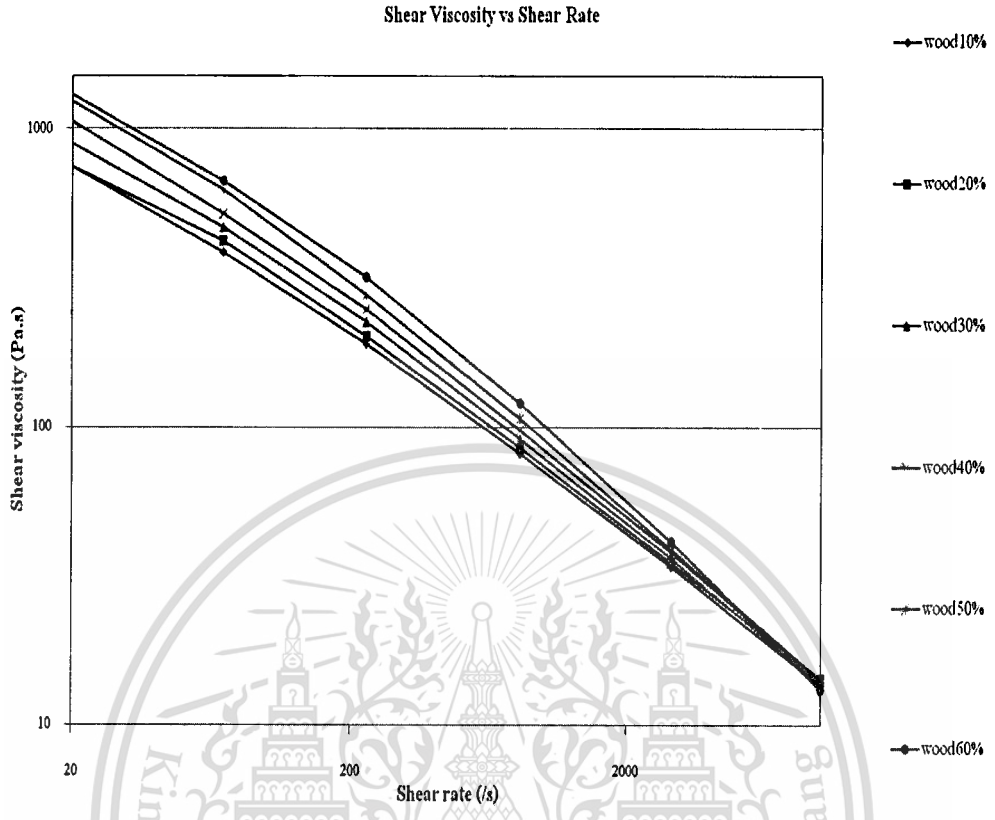

Figure 4.32 Plots of viscosities against shear rates at the various wood flour contents

4.3 Effect of wood plastic composite on mechanical properties

4.3.1 Effect of mechanical properties on sandwich structure

4.3.1.1 Effect of flexural properties

The flexural stress of sandwich specimens (Skin: PP HP420J, Core: wood plastic composite (PP HP500N+wood flour)) and (Skin: wood plastic composite (PP HP500N+wood flour), Core: PP HP420J) were shown in **Figure 4.33** and **4.34**, respectively. The specific of flexural stresses are also listed in **Table 4.2**. The Flexural stresses were increased when wood contents of sandwich specimens increased. Based on this result for sandwich structure with wood plastic composites, it can enhance the flexural stress.

Table 4.2 The specific flexural stress of sandwich specimens

Conditions		
Skin	Core	Flexural stress (Mpa)
PP(HP420J)	PP HP500N with wood10wt%	34.1144
PP(HP420J)	PP HP500N with wood20wt%	34.6806
PP(HP420J)	PP HP500N with wood30wt%	36.9034
PP HP500N with wood10wt%	PP(HP420J)	31.8982
PP HP500N with wood20wt%	PP(HP420J)	32.7456
PP HP500N with wood30wt%	PP(HP420J)	38.0387

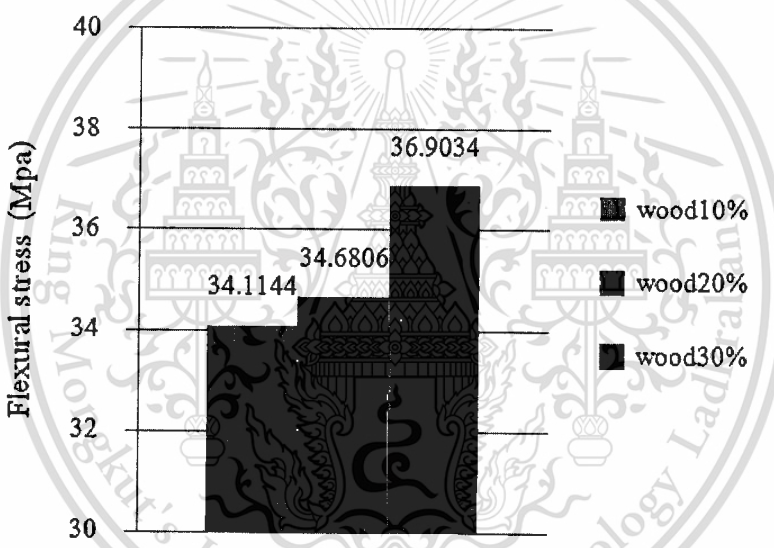

Figure 4.33 Flexural stress of sandwich structure (Skin: PP HP420J, Core: wood plastic composite (PP HP500N+wood flour)) by various wood contents

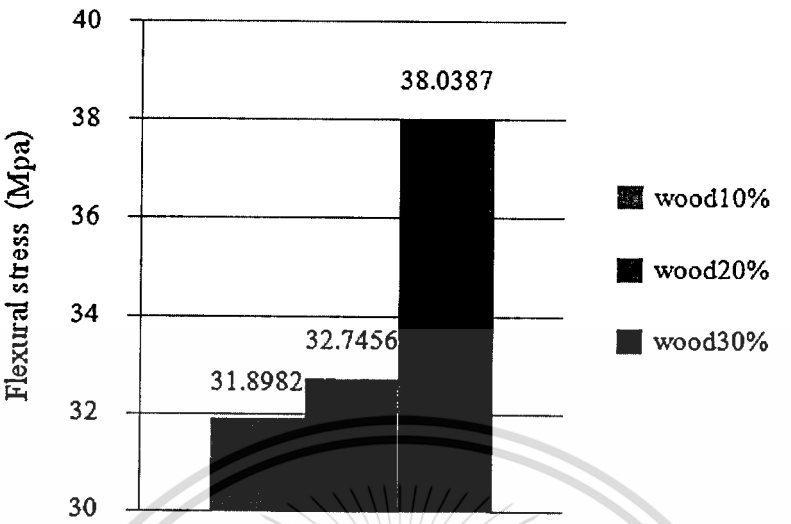

Figure 4.34 Flexural stress of sandwich structure (Skin: wood plastic composite (PP HP500N+wood flour), Core: PP HP420J) by various wood contents

Table 4.3 The specific flexural stress stress and skin-core viscosity ratios of sandwich specimens

Skin material	Skin material	Skin-core viscosity ratios	Flexural stress (Mpa)
PP(420J)	WPC (wood10%)	1.44	34.1144
PP(420J)	WPC (wood20%)	1.31	34.6806
PP(420J)	WPC (wood30%)	1.13	36.9034
WPC (wood10%)	PP(420J)	0.69	31.8982
WPC (wood20%)	PP(420J)	0.76	32.7456
WPC (wood30%)	PP(420J)	0.88	38.0387

Figure 4.35, Figure 4.36 and **Table 4.3** show the relationship between skin-core viscosity ratios and flexural stress of sandwich structure. Based on this result, the flexural stress of sandwich specimens (Skin: PP, Core: WPC) were decreased when increasing skin-core viscosity ratios because increasing skin-core viscosity ratios occurred with decreasing wood contents but the flexural stress of sandwich specimens (Skin: WPC, Core: PP) were increased when increasing skin-core viscosity ratios because increasing skin-core viscosity ratios occurred with increasing wood contents.

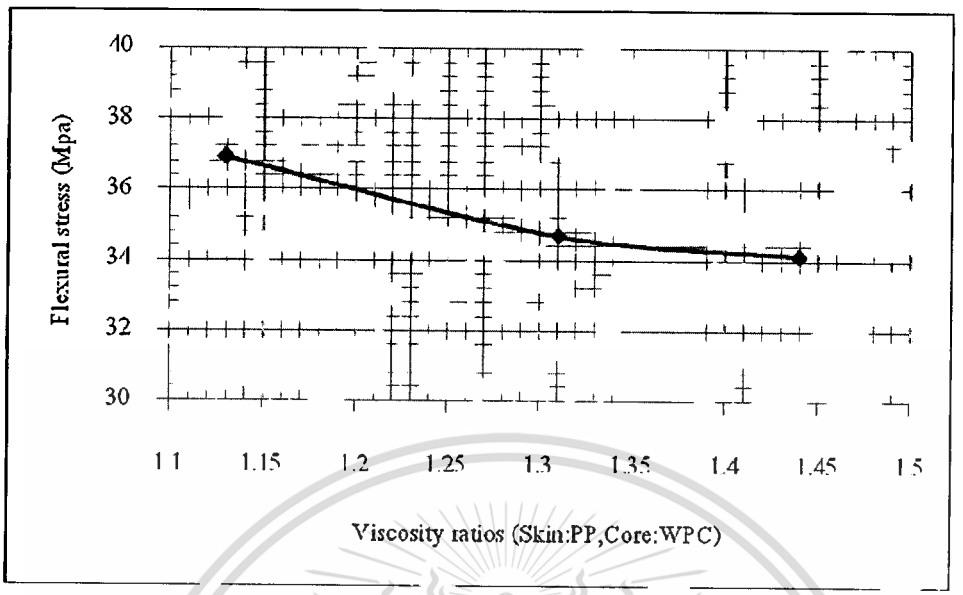

Figure 4.35 Relationship between skin-core viscosity ratios and flexural stress of sandwich structure (Skin: PP HP420J, Core: Wood plastic composite (PP HP500N+wood flour)) by various wood contents

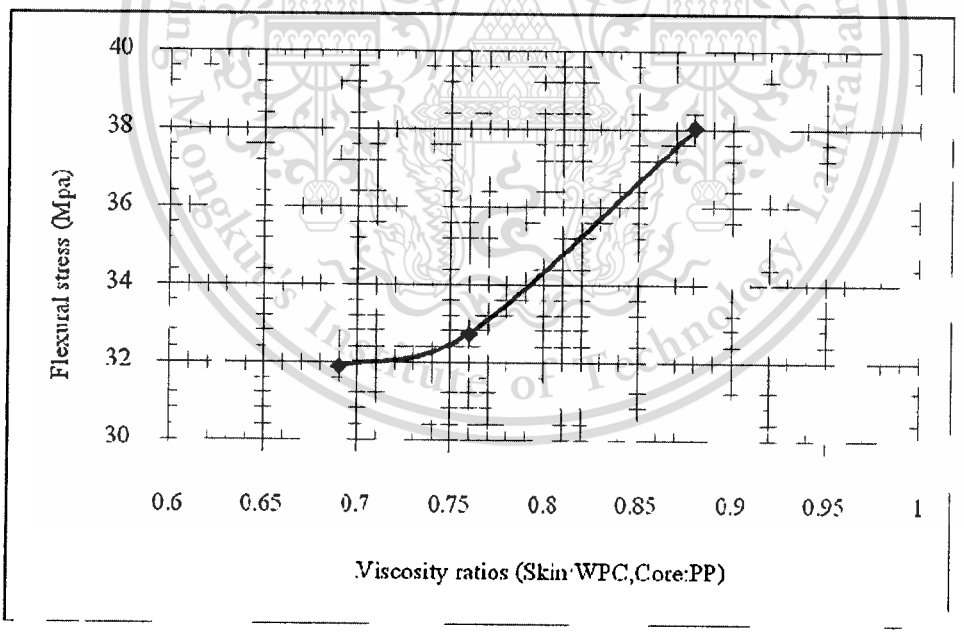

Figure 4.36 Relationship between skin-core viscosity ratios and flexural stress of sandwich structure (Skin: Wood plastic composite (PP HP500N+wood flour), Core: PP HP420J) by various wood contents

4.3.1.2 Effect of notched impact strength on wood plastic composite

Figure 4.37 show notched izod impact strength (energy absorbed/ thickness) of wood plastic composite (PP HP500N+wood flour). In this result, increasing fiber contents conduce to decreases energy to break. It can be observed the properties of wood flour used in WPC are high flexural but low impact strength.

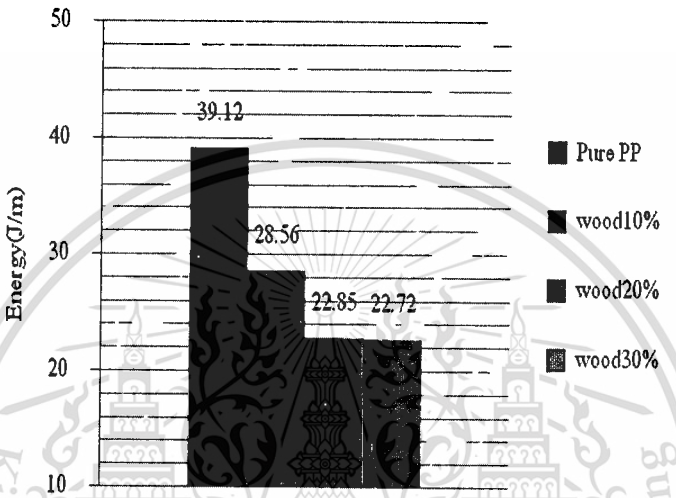

Figure 4.37 Notched izod impact strength (energy absorbed/ thickness) of wood plastic composite by various wood contents

4.3.1.3 Effect of notched impact properties on sandwich structure (Skin: PP, Core: wood plastic composite)

The results show the similar trends of notched impact strength on sandwich specimen as show in **Figure 4.38**. At low distance from the edge of component, high wood flour contents conduce to high notched impact strength with low core thickness fraction because the notched impact strength are depending on the percentage of wood flour contents and the profile of skin-core structures.

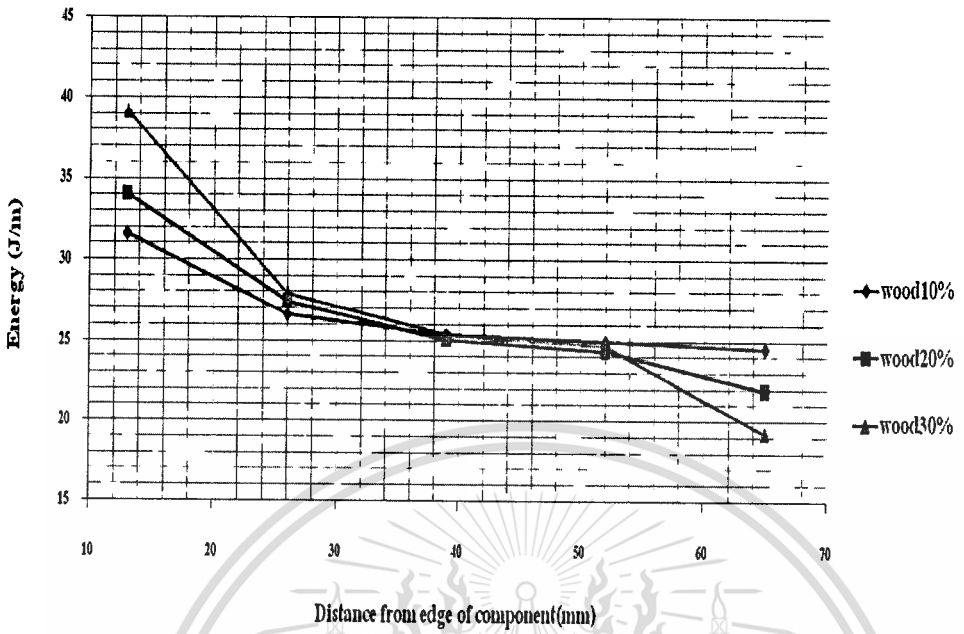

Figure 4.38 Notched impact strength (energy absorbed/ thickness) of sandwich specimen (Skin: PP HP 420J, Core: wood plastic composite (PP HP500N+wood flour)) by various wood contents in core layer

4.3.1.4 Comparing notched impact properties from experiment and calculation at wood contents 10wt% in core layer

The trend line of notched izod impact strength (energy absorbed/ thickness) of sandwich specimen (Skin: PP HP 420J, Core: wood plastic composite (PP HP500N+wood flour)) at wood contents 10wt% in core layer is shown in **Figure 4.39**. The results show a trend line of notched impact strength form experiment is slightly lower than calculation. The percentage error between calculation and experiment of five positions (first position started from the edge which opposite the gate) on sandwich specimen are shown in **Table 4.4**.

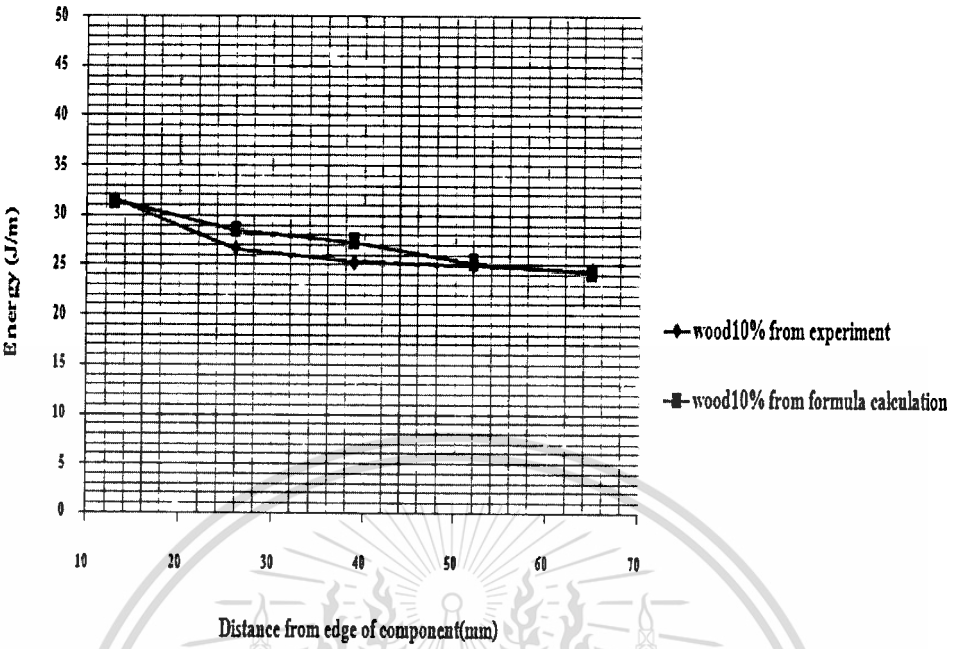

Figure 4.39 Comparing notched impact strength (energy absorbed/ thickness) of sandwich specimen (Skin: PP HP 420J, Core: wood plastic composite (PP HP500N+wood flour)) from experiment and formula calculation at wood contents 10wt% in core layer

Table 4.4 Percentage error of notched impact strength

Position	Percentage Error of Notched impact strength (energy absorbed/ cross-sectional thickness)
13	0.509
26	6.812
39	7.314
52	1.192
65	0.881

The morphology of this experiment was investigated by using SEM micrographs of sandwich specimens (Skin: PP HP420J, Core: wood plastic composite (PP HP500N+10% wood flour content)). The sandwich specimen was cut into three pieces perpendicular the flow direction by cutting start from the edge of component and prepared by fracture parallel the flow direction in liquid nitrogen. The excellent adhesion of skin-core structure was observed as show in **Figure 4.50, Figure 4.51, and Figure 4.52** (P.102).

4.4 The effect of moisture contents on wood plastic composites

The effect of moisture contents on wood plastic composites before and after reduce moisture by vacuum oven are shown in **Figure 4.40** and **Figure 4.41** respectively. As can be seen, the moisture contents of composites increased with increase wood flour contents because polypropylene is hydrophobic and the wood flour is hydrophilic, the absorption of water depends on the wood fibers alone.

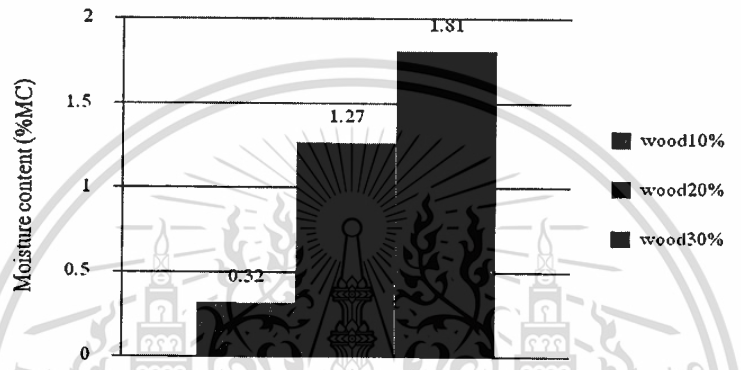

Figure 4.40 Moisture contents of wood plastic composite before reduce moisture by vacuum oven

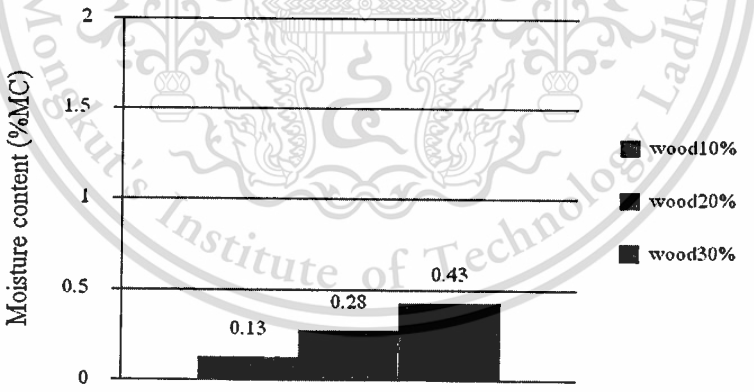

Figure 4.41 Moisture contents of wood plastic composite after reduce moisture by vacuum oven

Wood fiber variability has a significant effect on the mechanical and physical properties studied. This effect was explained by variations in wood fiber contents. Composites made with hardwood particles exhibit lower water absorption compared to softwood particles. Differences in chemical composition between hardwood and softwood were among the plausible explanations

for the differences in moisture. Increasing hardwood fiber contents lead to improve flexural property and high moisture contents but reduce energy to break.

4.5 Sieve analysis

This investigation was required to shake the wood flour over nested sieves. Sieves were selected to furnish information required by specification. The sieves were nested in order of decreasing size from the top to the bottom and the wood flour was placed on the top sieve. Sieves are shaken in a mechanical shaker to provide complete separation.

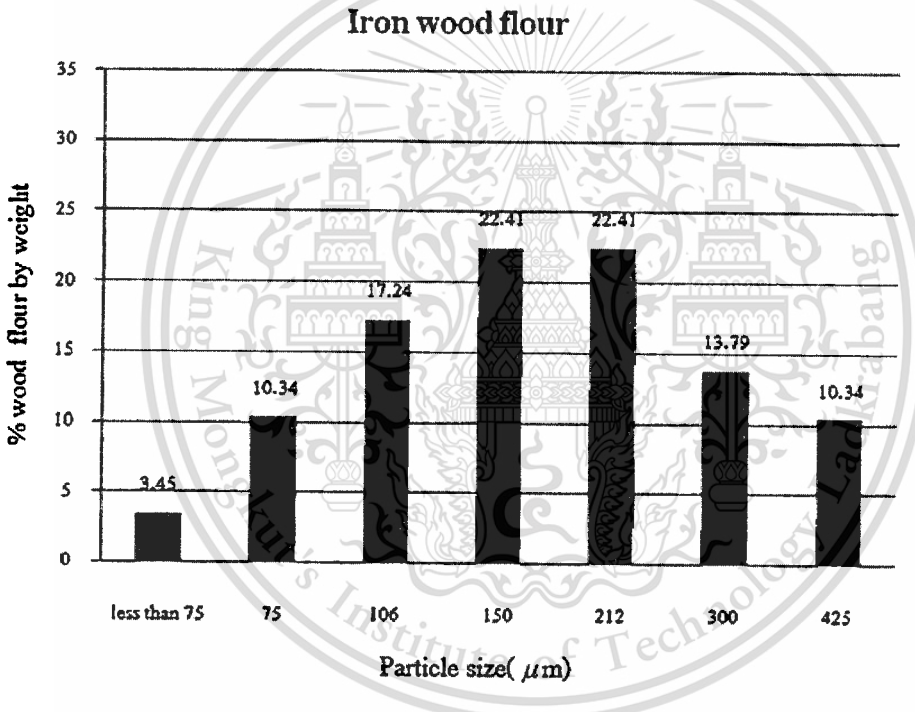

Figure 4.42 The particle size classification of wood flour by using Sieve analysis

The results show most of the particle sizes using Sieve analysis are around 150-212 μ m these are consistent with SEM micrograph (**Figure 4.42**).

4.6 Effect of wood flour percentage on Morphological structure

4.6.1 Scanning electron microscopy (SEM)

Scanning electron microscopy (SEM) was used to measure wood particle size and fracture surfaces of sandwich specimens. The SEM micrograph showing the particle characteristics of wood flour used in the study are shown in **Figure 4.43**. According to the micrograph, the average size of this particular wood flour is around 200 μm .

Figure 4.43 SEM micrograph showing the particle characteristics of wood flour used in the study

The fracture surfaces determined were parallel to the flow direction. The SEM micrographs of sandwich specimens (Skin: PP HP420J, Core: wood plastic composite (PP HP500N+wood flour)) and (Skin: wood plastic composite (PP HP500N+wood flour), Core: PP HP420J) by various wood flour contents are shown in **Figure 4.44, Figure 4.45, Figure 4.46, Figure 4.47, Figure 4.48** and **Figure 4.49** ,respectively.

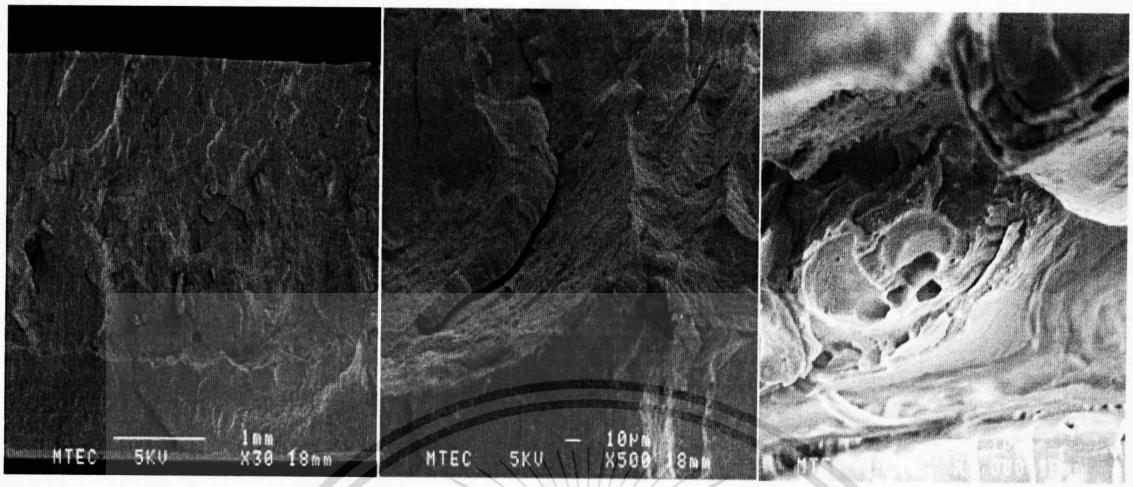

(a) (b) (c)

Figure 4.44 The SEM micrographs of sandwich specimens (Skin: PP HP420J, Core: wood plastic composite(PP HP500N+wood flour)) (a) 10% wood content per weight unit with magnification of 30x, (b) 10% wood content per weight unit with magnification of 500x, (c) 10% wood content per weight unit with magnification of 5000x

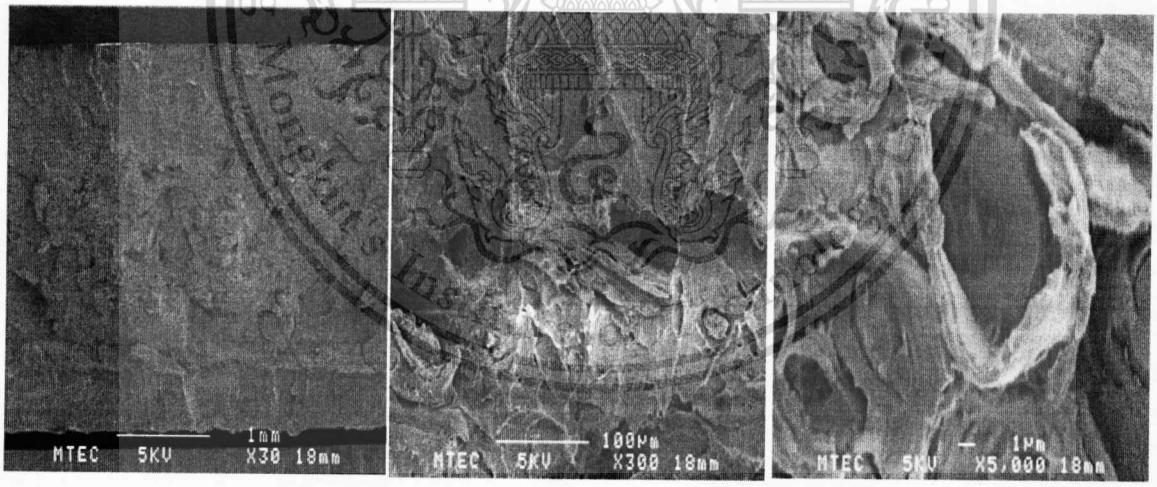

(a) (b) (c)

Figure 4.45 The SEM micrographs of sandwich specimens (Skin: PP HP420J, Core: wood plastic composite(PP HP500N+wood flour)) (a) 20% wood content per weight unit with magnification of 30x, (b) 20% wood content per weight unit with magnification of 300x, (c) 20% wood content per weight unit with magnification of 5000x

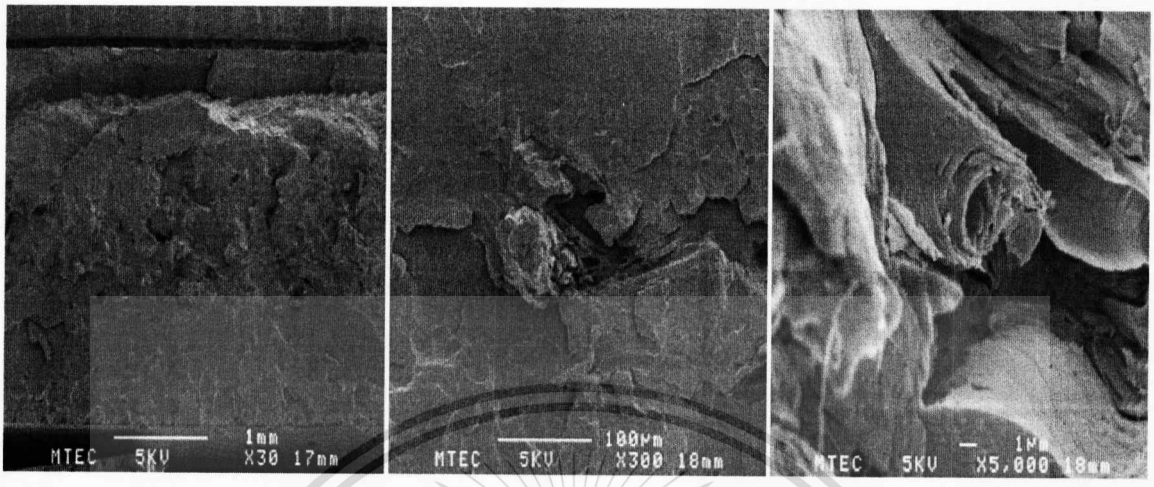

(a) (b) (c)

Figure 4.46 The SEM micrographs of sandwich specimens (Skin: PP HP420J, Core: wood plastic composite(PP HP500N+wood flour)) (a) 30% wood content per weight unit with magnification of 30x, (b) 30% wood content per weight unit with magnification of 300x, (c) 30% wood content per weight unit with magnification of 5000x

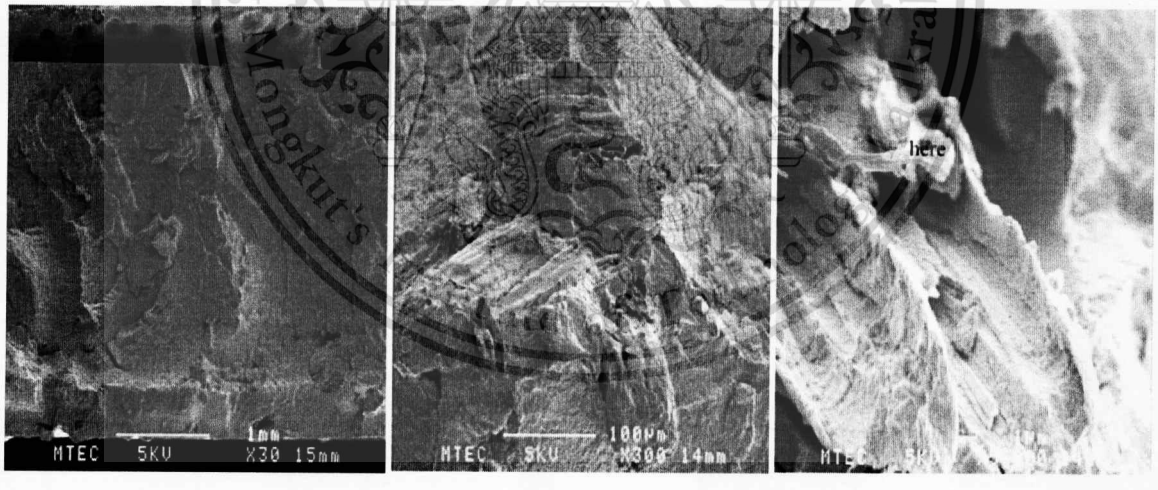

(a) (b) (c)

Figure 4.47 The SEM micrographs of sandwich specimens (Skin: wood plastic composite(PP HP500N+wood flour), Core: PP HP420J) (a) 10% wood content per weight unit with magnification of 30x, (b) 10% wood content per weight unit with magnification of 300x, (c) 10% wood content per weight unit with magnification of 5000x

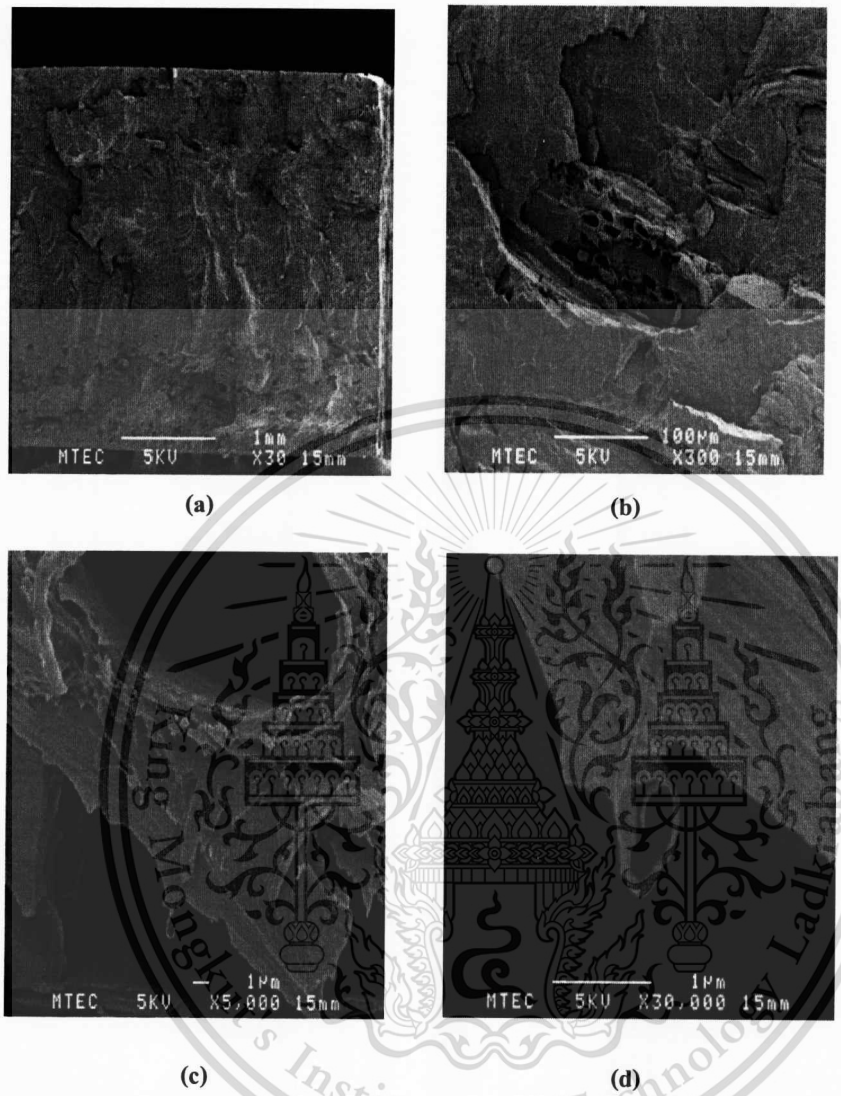

Figure 4.48 The SEM micrographs of sandwich specimens (Skin: wood plastic composite(PP HP500N+wood flour), Core: PP HP420J) (a) 20% wood content per weight unit with magnification of 30x, (b) 20% wood content per weight unit with magnification of 300x, (c) 20% wood content per weight unit with magnification of 5000x, (d) 20% wood content per weight unit with magnification of 30000x

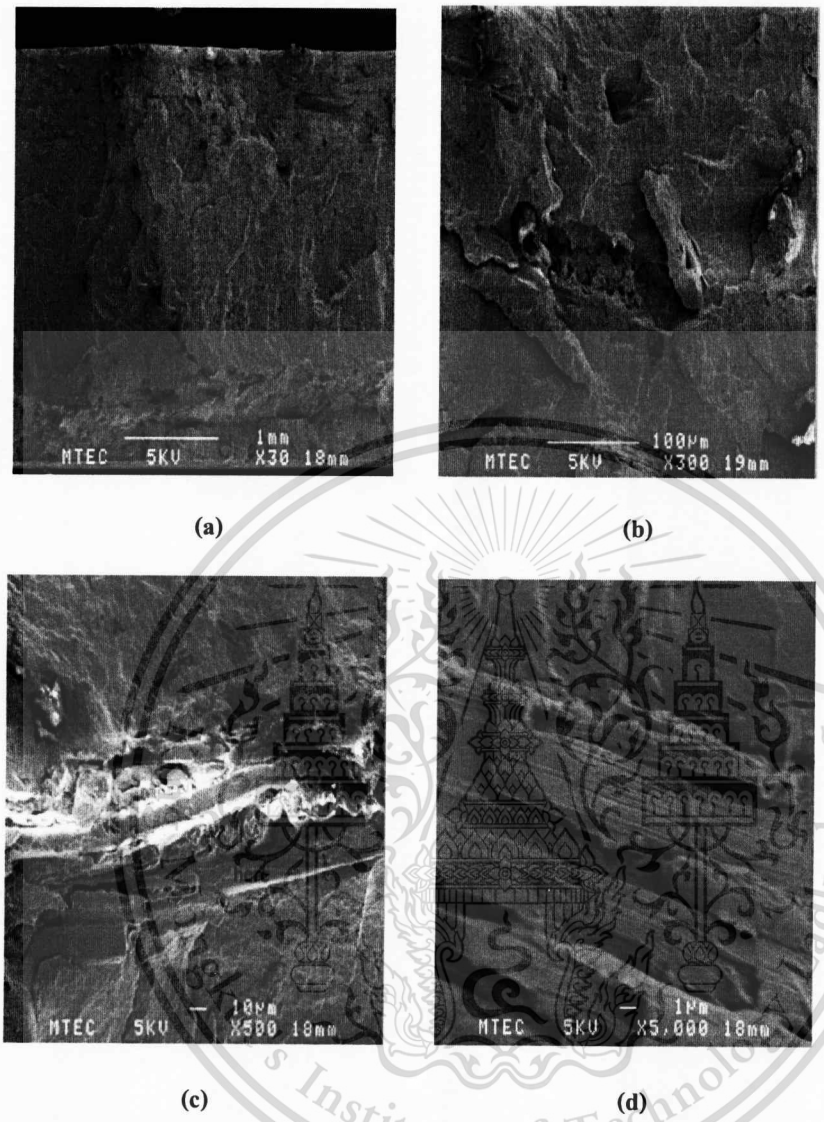

(a) (b)

(c) (d)

Figure 4.49 The SEM micrographs of sandwich specimens (Skin: wood plastic composite (PP HP500N+wood flour), Core: PP HP420J) (a) 30% wood content per weight unit with magnification of 30x, (b) 30% wood content per weight unit with magnification of 300x, (c) 30% wood content per weight unit with magnification of 500x, (d) 30% wood content per weight unit with magnification of 5000x

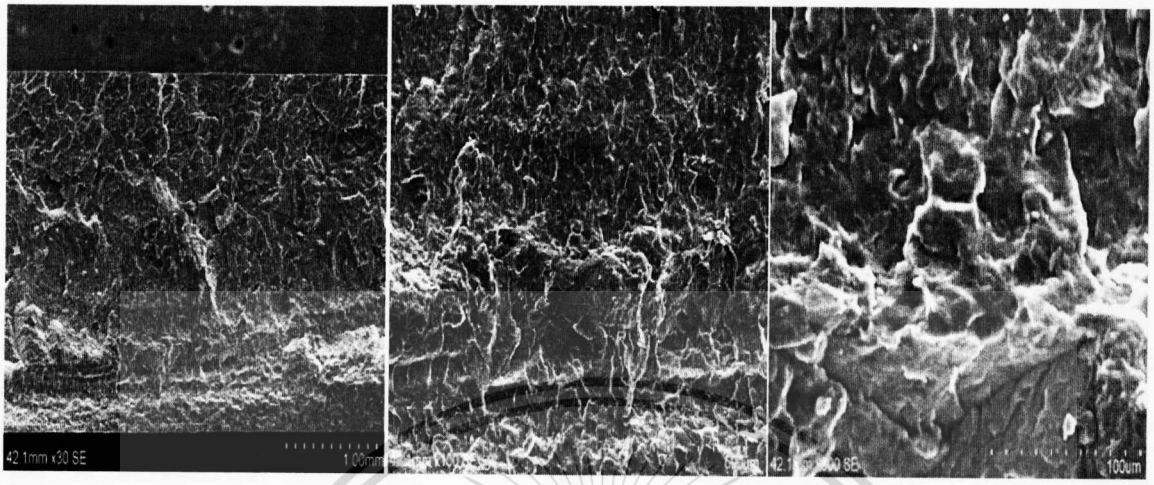

(a) (b) (c)

Figure 4.50 The SEM micrographs of sandwich specimens (Skin: PP HP420J, Core: wood plastic composite(PP HP500N+wood flour)) (a) 10% wood content per weight unit with magnification of 30x, (b) 10% wood content per weight unit with magnification of 100x, (c) 10% wood content per weight unit with magnification of 500x at first area

(a) (b) (c)

Figure 4.51 The SEM micrographs of sandwich specimens (Skin: PP HP420J, Core: wood plastic composite(PP HP500N+wood flour)) (a) 10% wood content per weight unit with magnification of 30x, (b) 30% wood content per weight unit with magnification of 100x, (c) 10% wood content per weight unit with magnification of 500x at second area

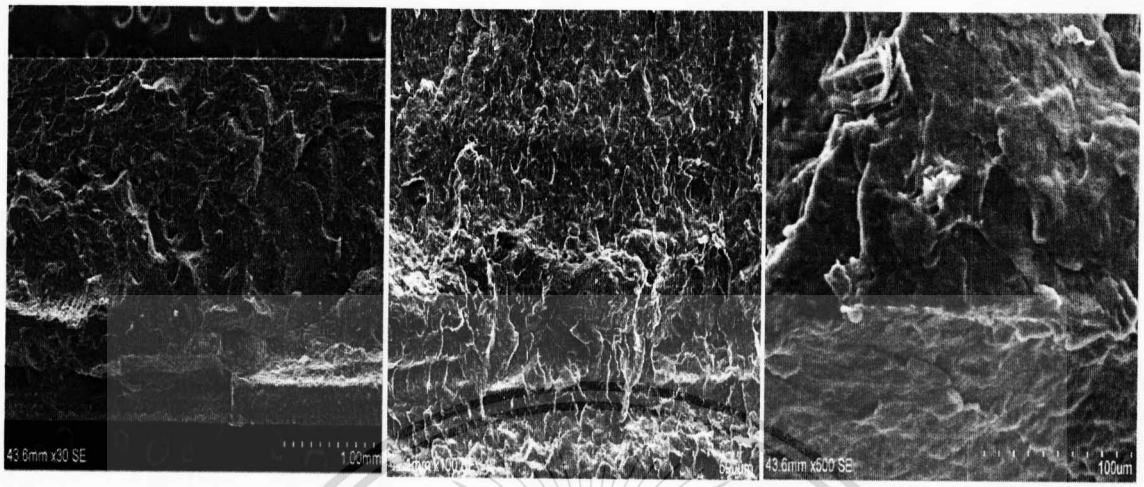

(a) (b) (c)

Figure 4.52 The SEM micrographs of sandwich specimens (Skin: PP HP420J, Core: wood plastic composite(PP HP500N+wood flour)) (a) 10% wood content per weight unit with magnification of 30x, (b) 10% wood content per weight unit with magnification of 100x, (c) 10% wood content per weight unit with magnification of 500x at third area

4.6.2 The Optical Microscope

The pictures from Optical Microscope (**Figure 4.53** and **Figure 4.54)** show the adhesion between skin-core layers with magnification of 50x and 100x in the left hand side and right hand side respectively. The surfaces determined were parallel to the flow direction.

(a)

(b)

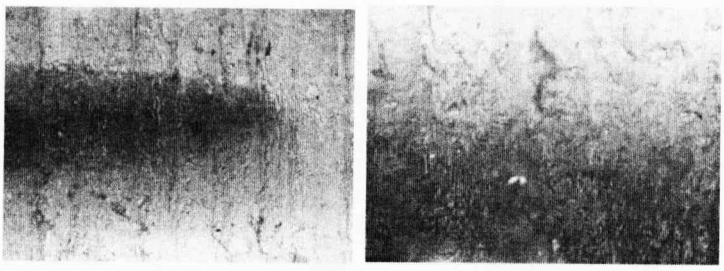

(c)

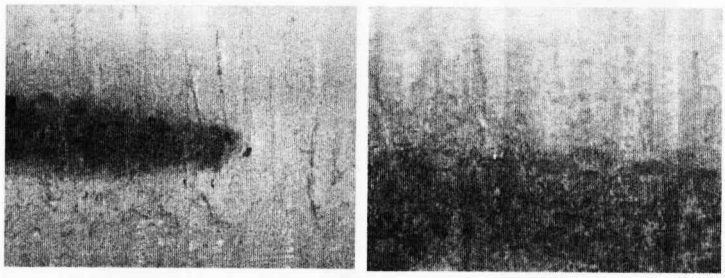

Figure 4.53 The pictures from Optical Microscope of sandwich specimens (Skin: PP HP420J, Core: wood plastic composite(PP HP500N+wood flour)) (a) 10% wood content per weight unit (b) 20% wood content per weight unit (c) 30% wood content per weight unit

(a)

(b)

(c)

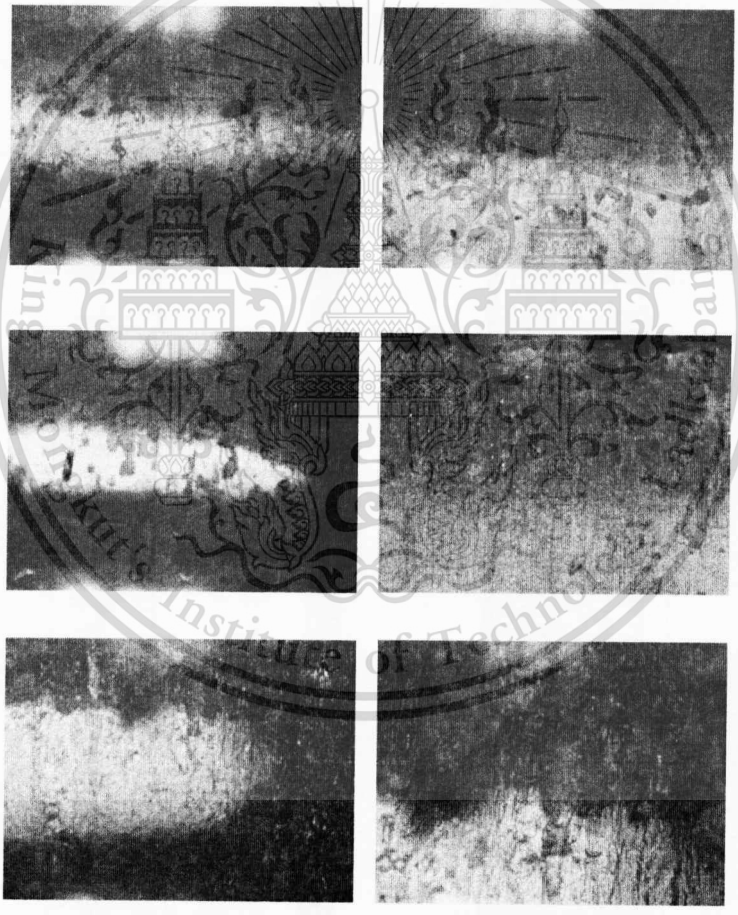

Figure 4.54 The pictures from Optical Microscope of sandwich specimens (Skin: wood plastic composite(PP HP500N+wood flour), Core: PP HP420J) (a) 10% wood content per weight unit (b) 20% wood content per weight unit (c) 30% wood content per weight unit

The SEM micrographs of fractured surfaces and Optical Microscope pictures show an excellent adhesion between skin and core layer. The fiber in wood plastic composite layer has been covered with a thin layer by the matrix. The wood particles are dispersed in the matrix of wood plastic composite. Excellent adhesion between the fiber and matrix makes it difficult to pull the fiber out of the matrix and the fracture path passes from the matrix through the interface and wood fibers. Obviously, the compatibilizer contributes a strong interfacial layer to be formed. Less voids and fiber pull out can be observed.

CHAPTER 5

CONCLUSION AND SUGGESTIONS

5.1 Conclusion

The molding parameters (viscosity, injection speed, volume proportion and temperature) were investigated to find major and minor parameters affecting on sandwich structure using sequential injection molding process. The results show viscosity parameter affect significantly influence the skin-core thickness fraction specimens while the optimum condition was obtained at volume fraction equal 1.5. In this experiment, there were found reduction of skin-core volume proportions, skin injection speeds, skin temperatures and core viscosities lead to high core thickness fractions but a large number of decreasing skin-core volume proportions conduce to core breakthrough. On the other hand, decreasing core injection speeds, core temperatures and skin viscosities lead to low core thickness fractions. From the results, injection speed and viscosity are the major factor and the melt temperature is the minor factor for controlling the profile of skin-core structures. Skin-core viscosities play important role on the sandwich structure profile because these are consistent with temperature and injection speed.

A Maleic anhydride (MA) grafted PP (PP-g-MA) was used as a compatibilizer to improve the poor interfacial interaction between the hydrophilic natural fibers and the hydrophobic matrix PP. The mechanical properties results of sandwich specimen with wood plastic composite (WPC) showed increasing wood flour contents in sandwich specimen lead to improve flexural stress but decreasing impact strength.

The fractured surfaces morphology and microstructure of sandwich specimen with wood plastic composite (WPC) were analyzed using the scanning electron microscopy (SEM) and Optical microscope. In this investigation, the morphology and microstructure of fractured surfaces results show wood fibers distribution in wood plastic composite layer and good adhesion between skin and core layers can be observed. Less voids and fiber pull out. The fiber in wood plastic composite layer has been covered with a thin layer by the matrix. The mechanical interlocking and interdiffusion occurred in skin and core layers. A large number of wood fibers dispersed in wood plastic composite layer at high wood contents. Thus, the microstructural parameters such as wood fiber size, void and percentage wood contents are consistent with mechanical properties of sandwich specimens.

5.2 Suggestions

Although this work was finished, it was only the first step Co-injection molding process. There are some suggestions to the work for further study as follow:

5.1.1 Further examine and analyze the effects of simultaneous process of Co-injection molding.

5.1.2 Another suggestion is softwood should be study and compare with hardwood from this investigation.

.

REFERENCES

1. P.J.Garner and D.F.Oxley.1971. **British Patent** No. 1, 156, 217.
2. Woodhams, R.T., G. Thomas and D.K. Rodgers. 1984. "Wood fibers as reinforcing fillers for polyolefin". **Polymer Engineering Science**. 24: 1166-1171.
3. Bledzki, A.K. and J. Gassan, 1999. "Composites reinforced with cellulose based fibers". **Polymer Engineering Science.** 24: 221-274.
4. James M. Margolis. 2006. **Engineering Plastics Handbook**. United States of America: The McGraw-Hill Companies.
5. Milton Ohring. 1995. **Engineering materials science**. United States of America: Academic Press Limited.
6. The university of Southern Mississippi, "**Ziegler-Natta vinyl polymerization**", [online]. Available: http://pslc.ws/macrog/ziegler.htm. 2005.
7. The university of Southern Mississippi, "**Metallocene catalysis polymerization**", [online].Available: http://pslc.ws/macrog/mcene.htm. 2005.
8. Maier, Clive; Calafut, Teresa (1998). Polypropylene: the definitive user's guide and databook. William Andrew. P. 14.
9. Nick Tucker, and Kevin Lindsey. 2002. **An Introduction to Automotive Composites**. UK : Rapra Technology Limited.
10. F.O. Anderegg, **Industrial Engineering Chemistry**, 1939 : 31,37
11. U.K.Dwivedi, Navin Chand. "Influence of MA-g-PP on abrasive wear behavior of chopped sisal fibre reinforced polypropylene composites". **Journal of Materials Processing Technology**. 209 (2009) : 5371-5375.
12. Goodship V.2001. "Interfacial Instabilities in multimaterial coinjection molding". University of Warwick.

REFERENCES (CONT.)

13. Chiu, Hsieh. 1987. ASME translation. **Journal of Engineering Material Technology**, Vol 109, No. 71.

14. Wilkinson A. N., Ryan A. J. 1999. **Polymer Processing and Structure Development**, Kluwer Academic Publishers, 1999.

15. Bushko W. C., Stokes V. K. "The Effects of Differential Mold-SurfaceTemperatures on The Warpage of Packed Injection-Molded Parts", **Proceedings of Antec** 94, San Francisco, Vol 1,1994, pp506-512.

16. Wuttipong Rungseesantivanon.2000. "Factors affecting adhesion of polymers during co-injection", University of Warwick.

17. Oxley D F and Sandiford D J H.1971. "Sandwich Molding". **Plastics &- polymers**,Vol. 39 (August), pp. 288-292.

18. Innovative Injection Molding.1996. **Ferromatik Milakron Company**.

19. Addmix@ Monosandwich Injection Moulding Technology. 1997. **Addmix Inc**.,Internet website http: //www.netlink.co.uk/users/addmix/main.html.

20. Kortec's Multigate Co-Injection Systems. 1997. **Kortec Inc**. Internet website http: //www.kortec.com.

21. Battenfeld's Operating Instructions for BMT-1100/2x300 Co-injection Molding Machine, **Battenfeld GmbH**.

22. Battenfeld's Operating Instructions for BM-2700/3x630 Co-injection Molding Machine, **Battenfeld GmbH**.

23. Wood R.1991. **Automotive Engineering Plastics**, Pentech Press.

REFERENCES (CONT.)

24. Eckardt H. 1986. "How to develop a successful co-injection application". Fourteenth annual structural foam conference and parts competition, **The socicty of the plastics industry,** Inc., Boston, Massachusetts, April 21-23.

25. White J L and Dee H B.1974. **Polym. Eng. Sci**. Vol. 14.pp.212.

26. Young S S, White J L, Clark E S, and Oyanagi Y. 1980. "A Basic Experimental Study of Sandwich Injection Molding with sequential injection", **SPE. ANTEC.** pp. 163-165.

27. Schlatter G, Davidoff A, Agassant J F, and Vincent M.1995. "Numerical Simulation of The Sandwich Injection Molding Process", **SPE ANTEC**. pp. 456-459.

28. Donovan R C, Rabe K S, Mammel W K, and Lord H A. 1975. "Recycling Plastics by Two-shot Molding". **Polymer Engineering and Science**.15(11). pp.774-780.

29. Lord H A and Williams G. 1975. **SPE ANTEC**, Tech. Papers Vol. 21.

30. Somnuk P, and Smith G F.1995."Experimental Study of Simultaneous Co-injection Molding Process". **SPE ANTEC**, Boston, Massachusetts, pp. 760-764.

31. Mark. Bikales. Overberger. Menges. 1985. **Encyclopedia of polymer science and engineering**. 2nd ed. Vol.01. New York : A wiley-interscience publication.

32. Chockchai N. 2006. "Parameters Influence on Inflow Pressure Loss in Injection Molding".**KMUTNB.**

33. Frederick W. 2010. "Catalytic pyrolysis of cellulose, hemicelluloses and lignin compound" **Virginia Polytechnic Institute.**

34. Mohan, D., C. U. Pittman, Jr., et al. (2006). "Pyrolysis of wood/biomass for bio oil: A critical review." **Energy & Fuels** 20(1): 848-889.

35. Bridgwater, A. V. (2004). Therm.Sci. 8: 21-89.

36. Sjostrom, Eero. 1981. **Wood Chemistry: Fundamentals and Applications**. Orlando:Academic Press.

37. Haygreen, John G. and Jim L Bowyer. 1996. "Forest Products and Wood Science". **An Introduction Third Edition**. Ames Iowa: Iowa State University Press.

38. Miller, Regis B. 1999. "Structure of Wood. p. 2-1 to 2-4". **In Wood Handbook: Wood as an Engineering Material**, General Technical Report FPL-GTR-113, Madison, Wisconsin: USDA Forest Products Laboratory.

APPENDIX A

MATERIAL AND PROCESSING INFORMATION

Appendix A-1: Product information of Polyprppylene HP500N

Product Data and Technical Information

Email this page Print this page

Name	Moplen
Grade	HP500N
Resin type	Polypropylene, Homopolymer
Description	*Moplen* HP500N is a homopolymer used for general purpose injection moulding applications. It exhibits good flow and stiffness. *Moplen* HP500N is suitable for food contact.
Availability	Europe, Asia-Pacific, Africa-Middle East
Technical data	
Density	0.9 g/cm³
Melt flow rate (MFR)	12 g/10 min (230°C/2.16kg)
Melt volume flow rate	16 cm³/10min (230°C/2.16kg)
Tensile Modulus	1550 MPa
Tensile Stress at Yield	35 MPa
Tensile Strain at Break	>50 %
Tensile Strain at Yield	10 %
Charpy unnotched impact strength	30 kJ/m² (0 °C)
Charpy unnotched impact strength	110 kJ/m² (23 °C)
Charpy notched impact strength	3 kJ/m² (23 °C)
Heat deflection temperature B (0.45 MPa) Unannealed	95 °C
Vicat softening temperature A/50	153 °C
Vicat softening temperature B/50	85 °C

Figure A-1 Scanned image of product information of Polypropylene HP500N

Appendix A-2: Product information of Polypropylene HP420J

Product Data and Technical Information

✉ Email this page 🖶 Print this page

Name	Moplen
Grade	HP420J
Resin type	Polypropylene, Homopolymer
Description	Moplen HP420J is a polypropylene homopolymer manufactured using the Spheripol process. It is particularly suitable for BOPP, with potential end use applications in general purpose packaging, lamination film and adhesive tape.
Availability	Asia-Pacific, Australia-NZ, Africa-Middle East

Technical data	
Density -Specific Gravity	0.90 g/cm³
Melt flow rate	3 g/10 min
Tensile Strength @ Yield	32 MPa
Flexural Modulus	1350 MPa
Tensile Elongation @ Yld	11 %
Notched izod impact	36 J/m (23 °C)
Heat deflection temperature at 0.46 N/mm2	96 °C

Figure A-2 Scanned image of product information of Polypropylene HP420J

Appendix A-3: Product information of Polyprppylene HP740H

Product Data and Technical Information

Email this page Print this page

Name	Moplen
Grade	HP740H
Resin type	Polypropylene, Homopolymer
Description	Moplen HP740H is a polypropylene homopolymer. With its good stiffness and top load strength, this grade is especially suitable for solid phase pressure thermoforming process. Potential end use products include drinking, margarine, noodle and dairy cups, etc. all of which can be hot fillable or microwaveable.
Availability	Asia-Pacific, Australia-NZ, Africa-Middle East

Technical data	
Density -Specific Gravity	0.90 g/cm³
Melt flow rate	2.1 g/10 min (230°C/2.16kg)
Tensile Strength @ Yield	36 MPa
Flexural Modulus	1750 MPa
Tensile Elongation @ Yld	9 %
Notched izod impact	40 J/m (23 °C)
Heat deflection temperature at 0.46 N/mm2	115 °C

Figure A-1 Scanned image of product information of Polypropylene HP740H

Appendix A-4: Product information of Polyprppylene P440J

SCG CHEMICALS

Technical Datasheet Polypropylene Impact Copolymer for Injection Molding

EL-Pro P440J

Product Description

EL-Pro P440J is an impact copolymer polypropylene resin suitable for injection molding process.
This resin is recommended for product that requires high impact strength with good processibility.

Typical Application

- Pail, Crates, Industrial uses
- Automotive and electrical appliance parts
- Furniture,Containers

Product Characteristics

- High impact strength
- Good processibility and stiffness
- Food contact applicable (Complies with U.S FDA 21 CFR 177.1520)

Physical Properties

Property	Test Method	Value	Unit
Melt Flow Rate	ASTM D 1238 @ 230°C, 2.16 kg	5	g/10 min
Density	ASTM D 1505	0.910	g/cm^3
Tensile Strength at Yield	ASTM D 638 @ Crosshead speed 50 mm/min	270	kg/cm^2
Tensile Strength at Break	ASTM D 638 @ Crosshead speed 50 mm/min	200	kg/cm^2
Elongation at Break	ASTM D 638 @ Crosshead speed 50 mm/min	520	%
Flexural Modulus	ASTM D 790	11500	kg/cm^2
Notched Izod Impact	ASTM D 256 @ 23°C	12	kg.cm/cm
Notched Izod Impact	ASTM D 256 @ 0°C	6	kg.cm/cm
Notched Izod Impact	ASTM D 256 @ -20°C	5	kg.cm/cm
Rockwell Hardness	ASTM D 785	60	R-Scale
Haze	ASTM D 1003	80	%
Gloss	ASTM D 2457	30	%
Melting Point	ASTM D 2117	163, 120	°C
Vicat Softening Point	ASTM D 1525	150	°C
Heat Deflection Temperature (HDT)	ASTM D 648 @ 4.6 kg/cm^2	100	°C
Heat Deflection Temperature (HDT)	ASTM D 648 @ 18.5 kg/cm^2	55	°C
Brittleness Temperature	ASTM D 746	-20	°C
% Shrinkage (2mmt) MD	TPE Method	1.19	%
TD	TPE Method	1.05	%
Flamability	UL - 94	HB	-

Note : Conversion factor for changing unit from kg/cm^2 to MPa is divided by 10.20

Figure A-4 Scanned image of product information of Polypropylene P440J

Appendix A-5: General specification

Tank capacity	50 litres
Pressure gauge display	Analog pressure gauge
The maximum working pressure	300bar
Hydraulic cylinder	∅40mm
Hydraulic control system	Solenoid valve
Motor "Mitsubishi"	220/380 Volt, 3 phase, 50Hz, 3HP
DC controller	AC 220 Volt
Hydraulic pump	Displacement (2.8 cm^3/rev), Flow (3.9litres/min)

Appendix A-6: Calculating hydraulic motor sizes

Define: The maximum working pressure (Δp) =300bar

Calculate flow rate of hydraulic pump (Q)

$Q = AV$ [litre/min]

$Q = V \cdot n \cdot 10^{-3}$ [litre/min]

$Q = 2.8 \cdot 1500 \cdot 10^{-3}$ [litre/min]

$Q = 4.2$ [litre/min]

Where V =displacement [cm^3/rotation], n= rotation speed [rev/min]

Calculate hydraulic power (P)

$P = (Q \cdot \Delta p)/(600)$ [kW]

$P = (4.2 \cdot 300)/(600)$ [kW]

$P = 2.1$ [kW]

$P = 2.81$ [HP] (1kW=1.34HP)

Where Q=flow rate [litre/min], Δp =pressure differential [bar]

Thus, the hydraulic Mitsubishi motor has enough horse power to operate with co-injection molding machine.

BIOGRAPHY

Name: Mr. Kriangkrai Jongprasertvittaya

Date of Birth: November 20, 1986

Place of Birth: Chonburi, Thailand

Education:

2005-2008	B. Eng. in Mechanical Engineering, Department of Mechanical Engineering, King Mongkut's Institute of Technology Ladkrabang (KMITL)
2009-2012	M. Eng. in Automotive Engineering (International program), International College, King Mongkut's Institute of Technology Ladkrabang (KMITL)

Honour and Scholarship:

2009-2012	Full scholarship for study in the master degree from National Science and Technology Development Agency (NSTDA)

Publications:

1. K. Jongprasertvittaya, W. Rungseesantivanon, N. Depaiwa, I. Satoh and T. Saito. "A study of factors affecting on PP/PP by Co-injection molding." **Proceeding of the 8th International Conference on Automotive Engineering**, Bangkok, Thailand, April 2-5, 2012.